RADC-TR-88-119
In-House Report
May 1988

INCREMENTAL DIFFRACTION COEFFICIENTS FOR PLANAR SURFACES, PART III: Pattern Effects of Narrow Cracks in the Surface of a Paraboloid Antenna

Dr. Robert A. Shore and Dr. Arthur D. Yaghjian

APPROVED FOR PUBLIC RELEASE; DISTRIBUTION UNLIMITED.

ROME AIR DEVELOPMENT CENTER
Air Force Systems Command
Griffiss AFB, NY 13441-5700

UNCLASSIFIED

SECURITY CLASSIFICATION OF THIS PAGE

REPORT DOCUMENTATION PAGE

1a. REPORT SECURITY CLASSIFICATION Unclassified	1b. RESTRICTIVE MARKINGS
2a. SECURITY CLASSIFICATION AUTHORITY	3. DISTRIBUTION / AVAILABILITY OF REPORT Approved for public release; distribution unlimited.
2b. DECLASSIFICATION / DOWNGRADING SCHEDULE	
4. PERFORMING ORGANIZATION REPORT NUMBER(S) RADC-TR-88-119	5. MONITORING ORGANIZATION REPORT NUMBER(S)
6a. NAME OF PERFORMING ORGANIZATION Rome Air Development Center 6b. OFFICE SYMBOL (If applicable) EEAS	7a. NAME OF MONITORING ORGANIZATION
6c. ADDRESS (City, State, and ZIP Code) Hanscom AFB Massachusetts 01731-5000	7b. ADDRESS (City, State, and ZIP Code)
8a. NAME OF FUNDING / SPONSORING ORGANIZATION Rome Air Development Center 8b. OFFICE SYMBOL (If applicable) EEAS	9. PROCUREMENT INSTRUMENT IDENTIFICATION NUMBER
8c. ADDRESS (City, State, and ZIP Code) Hanscom AFB Massachusetts 01731-5000	10. SOURCE OF FUNDING NUMBERS PROGRAM ELEMENT NO. / PROJECT NO. 4600 / TASK NO. 15 / WORK UNIT ACCESSION NO 07

11. TITLE (Include Security Classification)
Incremental Diffraction Coefficients for Planar Surfaces, Part III: Pattern Effects of Narrow Cracks in the Surface of a Paraboloid Antenna

12. PERSONAL AUTHOR(S)
Shore, Robert A. and Yaghjian, Arthur D.

13a. TYPE OF REPORT	13b. TIME COVERED	14. DATE OF REPORT (Year, Month, Day)	15. PAGE COUNT
Scientific, Interim	FROM Oct. 87 TO Mar. 88	May 1988	84

16. SUPPLEMENTARY NOTATION

17. COSATI CODES		
FIELD	GROUP	SUB-GROUP
0901	2003	

18. SUBJECT TERMS (Continue on reverse if necessary and identify by block number)
Incremental diffraction coefficients
Reflector antennas
Paraboloid

19. ABSTRACT (Continue on reverse if necessary and identify by block number)

In this report, incremental diffraction coefficients for a narrow slit in an infinite, perfectly conducting plane are used to investigate the effects of cracks in the surface of a focal-fed circular paraboloidal reflector antenna. Such cracks can result from the imperfect fitting together of panels to form a large reflector. The imperfections in fitting together are modeled by narrow slits in a paraboloidal surface. The far fields scattered by the cracks are computed by integrating the slit incremental diffraction coefficients (multiplied by the illuminating field) along the cracks. Two forms of cracks are modeled: azimuthal cracks, the projections of which on the aperture plane are concentric circles, and radial cracks, the projections of which on the aperture plane are radii of the projection of the paraboloid. The feed is assumed to be a Huygens source. It is found that narrow azimuthal cracks hardly change the H-plane pattern, moderately change the further out sidelobes of the E-plane pattern, and moderately change the entire cross-polarization pattern. Depending on their orientation the radial

(see over)

20. DISTRIBUTION / AVAILABILITY OF ABSTRACT	21. ABSTRACT SECURITY CLASSIFICATION
☒ UNCLASSIFIED/UNLIMITED ☐ SAME AS RPT. ☐ DTIC USERS	Unclassified
22a. NAME OF RESPONSIBLE INDIVIDUAL Robert A. Shore	22b. TELEPHONE (Include Area Code) 617/377-2058 22c. OFFICE SYMBOL EEAS

DD FORM 1473, 84 MAR — 83 APR edition may be used until exhausted. All other editions are obsolete.

SECURITY CLASSIFICATION OF THIS PAGE
UNCLASSIFIED

Block 19 (Contd.)

cracks can strongly change the E-plane and cross-polarization patterns. However, like the azimuthal cracks, the radial cracks hardly change the H-plane pattern.

Contents

Illustrations

Incremental Diffraction Coefficients for Planar Surfaces, Part III: Pattern Effects of Narrow Cracks in the Surface of a Paraboloid Antenna

1. INTRODUCTION

In Part I[1] of this series of reports we derived exact expressions for incremental diffraction coefficients at arbitrary angles of incidence and scattering directly in terms of the corresponding two-dimensional, cylindrical diffraction coefficients. We confirmed the validity of the general expressions by showing that, for the infinite wedge, the physical theory of diffraction, geometric theory of diffraction, and physical optics incremental diffraction coefficients obtained by direct substitution into the general expressions agreed with the results obtained by previous authors through integration of the currents on the surface of the wedge. In Part I we also applied our general method to obtain, for the first time, the incremental diffraction coefficients for the narrow strip and slit.

In Part II[2] we integrated the nonuniform incremental diffraction coefficients for the half plane around the rim of a reflector antenna to enhance the accuracy of the far fields computed from the physical optics current. Excellent agreement was obtained with the far fields obtained from a method of moments solution to

(Received for Publication 17 May 1988)

1. Shore, R.A., and Yaghjian, A.D. (1987) Incremental Diffraction Coefficients for Planar Surfaces, Part I: Theory, RADC-TR-87-35.
2. Shore, R.A., and Yaghjian, A.D. (1987) Incremental Diffraction Coefficients for Planar Surfaces, Part II: Calculation of the Nonuniform Current Correction to PO Reflector Antenna Patterns, RADC-TR-87-213.

the electric field integral equation applied to a 20-wavelength-diameter reflector. It was shown that the cross-polarized field, further-out sidelobes of the co-polarized field, and fields near nulls can be appreciably changed by inclusion of the fields of the nonuniform currents.

In this report (Part III) we use the incremental diffraction coefficients for a narrow slit in an infinite, perfectly conducting plane derived in Part I to investigate the effect of cracks in the surface of a focal-fed circular paraboloidal reflector antenna. Such cracks can result from the imperfect fitting together of panels to form a large reflector. The cracks are modeled by narrow slits in a paraboloidal surface, and the far fields scattered by the cracks are computed by integrating the slit incremental diffraction coefficients (multiplied by the illuminating field) along the cracks. Two forms of cracks are considered here: "azimuthal" cracks, the projections of which on the aperture plane are circles concentric with the projection of the reflector rim; and "radial" cracks, the projections of which on the aperture plane are radii of the projection of the paraboloid.

It is found that narrow azimuthal cracks hardly change the H-plane pattern, moderately change the further-out sidelobes of the E-plane pattern, and moderately change the entire cross-polarization pattern. Depending on their orientation, the radial cracks can strongly change the E-plane and cross-polarization patterns. However, like the azimuthal cracks, the radial cracks hardly change the H-plane pattern.

We also compare the far fields scattered by the azimuthal and radial cracks as computed by numerical integration of the incremental diffraction coefficients with the far fields obtained by asymptotic evaluation of the same diffraction integrals. Significantly, it is found that the asymptotically evaluated far fields of both radial and azimuthal cracks can deviate greatly from the far fields determined by numerical integration. An investigation of the discrepancies revealed that the usual asymptotic evaluation by the method of stationary phase applied to the cracks could be a highly inaccurate approximation over a significant portion of the far field.

2. ANALYSIS

We wish to investigate the effects of narrow cracks in the surface of a paraboloidal reflector antenna on the antenna far field. It is assumed that the reflector can be modeled by an infinitesimally thin, perfectly conducting surface, and that each crack, locally, appears to be a portion of a narrow infinite slit in a perfectly conducting screen. The effect of the cracks can then be approximated by the integral of the incremental diffraction coefficients of a slit along the cracks.

2.1 Incremental Diffraction Coefficients of an Infinite Slit

The incremental diffraction coefficients for a narrow infinite slit in a perfectly conducting screen illuminated by a plane wave were derived in Part I[1]. The slit, of width d, is defined in terms of Cartesian coordinates (x, y, z) by $y = 0$, $|x| \leq d/2$, so that the slit lies in the xz-plane with the edges of the slit parallel to the z-axis as shown in Figure 1. The direction vector $\bar{k}$ of the incident plane wave forms angles of $\pi + \phi_o$ and $\pi - \theta_o$ with the positive x- and z-axes respectively.

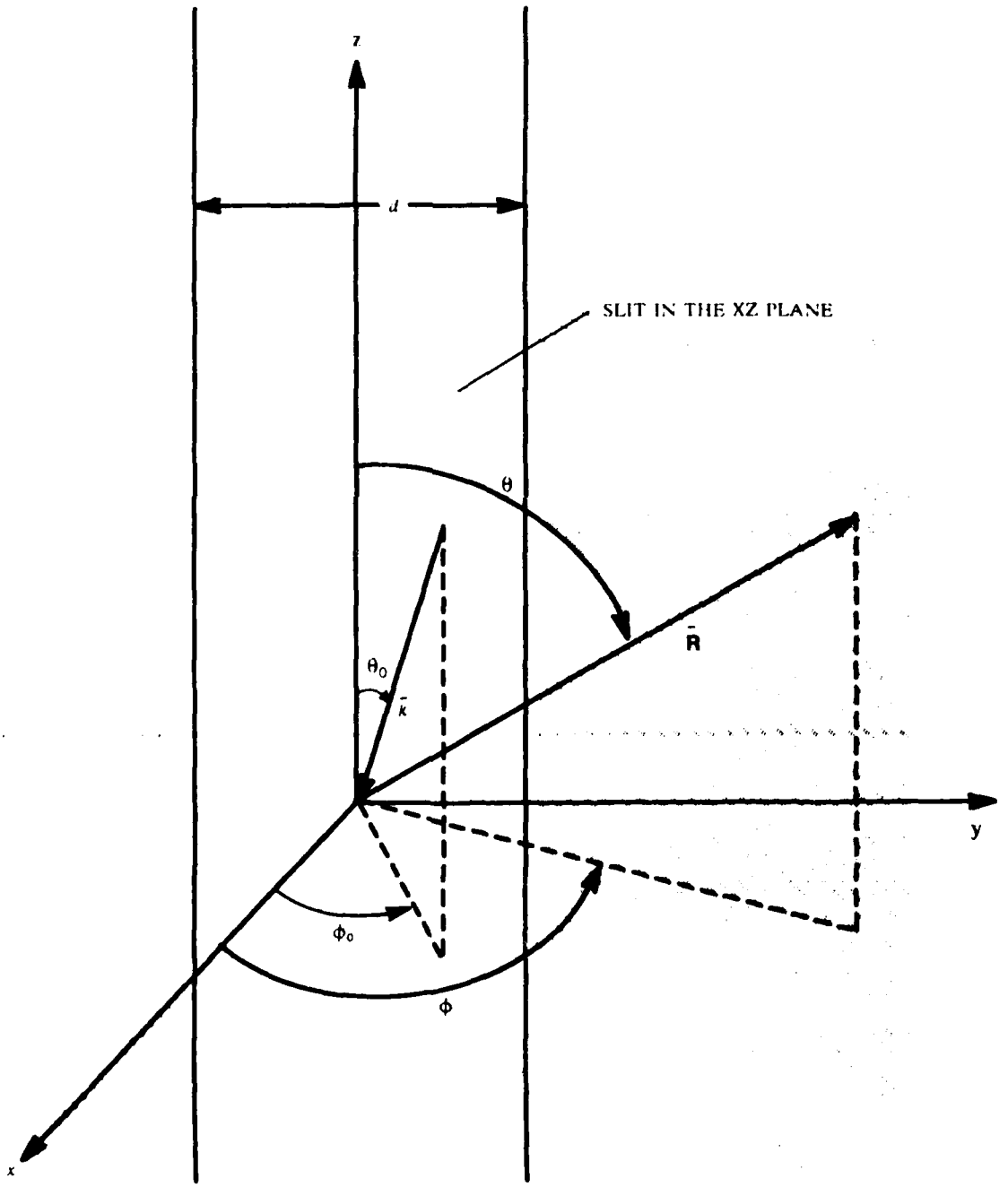

Figure 1. Geometry of Slit, Incident Wave, and Observation Point

The magnitude of $\bar{k}$ is

$$k = 2\pi/\lambda = \omega/c \quad ,$$

where λ is the free-space wavelength, ω is the angular frequency of the suppressed exp ($-i\omega t$) time dependence ($\omega > 0$), and c is the speed of light in free space. The observation direction is defined by the azimuth and elevation angles ϕ and θ respectively. The transverse electric and transverse magnetic incremental diffraction coefficients, $\overline{dE}_d^{TE}(\bar{r})$ and $\overline{dE}_d^{TM}(\bar{r})$ are[1]

$$\overline{dE}_d^{TE}(\bar{r}) \underset{\sim}{r \to \infty} dz' Z_o \frac{H_{iz}}{\sin \theta_o} \frac{e^{ikr}}{4\pi r} \frac{4P_1(\alpha, \phi_o, kd \sin \theta_o)}{\sin \alpha} \frac{\sin \phi}{|\sin \phi|}$$

$$\cdot [\sin \phi \, \hat{\phi} - (\cos \phi \cos \theta + \cos \alpha \sin \theta \cot \theta_o)\hat{\theta}] \tag{1a}$$

and

$$\overline{dE}_d^{TM}(\bar{r}) \underset{\sim}{r \to \infty} - dz' E_{iz} \frac{\sin \theta}{\sin^2 \theta_o} \frac{e^{ikr}}{4\pi r} 4P_2(\alpha, \phi_o, kd \sin \theta_o) \frac{\sin \phi}{|\sin \phi|} \hat{\theta} \quad , \tag{1b}$$

where E_{iz} and H_{iz} are the complex amplitudes of the electric and magnetic components, respectively, of the illuminating plane waves parallel to the edge of the slit at the origin, Z_o is the free-space impedance, $r = |\bar{r}|$, the distance from the origin to the field point,

$$\alpha = \cos^{-1}\left(\frac{\sin \theta \cos \phi}{\sin \theta_o}\right) \quad , \tag{2}$$

$$P_1(\phi, \phi_o, kd) = \pi \sum_{n=0}^{2} T_{2n}(\phi, \phi_o, p) \, c^{2n} + o(c^5) \quad , \tag{3a}$$

$$P_2(\phi, \phi_o, kd) = \pi c^2 \sum_{n=0}^{1} U_{2n}(\phi, \phi_o, p) c^{2n} + o(c^5) \quad , \tag{3b}$$

with

$$c = kd/2,$$

$$p = \ln(c/4) + \gamma - i\pi/2,$$

$\gamma = 0.5772157\ldots$ = Euler's constant,

$$T_o = \frac{1}{2p},$$

$$T_2 = -\frac{1}{4}\left(\frac{\cos^2\phi}{2p} - \cos\phi_o\cos\phi - \frac{\sin^2\phi_o}{2p}\right),$$

$$T_4 = \frac{\cos^4\phi}{128p} - \frac{1}{32}\cos\phi_o\cos^3\phi$$

$$- \frac{1}{32}\left(\frac{\sin^2\phi_o}{p} + \cos^2\phi_o - \frac{1}{2} - \frac{1}{4p}\right)\cos^2\phi$$

$$+ \frac{1}{16}\left[-\frac{1}{2}\cos^3\phi_o + \left(p + \frac{1}{4}\right)\cos\phi_o\right]\cos\phi$$

$$+ \left[\frac{\cos^4\phi_o}{128p} + \frac{1}{64}\left(1 - \frac{3}{2p}\right)\cos^2\phi_o + \frac{1}{256}\left(\frac{1}{p^2} + \frac{3}{2p} - 2\right)\right],$$

$$U_o = -\frac{1}{4}\sin\phi_o\sin\phi,$$

and

$$U_2 = \frac{1}{16}\sin\phi_o\sin\phi\left[\frac{1}{2}\cos^2\phi + \frac{1}{2}\cos\phi_o\cos\phi + \left(p - \frac{3}{4} + \frac{1}{2}\cos^2\phi_o\right)\right].$$

Expressions for higher order terms in the series for P_1 and P_2 are given in Refs. 3 and 4.

---

3. Millar, R.F. (1960) A note on diffraction by an infinite slit, Can. J. Phys., 38:38-47.

4. Asvestas, J.S., and Kleinman, R.E. (1969) The strip, Ch. 4 of Electromagnetic and Acoustic Scattering by Simple Shapes, Bowman, J.J., Senior, T.B.A., and Uslenghi, P.L.E., Eds., Amsterdam: North-Holland.

For arbitrarily polarized plane-wave illumination, the slit incremental diffraction coefficient is obtained by summing (1a) and (1b):

$$\overline{dE_d}(r_\ell) \overset{r_\ell \to \infty}{\sim} -dz'_\ell \frac{e^{ikr_\ell}}{4\pi r_\ell} \frac{1}{\sin\theta_{o\ell}} \left[E_{iz_\ell} \frac{\sin\theta_\ell}{\sin\theta_{o\ell}} 4P_2(\alpha, \phi_{o\ell}, kd\sin\theta_{o\ell}) \right.$$

$$\left. + Z_o H_{iz_\ell} \frac{4P_1(\alpha, \phi_{o\ell}, kd\sin\theta_{o\ell})}{\sin\alpha} (\cos\phi_\ell \cos\theta_\ell + \cos\alpha \sin\theta_\ell \cot\theta_{o\ell}) \right] \frac{\sin\phi_\ell}{|\sin\phi_\ell|} \hat{\theta}_\ell$$

$$+ dz'_\ell \frac{e^{ikr_\ell}}{4\pi r_\ell} Z_o \frac{H_{iz_\ell}}{\sin\theta_{o\ell}} \frac{4P_1(\alpha, \phi_o, kd\sin\theta_{o\ell})}{\sin\alpha} \sin\phi_\ell \frac{\sin\phi_\ell}{|\sin\phi_\ell|} \hat{\phi}_\ell \qquad (4)$$

with

$$\alpha = \cos^{-1}\left(\frac{\sin\theta_\ell \cos\phi_\ell}{\sin\theta_{o\ell}}\right) .$$

We have inserted the subscripts "ℓ" in the above expression, indicating that the subscripted quantities are defined with reference to a local coordinate system with origin at the point of integration, to clearly distinguish the locally defined quantities from those defined with reference to the global coordinate system of the reflector antenna introduced in the next subsection.

The total field in the illuminated half space, $y \geq 0$, is obtained by adding the diffracted field to the field that would be present if no slit were there—the incident field plus the reflected field—whereas in the half-space $y \leq 0$ behind the screen, the total field is given by the diffracted field. The reflected field is the field radiated by the physical optics current excited on the screen in the absence of the slit. In our application we will be concerned solely with the field in the illuminated region, i.e., the forward portion of the reflector pattern. This restriction to the forward region arises because, in calculating the effect of narrow cracks in the surface of a paraboloidal reflector as the integral of the incremental slit-diffracted fields along the cracks, we are limited to the cone of observation angles within the intersection of the cones formed by rays to the reflector rim from the integration points on the cracks. For observation directions beyond that cone it would be necessary to take into account the secondary diffraction of the crack-diffracted fields by the reflector rim, a task of considerable complexity that will

not be undertaken here. Within this cone we will also neglect the reflection of the crack diffracted fields by the reflector.

2.2 Transformation to the Global Coordinate System of the Reflector

The effect of cracks in the reflector surface is obtained as indicated above by integrating (4) along the cracks and adding the result to the far field of the reflector without the cracks to obtain the total far field. The far field of the reflector without the cracks is calculated, as described in Part II,[2] by adding the integral of the half-plane nonuniform current incremental diffraction coefficient around the reflector rim to the PO reflector far field. Since all quantities in (4) are defined with respect to a local coordinate system with its origin at a differential element of a crack, it is first necessary to transform (4) to a global coordinate system which we will take here to be that shown in Figure 2. The origin of the global coordinate system is the focus of the paraboloid reflector of focal length F and diameter D, and the z-axis is the axis of the reflector directed

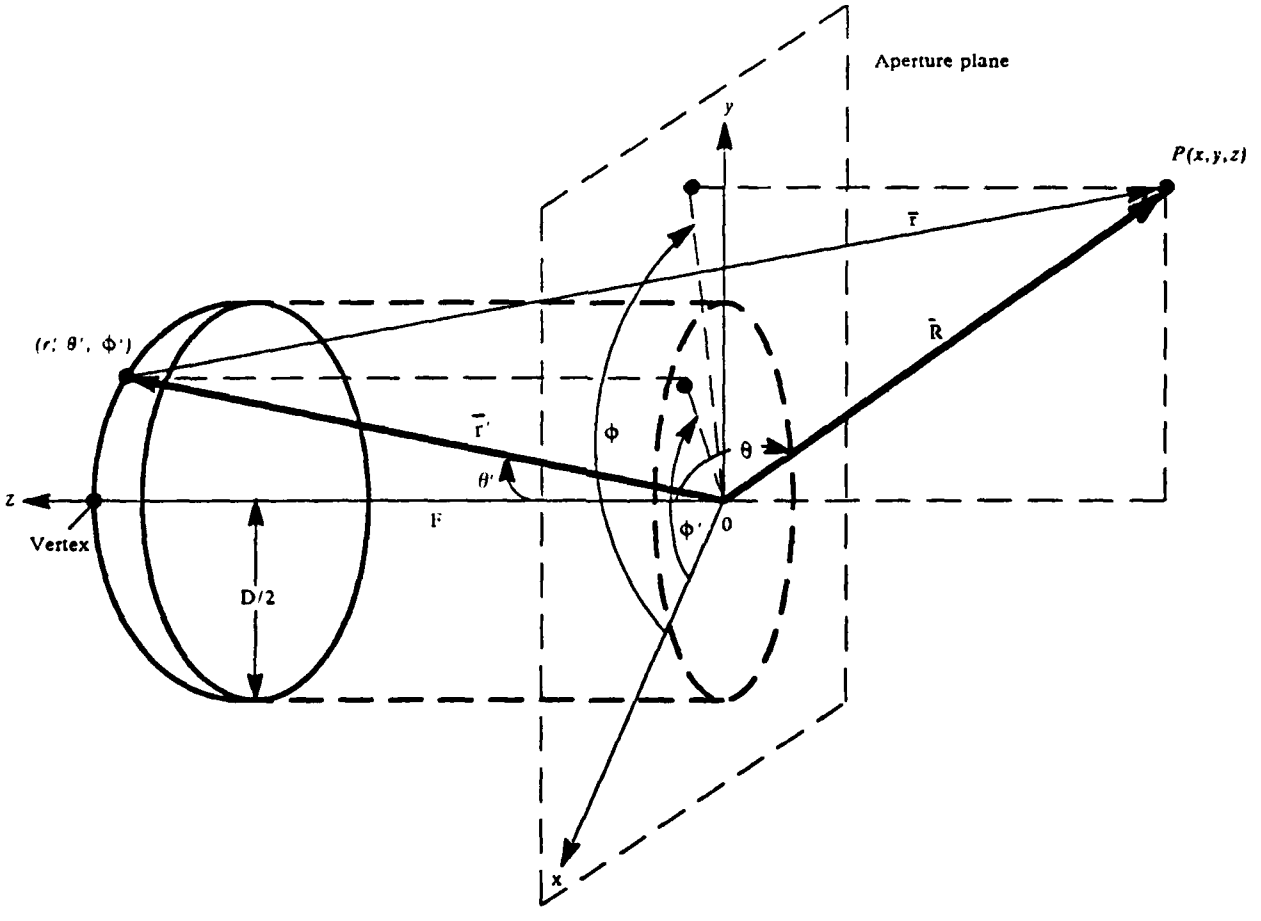

Figure 2. Global Coordinate System for Paraboloidal Reflector

towards the center of the reflector. Primed quantities are used to indicate integration points on the cracks, and unprimed quantities to indicate the field points.

Two types of cracks will be considered here: (1) azimuthal cracks defined in the global coordinate system by $\theta' = \theta'_c$; and (2) radial cracks defined by $\phi' = \phi'_c$. We will consider each of these types of cracks in turn.

2.2.1 AZIMUTHAL CRACKS

The analysis is almost identical to that described in Part II,[2] Section 2.2, for integrating the half-plane incremental diffraction coefficient around the reflector rim, the only difference being that in Part II, θ' was the angle $2\cot^{-1}(4F/D)$ at the focus between the reflector axis and rays from the focus to the reflector rim, whereas here θ'_c can be any angle between 0 and $2\cot^{-1}(4F/D)$. We can then immediately write down the relevant equations of Part II for use here.

In the local coordinate system, the local x-axis is tangent to the reflector at the crack, perpendicular to the crack, and directed towards the reflector center from the crack; the local y-axis is the inwardly directed normal to the paraboloid at the crack. Thus

$$\hat{x}_\ell = -\sin\frac{\theta'_c}{2}\,\hat{r}' - \cos\frac{\theta'_c}{2}\,\hat{\theta}' \quad , \tag{5a}$$

$$\hat{y}_\ell = -\cos\frac{\theta'_c}{2}\,\hat{r}' + \sin\frac{\theta'_c}{2}\,\hat{\theta}' \quad , \tag{5b}$$

and

$$\hat{z}_\ell = \hat{x}_\ell \times \hat{y}_\ell = -\hat{\phi}'_\ell \quad . \tag{5c}$$

The angle $\theta_{o\ell}$ between the local unit z-vector, $-\hat{\phi}'$, and the ray $-\bar{r}'$ from the crack point to the feed at the focus, is equal to $\pi/2$ so that

$$\cos\theta_{o\ell} = 0 \tag{6a}$$

and

$$\sin\theta_{o\ell} = 1 \quad . \tag{6b}$$

The trigonometric functions of $\phi_{o\ell}$, the angle between $\hat{x}_\ell$ and the projection of $-\bar{r}'$ on the $x_\ell y_\ell$-plane are

$$\cos\phi_{o\ell} = \sin\theta'_c/2 \tag{7a}$$

and

$$\sin \phi_{o\ell} = \cos \theta'_c/2 \quad . \tag{7b}$$

The trigonometric functions of the local field point elevation angle are

$$\cos \theta_\ell = \sin \theta \sin(\phi' - \phi) \tag{8a}$$

and

$$\sin \theta_\ell = [1 - \sin^2 \theta \sin^2(\phi' - \phi)]^{1/2} \quad , \tag{8b}$$

where the positive root must be taken since $0 \leq \theta_\ell \leq \pi$.

The cosine and sine of ϕ_ℓ, the local field point azimuth angle, are given by

$$\cos \phi_\ell = \left[- \cos \frac{\theta'_c}{2} \sin \theta \cos(\phi' - \phi) + \sin \frac{\theta'_c}{2} \cos \theta \right] \Big/ \sin \theta_\ell \tag{9a}$$

and

$$\sin \phi_\ell = \left[- \sin \frac{\theta'_c}{2} \sin \theta \cos(\phi' - \phi) - \cos \frac{\theta'_c}{2} \cos \theta \right] \Big/ \sin \theta_\ell \quad . \tag{9b}$$

The cosine and sine of $\alpha = \cos^{-1} \left(\dfrac{\sin \theta_\ell \cos \phi_\ell}{\sin \theta_{o\ell}} \right)$ are now known from (6b), (8b), and (9a):

$$\cos \alpha = \sin \theta_\ell \cos \phi_\ell \tag{10a}$$

and

$$\sin \alpha = (1 - \sin^2 \theta_\ell \cos^2 \phi_\ell)^{1/2} \quad , \tag{10b}$$

with the sign of $\sin \alpha$ being plus if $\phi_\ell = \tan^{-1} \left(\dfrac{\sin \phi_\ell}{\cos \phi_\ell} \right)$ is in quadrant I or II, and minus if ϕ_ℓ is in quadrants III or IV.

The θ- and ϕ- components of $\hat{\theta}_\ell$ and $\hat{\phi}_\ell$ are as follows:

$$\sigma = \hat{\theta}_\ell \cdot \hat{\theta}$$

$$= - \frac{\cos \theta \sin u}{(1 - \sin^2 \theta \sin^2 u)^{1/2}} \tag{11a}$$

$$\tau = \hat{\theta}_\ell \cdot \hat{\phi}$$

$$= \frac{\cos u}{(1 - \sin^2 \theta \sin^2 u)^{1/2}} \tag{11b}$$

$$\mu = \hat{\phi}_\ell \cdot \hat{\theta}$$

$$= - \frac{\cos u}{(1 - \sin^2 \theta \sin^2 u)^{1/2}} \tag{11c}$$

and

$$\nu = \hat{\phi}_\ell \cdot \hat{\phi}$$

$$= - \frac{\cos \theta \sin u}{(1 - \sin^2 \theta \sin^2 u)^{1/2}} \tag{11d}$$

with

$$u = \phi' - \phi \quad . \tag{12}$$

The factor

$$\frac{e^{ikr_\ell}}{r_\ell} = \frac{e^{ikr}}{r} \underset{\sim}{r \to \infty} \frac{e^{ik(R - \bar{r}' \cdot \hat{R})}}{R} \quad , \tag{13a}$$

with

$$\bar{r}' \cdot \hat{R} = r' [\sin \theta'_c \sin \theta \cos (\phi' - \phi) + \cos \theta'_c \cos \theta] \tag{13b}$$

and

$$r' = \frac{2F}{1 + \cos \theta'_c} = F \sec^2 \frac{\theta'_c}{2} \quad . \tag{13c}$$

Finally,

$$dz'_\ell = - r' \sin \theta'_c \, d\phi' = -2F \tan \frac{\theta'_c}{2} \, d\phi' \quad , \tag{14}$$

and

$$E_{iz_\ell} = - E_{i\phi'} \quad , \tag{15a}$$

$$H_{iz_\ell} = - H_{i\phi'} \quad . \tag{15b}$$

Substituting explicit expressions for $\cos \theta_{o\ell}$, $\sin \theta_{o\ell}$, r_ℓ, dz'_ℓ, E_{iz_ℓ}, and H_{iz_ℓ} in (4) and taking the θ- and ϕ- components gives

$$dE_{d \begin{Bmatrix} \theta \\ \phi \end{Bmatrix}}(\bar{r}) \overset{r \to \infty}{\sim}$$

$$- d\phi' \frac{e^{ikR}}{4\pi R} r' \sin \theta'_c \, e^{-ik\bar{r}' \cdot \hat{R}} \frac{\sin \phi_\ell}{|\sin \phi_\ell|} \left\{ \left[E_{i\phi'} \sin \theta_\ell \, 4P_2(\alpha, \phi_{o\ell}, kd) \right.\right.$$

$$\left.\left. + Z_o H_{i\phi'} \frac{4P_1(\alpha, \phi_{o\ell}, kd)}{\sin \alpha} \cos \phi_\ell \cos \theta_\ell \right] \begin{Bmatrix} \sigma \\ \tau \end{Bmatrix} \right.$$

$$\left. - Z_o H_{i\phi'} \frac{4P_1(\alpha, \phi_{o\ell}, kd)}{\sin \alpha} \sin \phi_\ell \begin{Bmatrix} \mu \\ \nu \end{Bmatrix} \right\} \quad . \tag{16a, b}$$

2.2.2 RADIAL CRACKS

For the radially directed cracks we take the local z-axis to be in the direction of the crack, from the center of the paraboloid outward, and the local y-axis to be the inwardly directed normal to the paraboloid. Thus

$$\hat{y}_\ell = - \cos \frac{\theta'}{2} \hat{r}' + \sin \frac{\theta'}{2} \hat{\theta}' \quad , \tag{17a}$$

$$\hat{z}_\ell = \sin \frac{\theta'}{2} \hat{r}' + \cos \frac{\theta'}{2} \hat{\theta}' \quad , \tag{17b}$$

and

$$\hat{x}_\ell = \hat{y}_\ell \times \hat{z}_\ell = -\hat{\phi}' \quad . \tag{17c}$$

The cosine of $\theta_{o\ell}$, the local elevation angle of the direction from which the illuminating plane wave is coming, is given by

$$\cos \theta_{o\ell} = \hat{z}_\ell \cdot -\hat{r}' = -\sin \frac{\theta'}{2} \quad , \tag{18a}$$

from which we obtain

$$\sin \theta_{o\ell} = \cos \frac{\theta'}{2} \quad . \tag{18b}$$

The trigonometric functions of $\phi_{o\ell}$, the angle between $\hat{x}_\ell$ and the projection of $-\bar{r}'$ on the $x_\ell y_\ell$-plane are

$$\cos \phi_{o\ell} = -\hat{r}' \cdot \hat{x}_\ell / \sin \theta_{o\ell} = 0 \quad , \tag{19a}$$

and

$$\sin \phi_{o\ell} = -\hat{r}' \cdot \hat{y}_\ell / \sin \theta_{o\ell} = 1 \quad . \tag{19b}$$

For the cosine and sine of θ_ℓ, the angle between $\hat{z}_\ell$ and the ray from the point on the crack to the far field point, we have

$$\cos \theta_\ell = \hat{z}_\ell \cdot \hat{r}_\ell = \hat{z}_\ell \cdot \hat{R}$$

$$= \sin \theta \cos \frac{\theta'}{2} \cos (\phi'_c - \phi) - \cos \theta \sin \frac{\theta'}{2} \quad , \tag{20a}$$

and

$$\sin \theta_\ell = + (1 - \cos^2 \theta_\ell)^{1/2} \quad , \tag{20b}$$

while for the local field-point azimuth angle ϕ_ℓ,

$$\cos \phi_\ell = \hat{r}_\ell \cdot \hat{x}_\ell / \sin \theta_\ell = \hat{R} \cdot \hat{x}_\ell / \sin \theta_\ell$$

$$= \sin \theta \sin (\phi'_c - \phi) / \sin \theta_\ell \quad , \tag{21a}$$

and

$$\sin \phi_\ell = \hat{r}_\ell \cdot \hat{y}_\ell / \sin \theta_\ell = \hat{R} \cdot \hat{y}_\ell / \sin \theta_\ell$$

$$= - \left[\sin \theta \sin \frac{\theta'}{2} \cos (\phi'_c - \phi) + \cos \theta \cos \frac{\theta'}{2} \right] \Big/ \sin \theta_\ell \quad . \tag{21b}$$

From (18b), (20b), and (21a),

$$\cos\alpha \equiv \frac{\sin\theta_\ell \cos\phi_\ell}{\sin\theta_{o\ell}} = \frac{\sin\theta \sin(\phi'_c - \phi)}{\cos\frac{\theta'}{2}} \tag{22}$$

Showing that $|\cos\alpha| < 1$ for observation directions within the allowable forward cone is straightforward† (see p. 6). Then

$$\sin\alpha = (1 - \cos^2\alpha)^{1/2}$$

with the sign of $\sin\alpha$ determined in the same way as that for the azimuthal cracks (see p. 9).

---

† The magnitude of $\cos\alpha$ is bounded by $\sin\theta/\cos(\theta'/2)$. The minimum value of $\cos(\theta'/2)$ occurs for points on the reflector rim. For these points the maximum value of $\sin\theta$ occurs for the minimum allowable value of θ (recall that in our global coordinate system the z-axis is directed from the focus to the reflector center so that the forward direction is given by $\theta = \pi$) determined, as noted above, by the cones of observation angles formed by rays from the points on the cracks to the reflector rim. Let P be a point on a crack and consider the cone of rays from P to the reflector rim. If we let ψ be the angle between a ray and the forward direction, then ψ takes on its smallest value, ψ_{min}, for the ray to the nearest rim point in the plane determined by P and the z-axis. As P approaches the rim, ψ_{min} decreases. The limiting value of ψ_{min} is the maximum allowable value of $\pi - \theta$. This limiting value is given by the arc tangent of the negative of the slope of the paraboloid. Since the paraboloid is defined by the equation

$$\rho^2 = 4F(F - z) \quad ,$$

the negative of the slope is

$$-\frac{d\rho}{dz} = 2F/\rho \quad .$$

At the reflector rim $\rho = D/2$ so that

$$\lim_{\rho \to D/2} \psi_{min} = \tan^{-1}(4F/D) \quad .$$

Then

$$\cos\alpha \leq \frac{\sin\theta_{min}}{\cos\frac{\theta'_{max}}{2}} = \frac{4F/D}{4F/D} = 1$$

with strict inequality holding for observation directions for which $\theta > \pi - \tan^{-1}(4F/D)$. It is worth noting that within this forward cone of observation angles $\pi/2 \leq \phi_\ell \leq \pi$ so that $\sin\phi_\ell$ is positive and the factor $\sin\phi_\ell / |\sin\phi_\ell|$ which appears in (4) and (16a, b) equals +1. This can easily be seen by referring to the definitions of the local coordinates on p. 8 and p. 11, and can also be demonstrated analytically starting with (9b) or (21b) and using the fact that the maximum value of θ'_c in (9b) or θ' in (21b), the angle at the focus subtended by points on the reflector rim, is given by $2\cot^{-1}(4F/D)$.

A straightforward though algebraically lengthy procedure starting with

$$\hat{\theta}_\ell = \cos\theta_\ell \cos\phi_\ell \hat{x}_\ell + \cos\theta_\ell \sin\phi_\ell \hat{y}_\ell - \sin\theta_\ell \hat{z}_\ell$$

and

$$\hat{\phi}_\ell = -\sin\phi_\ell \hat{x}_\ell + \cos\phi_\ell \hat{y}_\ell$$

leads to expressions for the θ- and ϕ-components of $\hat{\theta}_\ell$ and $\hat{\phi}_\ell$:

$$\sigma = \hat{\theta}_\ell \cdot \hat{\theta}$$

$$= -\frac{\left[\cos\frac{\theta'}{2}\cos\theta\cos(\phi'_c - \phi) + \sin\frac{\theta'}{2}\sin\theta\right]}{\sin\theta_\ell} \tag{23a}$$

$$\tau = \hat{\theta}_\ell \cdot \hat{\phi}$$

$$= -\frac{\cos\frac{\theta'}{2}\sin(\phi'_c - \phi)}{\sin\theta_\ell} \tag{23b}$$

$$\mu = \hat{\phi}_\ell \cdot \hat{\theta}$$

$$= \frac{\left[\cos\frac{\theta'}{2}\sin(\phi'_c - \phi)\right]}{\sin\theta_\ell} \tag{23c}$$

and

$$\nu = \hat{\phi}_\ell \cdot \hat{\phi}$$

$$= -\frac{\left[\sin\frac{\theta'}{2}\sin\theta + \cos\frac{\theta'}{2}\cos\theta\cos(\phi'_c - \phi)\right]}{\sin\theta_\ell} \tag{23d}$$

The factor $\exp(ikr_\ell)/r_\ell$ is given by (13a), the same expression as that for the azimuthal gap with ϕ', of course, now fixed at the crack azimuthal angle ϕ'_c and θ' variable along the crack instead of θ' fixed at the crack elevation angle θ'_c and ϕ' variable as for the azimuthal crack. Finally, the differential length

$$dz'_\ell = r' \sec \frac{\theta'}{2}\, d\theta' \tag{24}$$

and the components of the incident electric and magnetic field in the z_ℓ direction are given by

$$E_{iz_\ell} = \overline{E}_i \cdot \left(\sin \frac{\theta'}{2}\, \hat{r}' + \cos \frac{\theta'}{2}\, \hat{\theta}'\right) \tag{25a}$$

and

$$H_{iz_\ell} = \overline{H}_i \cdot \left(\sin \frac{\theta'}{2}\, \hat{r}' + \cos \frac{\theta'}{2}\, \hat{\theta}'\right) \quad . \tag{25b}$$

Substituting explicit expressions for $\cos \theta_{o\ell}$, $\sin \theta_{o\ell}$, $\cos \phi_{o\ell}$, $\sin \phi_{o\ell}$, r_ℓ, and dz'_ℓ in (4) and taking the θ- and ϕ-components gives

$$dE \begin{matrix} \theta \\ \phi \end{matrix} (\overline{r}) \overset{r \to \infty}{\sim} - d\theta' \frac{e^{ikR}}{4\pi R} \frac{r'}{\cos^2 \frac{\theta'}{2}}\, e^{-ik\overline{r}' \cdot \hat{R}}$$

$$\cdot \left\{ \left[E_{iz_\ell} \frac{\sin \theta_\ell}{\cos \frac{\theta'}{2}}\, 4P_2\left(\alpha, \pi/2, kd \cos \frac{\theta'}{2}\right) \right.\right.$$

$$\left.\left. + Z_o H_{iz_\ell} \frac{4P_1\left(\alpha, \pi/2, kd \cos \frac{\theta'}{2}\right)}{\sin \alpha} \left(\cos \phi_\ell \cos \theta_\ell - \cos \alpha \sin \theta_\ell \tan \frac{\theta'}{2}\right) \right] \begin{Bmatrix} \sigma \\ \nu \end{Bmatrix} \right.$$

$$\left. - Z_o H_{iz_\ell} \frac{4P_1\left(\alpha, \pi/2, kd \cos \frac{\theta'}{2}\right)}{\sin \alpha} \sin \phi_\ell \begin{Bmatrix} \mu \\ \nu \end{Bmatrix} \right\} . \tag{26a, b}$$

2.3 Feed Illumination

The form of the feed illumination of the reflector is chosen, as in Part II, to be

$$\overline{E}_i = \frac{e^{ikr'}}{r'} \left[a(\theta') \cos \phi'\, \hat{\theta}' + d(\theta') \sin \phi'\, \hat{\phi}'\right] \tag{27a}$$

$$\overline{H}_i = \frac{e^{ikr'}}{Z_o r'} \left[a(\theta') \cos \phi'\, \hat{\phi}' - d(\theta') \sin \phi'\, \hat{\theta}'\right] \tag{27b}$$

so that the E-plane is the xz-plane and the H-plane is the yz-plane. For an x-directed electric dipole source,

$$a(\theta') = \cos\theta' \quad , \quad d(\theta') = -1 \quad , \tag{28}$$

while for a Huygens source with an x-directed electric dipole and a y-directed magnetic dipole,

$$a(\theta') = 1 + \cos\theta' \quad , \quad d(\theta') = -(1 + \cos\theta') \quad . \tag{29}$$

Thus $E_{i\phi'}$ and $H_{i\phi'}$ in (16a, b), for the components of the diffraction coefficient for an incremental length of an azimuthal crack, are

$$E_{i\phi'} = \frac{e^{ikr'}}{r'} d(\theta'_c) \sin\phi' = \frac{e^{ikr'}}{r'} d(\theta'_c)(\sin\phi\cos u + \cos\phi\sin u) \tag{30a}$$

and

$$H_{i\phi'} = \frac{e^{ikr'}}{r'} a(\theta'_c) \cos\phi' = \frac{e^{ikr'}}{r'} a(\theta'_c)(\cos\phi\cos u - \sin\phi\sin u) \tag{30b}$$

with

$$u \equiv \phi' - \phi \quad .$$

Substituting (30a) and (30b) in (16a, b) and replacing $d\phi'$ by du gives

$$\begin{aligned} dE^{\theta}_{\phi}(\bar{r}) \overset{r\to\infty}{\sim} & - du \frac{e^{ikR}}{4\pi R} \sin\theta'_c \, e^{ik(r' - \bar{r}'\cdot\hat{R})} \\ & \cdot \Bigg[d(\theta'_c)(\sin\phi\cos u + \cos\phi\sin u) \sin\theta_\ell \, 4P_2(\alpha, \phi_{o\ell}, kd) \{^{\sigma}_{\tau} \\ & + a(\theta'_c)(\cos\phi\cos u - \sin\phi\sin u) \frac{4P_1(\alpha, \phi_{o\ell}, kd)}{\sin\alpha} \Big(\cos\theta_\ell \cos\phi_\ell \{^{\sigma}_{\tau} \\ & - \sin\phi_\ell \{^{\mu}_{\nu} \Big) \Bigg] \quad . \end{aligned} \tag{31a, b}$$

For the radial cracks, (27a) and (27b) combined with (25a) and (25b) give

$$E_{iz_\ell} = \frac{e^{ikr'}}{r'} a(\theta') \cos \phi'_c \cos \frac{\theta'}{2} \tag{32a}$$

and

$$H_{iz_\ell} = -\frac{e^{ikr'}}{r'} d(\theta') \sin \phi'_c \cos \frac{\theta'}{2} \quad . \tag{32b}$$

Substituting (32a) and (32b) in (26a, b) we obtain for the θ- and ϕ-components of the electric field of an incremental length of a radial crack

$$dE_{d\begin{Bmatrix}\theta\\ \phi\end{Bmatrix}}(\bar{r}) \overset{r\to\infty}{\sim} -d\theta' \frac{e^{ikR}}{4\pi R} e^{ik(r' - \bar{r}'\cdot\hat{R})} \frac{1}{\cos^2 \frac{\theta'}{2}}$$

$$\cdot \left\{ a(\theta') \cos \phi'_c \sin \theta_\ell \, 4P_2\left(\alpha, \pi/2, kd \cos \frac{\theta'}{2}\right) \begin{Bmatrix}\sigma\\ \tau\end{Bmatrix} \right.$$

$$\left. - d(\theta') \sin \phi'_c \cos \frac{\theta'}{2} \frac{4P_1\left(\alpha, \pi/2, kd \cos \frac{\theta'}{2}\right)}{\sin \alpha} \right.$$

$$\left. \left[\left(\cos \phi_\ell \cos \theta_\ell - \cos \alpha \sin \theta_\ell \tan \frac{\theta'}{2} \right) \begin{Bmatrix}\sigma\\ \tau\end{Bmatrix} - \sin \phi_\ell \begin{Bmatrix}\mu\\ \nu\end{Bmatrix} \right] \right\} \quad . \tag{33a, b}$$

2.4 Integration of the Incremental Fields

Although it is possible to numerically integrate (31a, b) as they stand along an azimuthal crack forming a complete circle on the reflector surface, the integration can be substantially simplified by eliminating those parts of the integrands that are odd functions of u and hence vanish when integrated with respect to u from $-\pi$ to $+\pi$. [Note from (5c) that, in order to obtain the proper sign of the far field components, the integration must be performed in the negative u- or negative ϕ'-direction since this corresponds to integration in the positive local z-direction.] It is straightforward to show that all terms in $dE_{d\theta}(\bar{r})$ containing $\sin \phi$ and all terms in $dE_{d\phi}(\bar{r})$ containing $\cos \phi$ are odd functions of u so that

$$E_{d\theta}(\bar{R}) \overset{R\to\infty}{\sim} -\cos\phi \frac{e^{ikR}}{4\pi R} \sin\theta'_c \int_{\pi}^{-\pi} du\, e^{ik(r' - \bar{r}'\cdot\hat{R})}$$

$$\cdot \left[d(\theta'_c) \sin u \sin\theta_\ell \; 4P_2(\alpha, \phi_{o\ell}, kd)\sigma \right.$$

$$\left. + a(\theta'_c) \cos u \frac{4P_1(\alpha, \phi_{o\ell}, kd)}{\sin\alpha} (\cos\theta_\ell \cos\phi_\ell \, \sigma - \sin\phi_\ell \, \mu) \right] , \qquad (34a)$$

and

$$E_{d\phi}(\bar{R}) \overset{R\to\infty}{\sim} -\sin\phi \frac{e^{ikR}}{4\pi R} \sin\theta'_c \int_{\pi}^{-\pi} du\, e^{ik(r' - \bar{r}'\cdot\hat{R})}$$

$$\cdot \left[d(\theta'_c) \cos u \sin\theta_\ell \; 4P_2(\alpha, \phi_{o\ell}, kd)\tau \right.$$

$$\left. - a(\theta'_c) \sin u \frac{4P_1(\alpha, \phi_{o\ell}, kd)}{\sin\alpha} (\cos\theta_\ell \cos\phi_\ell \, \tau - \sin\phi_\ell \, \nu) \right] . \qquad (34b)$$

Thus $E_{d\theta}(R)$ and $E_{d\phi}(R)$ vary as $\cos\phi$ and $\sin\phi$ respectively. If the co- and cross-polarized field components, E_{co} and E_{cr}, are defined according to Ludwig's third definition[5]

$$E_{co} = E_\theta \cos\phi + E_\phi \sin\phi \qquad (35a)$$

and

$$E_{cr} = E_\theta \sin\phi - E_\phi \cos\phi , \qquad (35b)$$

then there is no cross-polarized field in either the E- or H-planes resulting from the integration of the incremental diffraction coefficients along a complete azimuthal crack.

For the radial cracks, no such simplification can be effected in general, and (33a, b) must be integrated as given along the radial cracks.

---

5. Ludwig, A.C. (1973) The definition of cross polarization, IEEE Trans. Antennas and Propagat, AP-21:116-119.

3. CALCULATIONS

In Section 3.1 we present the results of calculations performed to investigate the effects of cracks in the surface of a paraboloidal reflector antenna by numerically integrating the slit incremental diffraction coefficients along the cracks. The calculations were made on a CDC Cyber 860 computer using the IMSL program *DCADRE* with a relative error criterion of 10^{-9} to carry out the numerical integrations. The paraboloid itself was the same as that used in Part II: $D = 20\lambda$, $F = 8\lambda$. The feed is a Huygens source located at the focus with an x-directed ($\phi' = 0°$) electric dipole, and a y-directed ($\phi' = 90°$) magnetic dipole. The pattern of the antenna without cracks on the surface was calculated, as described in Part II, using the integral of the nonuniform current half-plane incremental diffraction coefficient along the rim of the reflector to enhance the accuracy of the PO reflector pattern. The basic configuration of cracks assumed here (see Figure 3) consists of an azimuthal crack halfway in angular measure from the center of the paraboloid—$\theta_c = \cot^{-1}(4F/D) = 32.01°$—and four radial cracks at the azimuth angles $\phi_c = 45°$, $135°$, $-45°$, and $-135°$ (i.e., two "diameter" cracks). The width of the cracks was taken to be 0.1λ. Co-polar patterns were calculated for the E- and H-planes, and cross-polar patterns for the $\phi = 45°$ plane. The range of θ for the patterns was from 180° (the forward direction) to 130°. As mentioned in Section 2 (see footnote, p. 13), the validity of the formulation is restricted to the forward cone of observation angles $\theta = [180°, 180° - \tan^{-1}(4F/D)] = [180°, 122.01°]$. In the calculations performed, terms of higher order than c^2 in the series for P_1 and P_2 [see (3a) and (3b)] were neglected. To facilitate interpretation of the results, calculations were also performed for the azimuth and diameter cracks separately. Additional patterns were obtained for the paraboloid with a single diameter crack defined by $\phi'_c = 0°$, $180°$; and with a single diameter crack defined by $\phi'_c = \pm 90°$.

In Section 3.2 we compare the amplitude of the far field due to the azimuthal crack, and to single diameter cracks defined by $\phi'_c = 0°$, $180°$; and by $\phi'_c = \pm 90°$, calculated by numerical integration of the slit incremental diffraction coefficients and by conventional asymptotic evaluation of the diffraction integrals.

3.1 Pattern Effects of Cracks Obtained by Numerical Integration of the Slit Incremental Diffraction Coefficients

Figures 4(a), 4(b) and 4(c), respectively, show the E- and H-plane co-polar amplitude patterns and the cross-polar amplitude pattern in the 45° plane. (The cross-polarized fields in the E- and H-plane are zero.) The corresponding phase patterns are shown in Figures 5(a), 5(b) and 5(c). The dashed-line patterns,

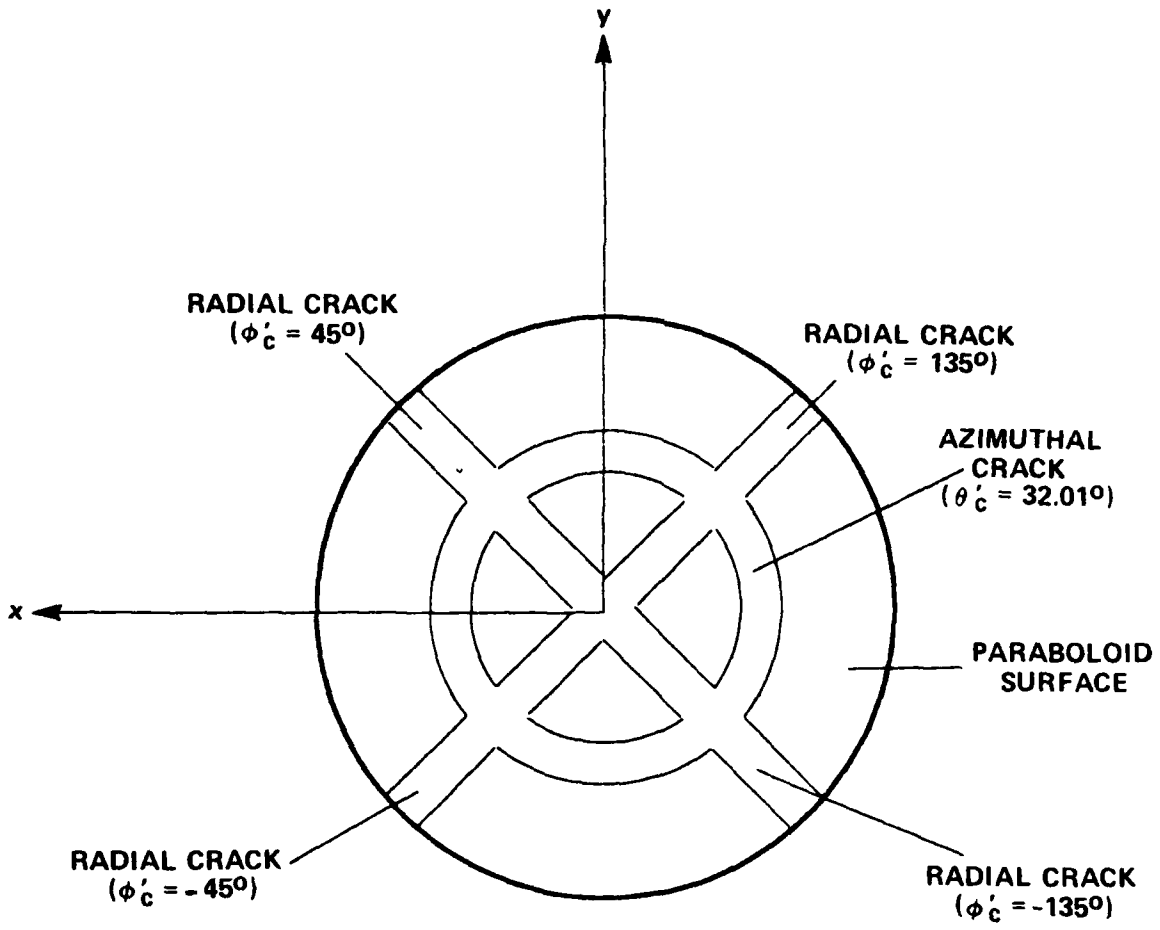

Figure 3. Basic Configuration of Cracks on the Surface of the Paraboloidal Reflector

given for reference in these figures, are those obtained for the paraboloid without cracks, while the solid-line patterns are those for the paraboloid with the basic crack configuration. All patterns are normalized to the value of the pattern of the paraboloid without cracks in the mainbeam direction of θ = 180° (amplitude = 35.0376 dB, phase = -90°). The primary Huygens-feed field is added to the secondary reflector field in all the patterns shown in this subsection.

It can be seen from Figures 4(a), 4(b), 5(a) and 5(b) that the presence of the cracks has a considerably greater effect on the E-plane patterns than on the H-plane patterns. This difference can be explained by first noting from Figures 6(a), 6(b), 7(a) and 7(b) for the amplitude and phase of the E- and H-plane patterns with only the two diameter cracks present (at ϕ'_c = 45°, -135°; and at ϕ'_c = 135°, -45°) and from Figures 8(a), 8(b), 9(a) and 9(b) for the patterns when only the azimuthal

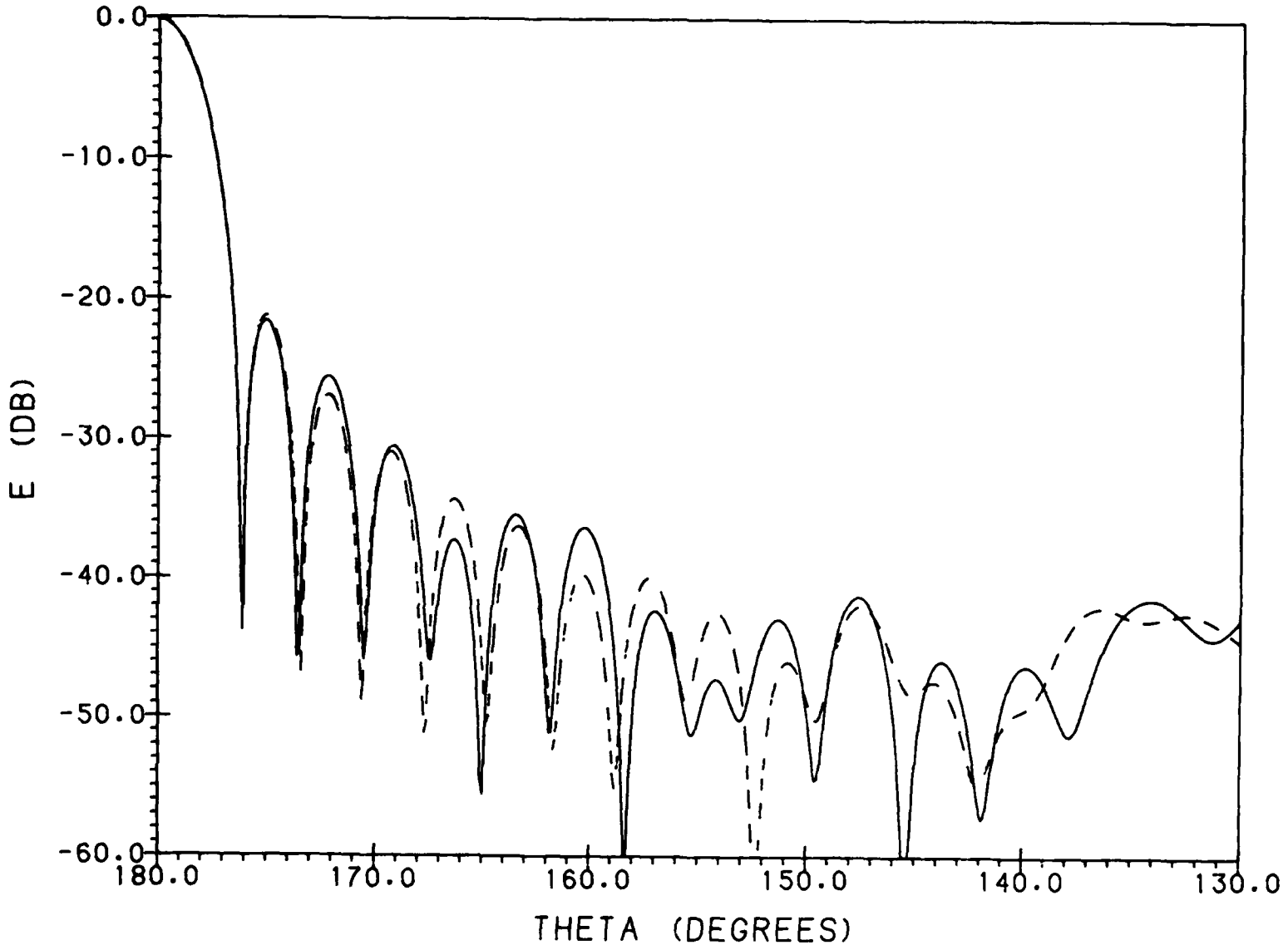

Figure 4a. Co-Polar E-Plane Amplitude Pattern of Paraboloid With Basic Crack Configuration (———) and of Paraboloid Without Cracks (------)

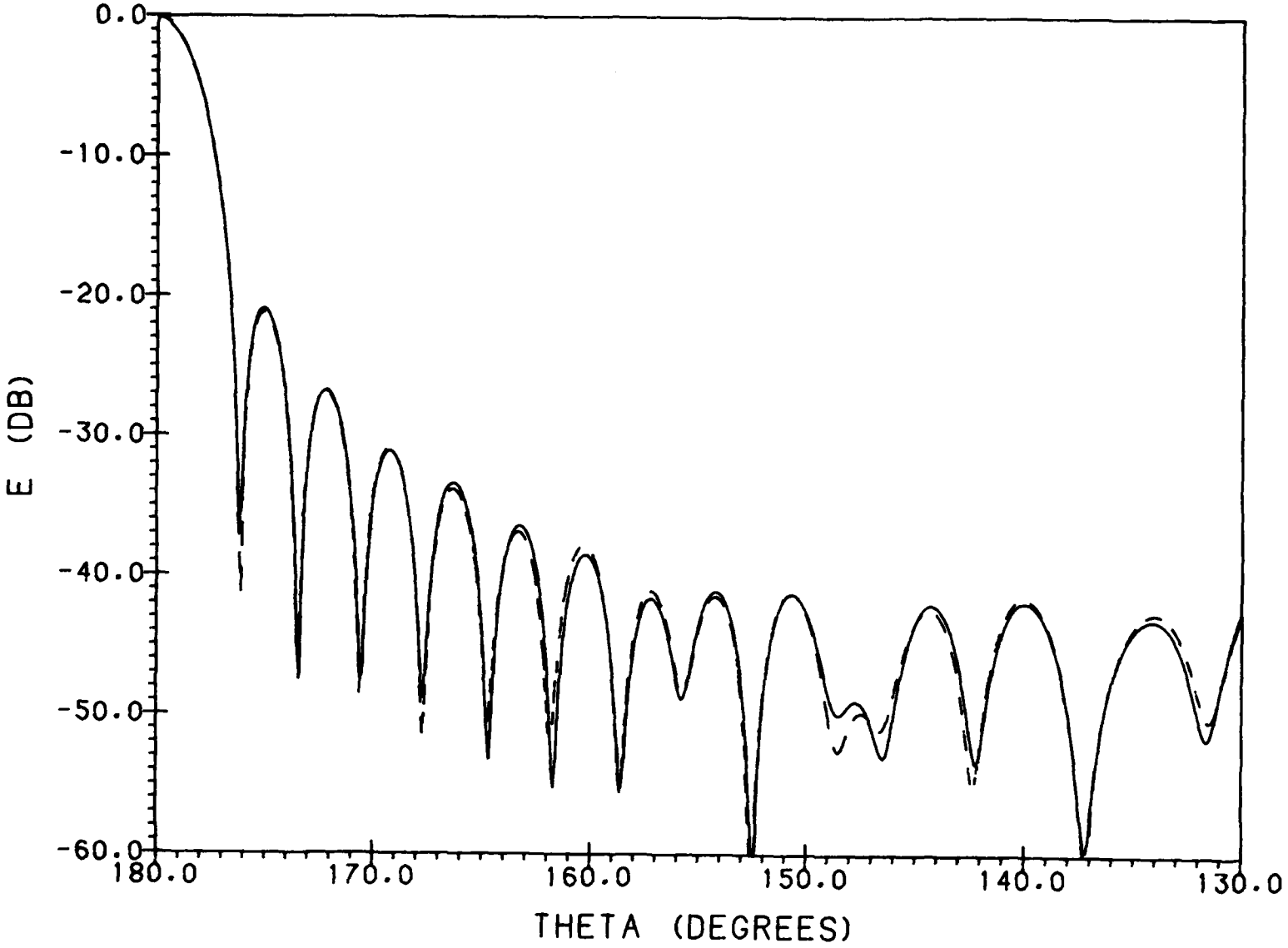

Figure 4b. Co-Polar H-Plane Amplitude Pattern of Paraboloid With Basic Crack Configuration (———) and of Paraboloid Without Cracks (------)

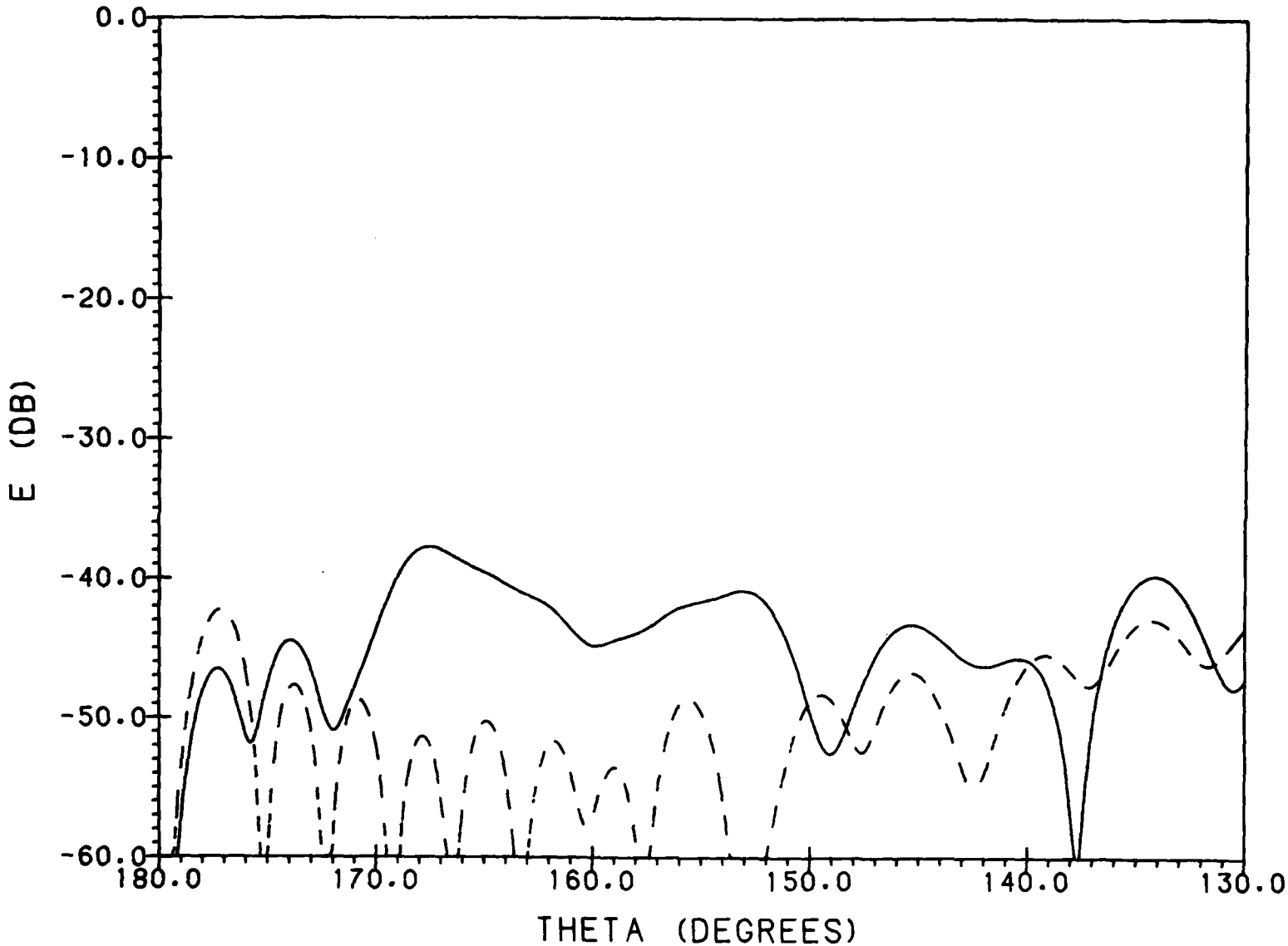

Figure 4c. Cross-Polar Amplitude Pattern in $\phi = 45°$ Plane of Paraboloid With Basic Crack Configuration (———) and of Paraboloid Without Cracks (------)

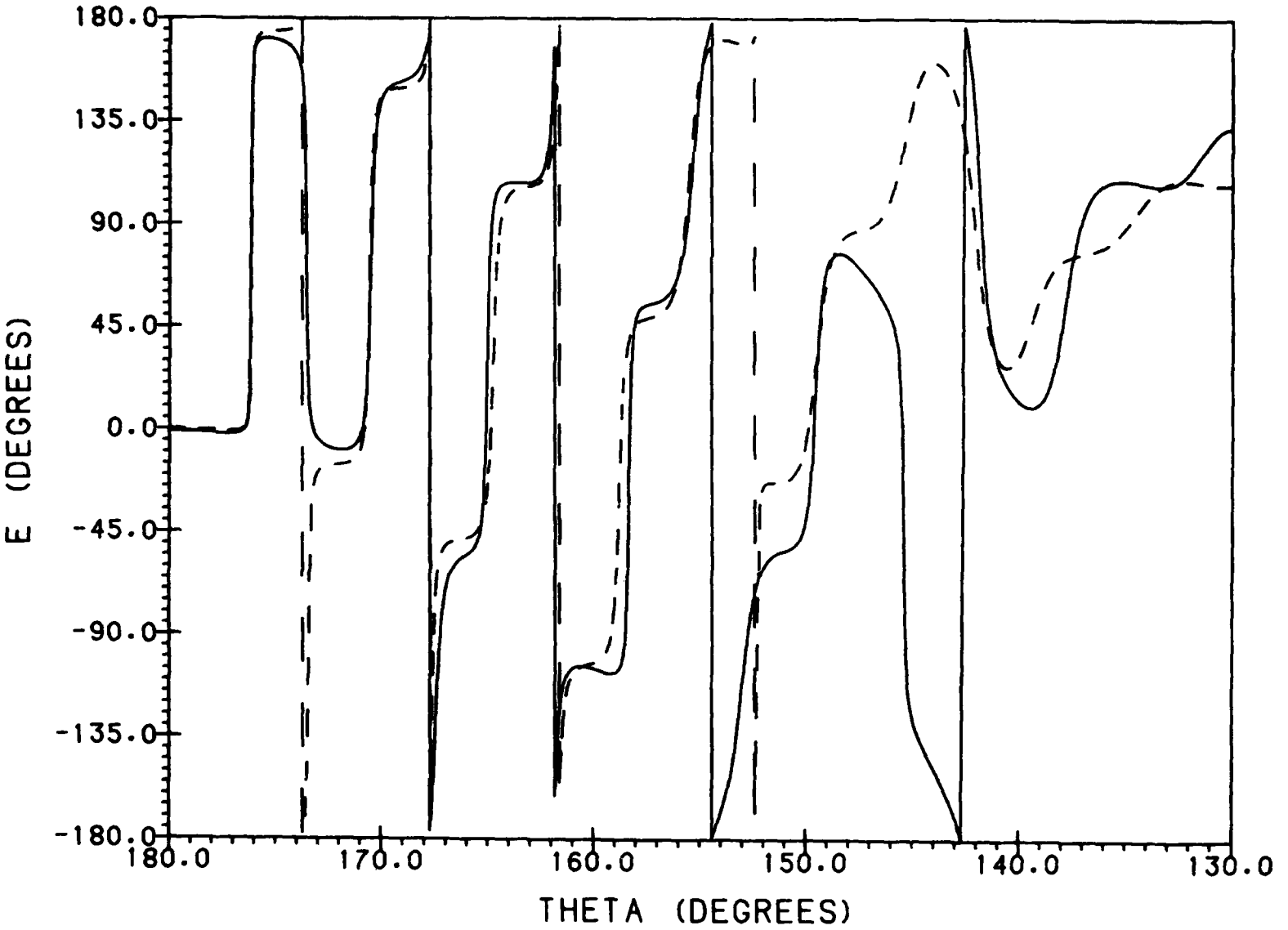

Figure 5a. Co-Polar E-Plane Phase Pattern of Paraboloid With Basic Crack Configuration (———) and of Paraboloid Without Cracks (------)

Figure 5b. Co-Polar H-Plane Phase Pattern of Paraboloid With Basic Crack Configuration (_____) and of Paraboloid Without Cracks (- - - - -)

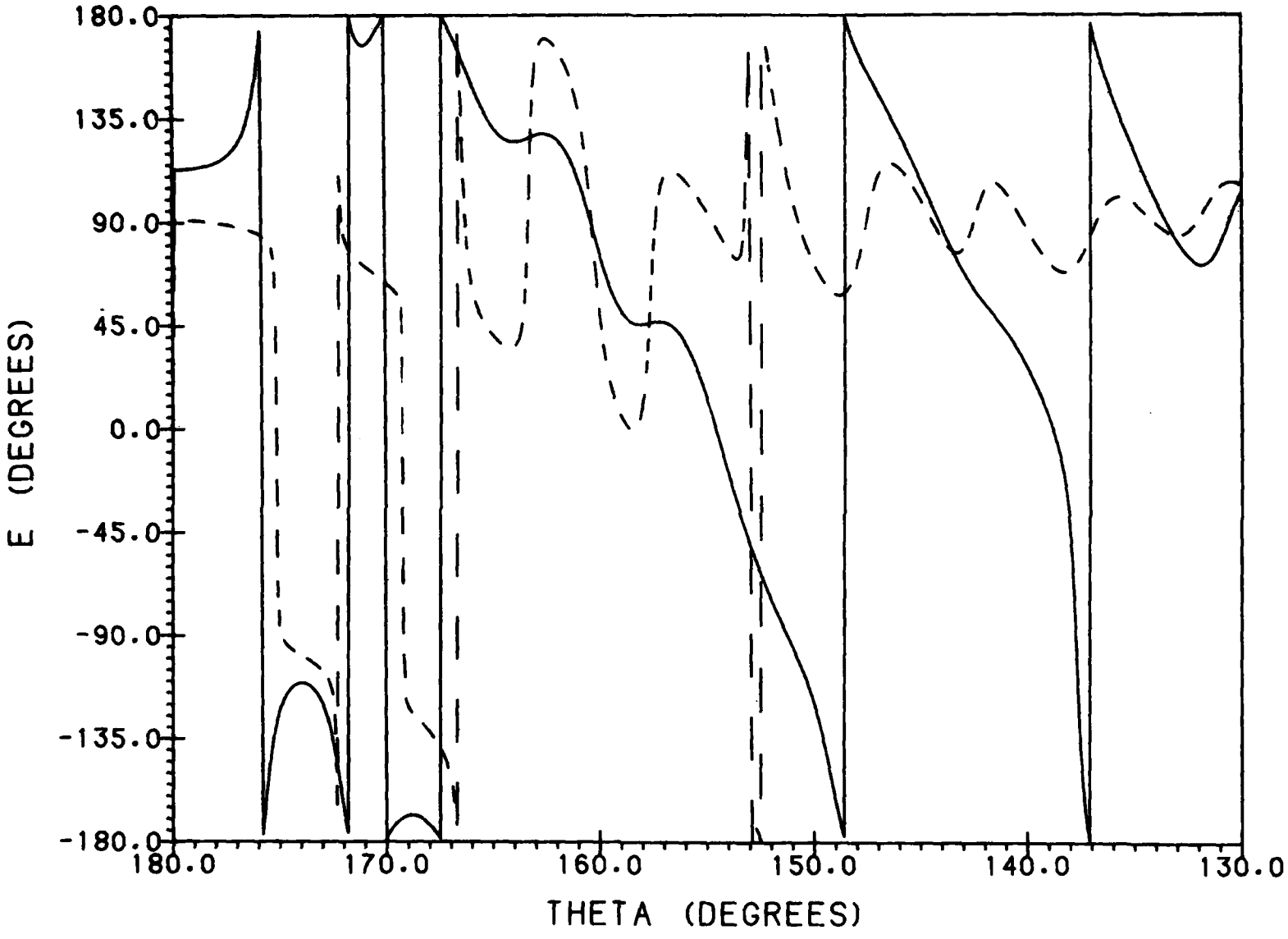

Figure 5c. Cross-Polar Phase Pattern in $\phi = 45^\circ$ Plane of Paraboloid With Crack Configuration (———) and of Paraboloid Without Cracks (------)

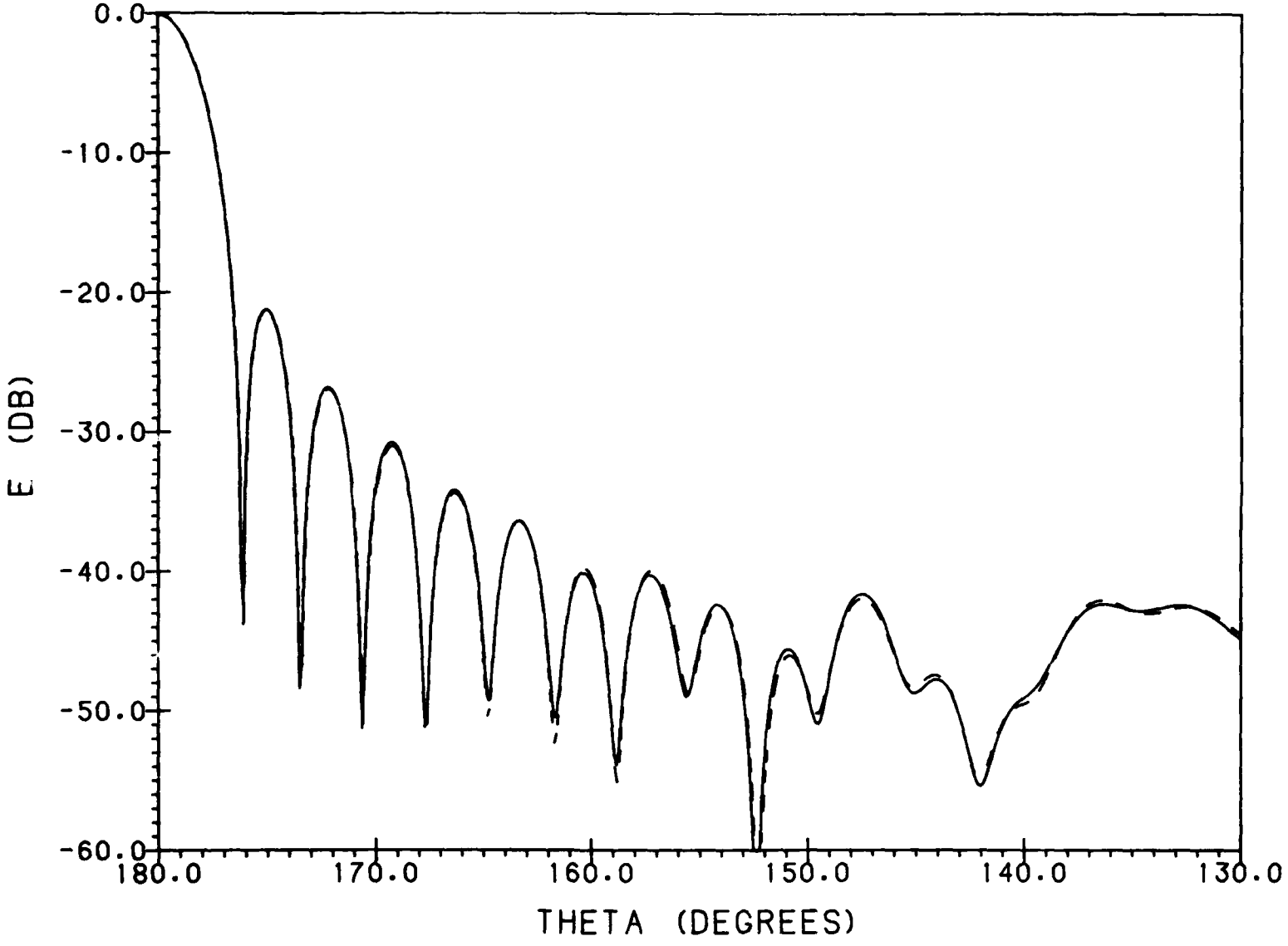

Figure 6a. Co-Polar E-Plane Amplitude Pattern of Paraboloid With Two Diameter Cracks Defined by $\phi_c' = 45°, -135°$, and by $\phi_c' = 135°, -45°$ (———) and of Paraboloid Without Cracks (------)

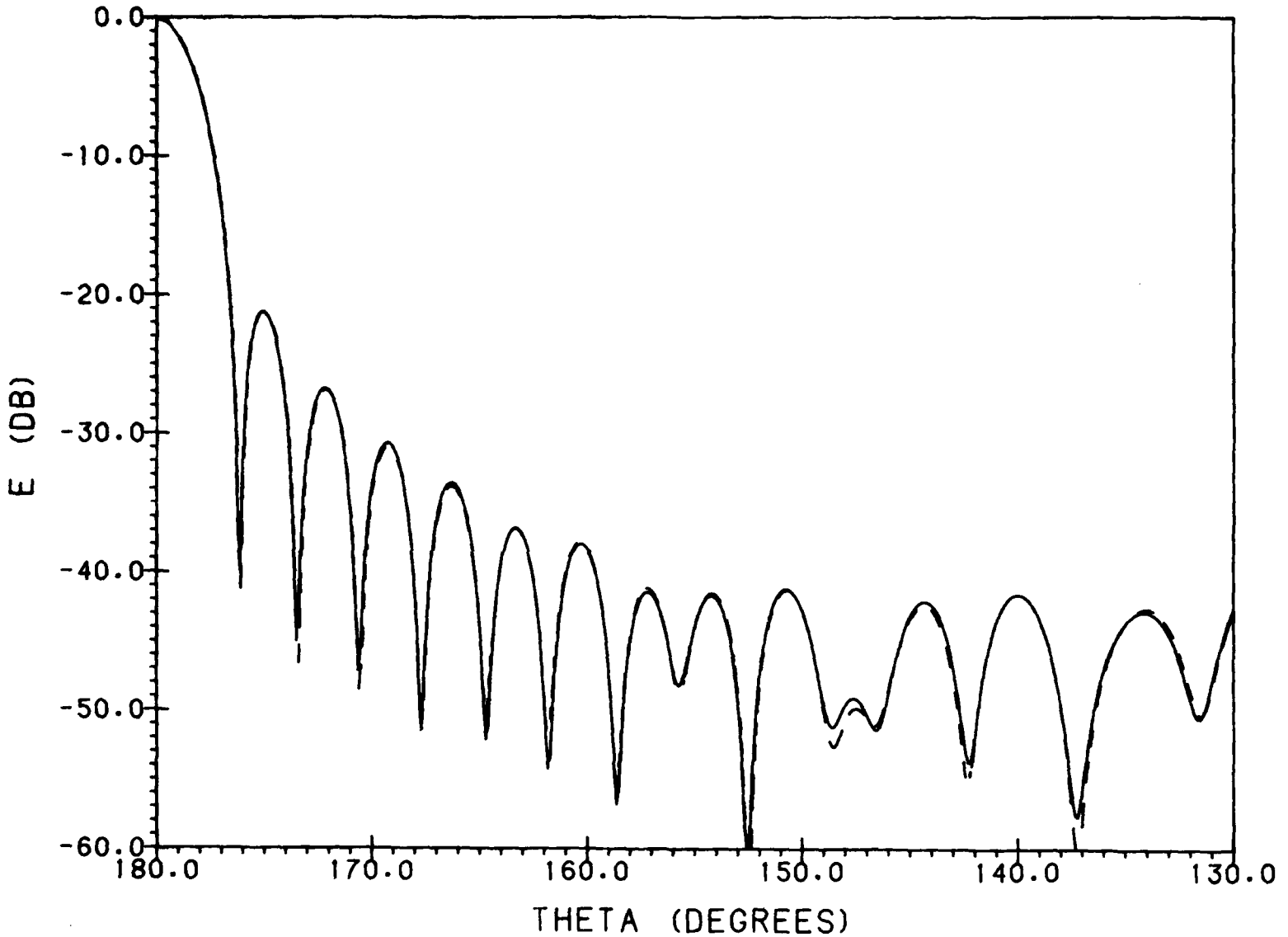

Figure 6b. Co-Polar H-Plane Amplitude Pattern of Paraboloid With Two Diameter Cracks Defined by $\phi_c' = 45°, -135°$, and by $\phi_c' = 135°, -45°$ (———) and of Paraboloid Without Cracks (------)

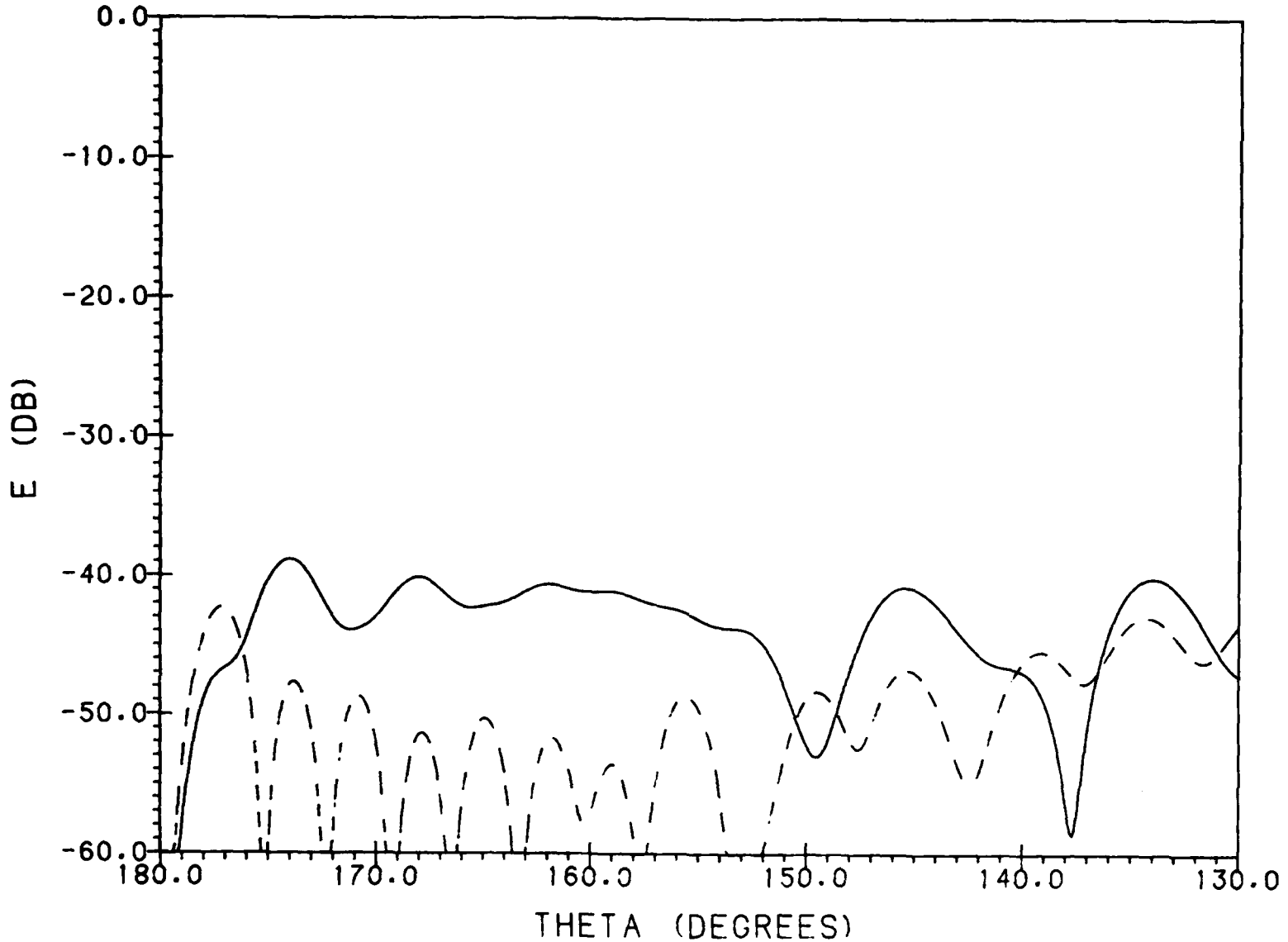

Figure 6c. Cross-Polar Amplitude Pattern in $\phi = 45°$ Plane of Paraboloid With Two Diameter Cracks Defined by $\phi'_c = 45°, -135°$, and by $\phi'_c = 135°, -45°$ (———) and of Paraboloid Without Cracks (------)

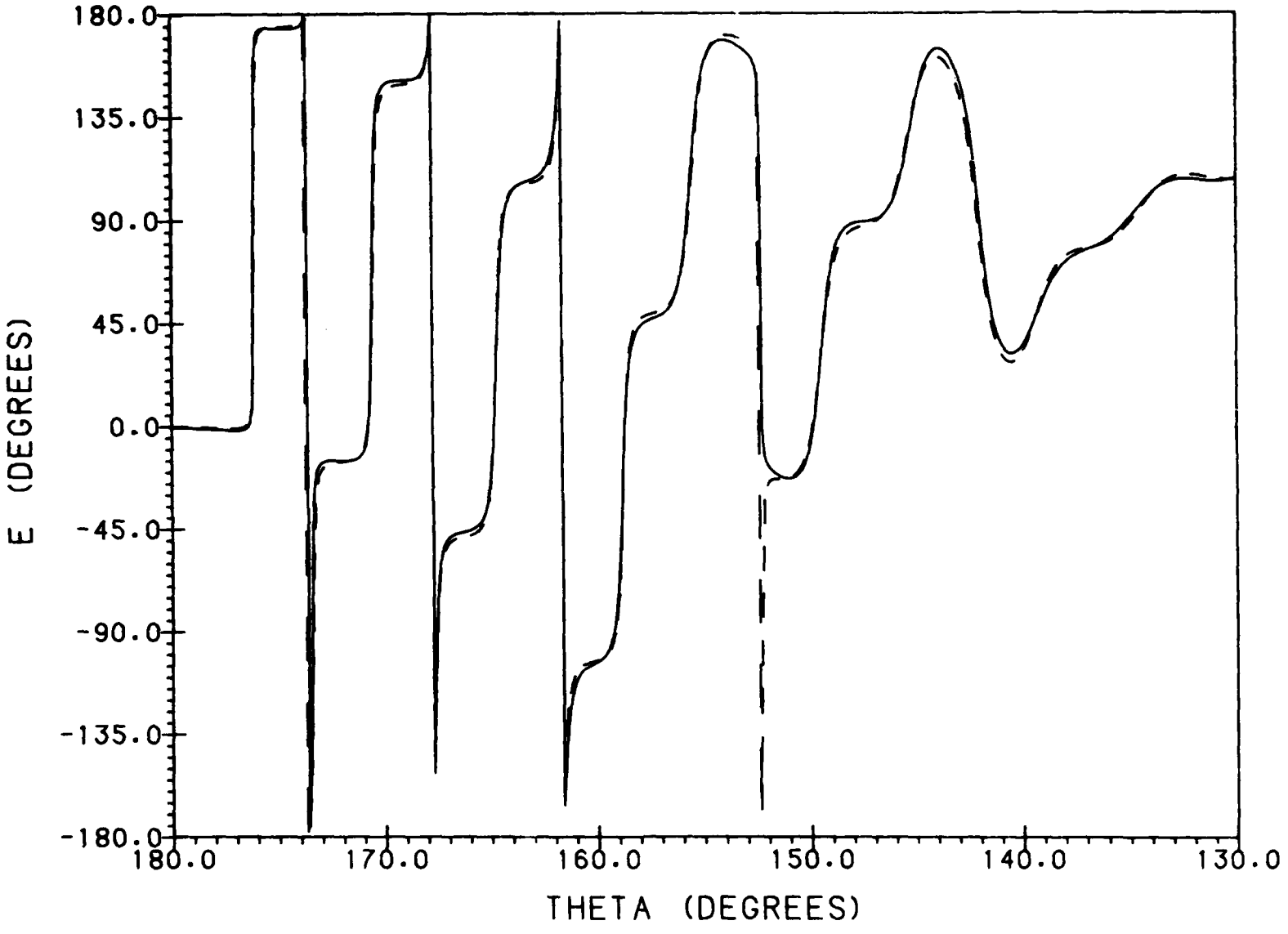

Figure 7a. Co-Polar E-Plane Phase Pattern of Paraboloid With Two Diameter Cracks Defined by $\phi_c' = 45^\circ, -135^\circ$, and by $\phi_c' = 135^\circ, -45^\circ$ (———) and of Paraboloid Without Cracks (------)

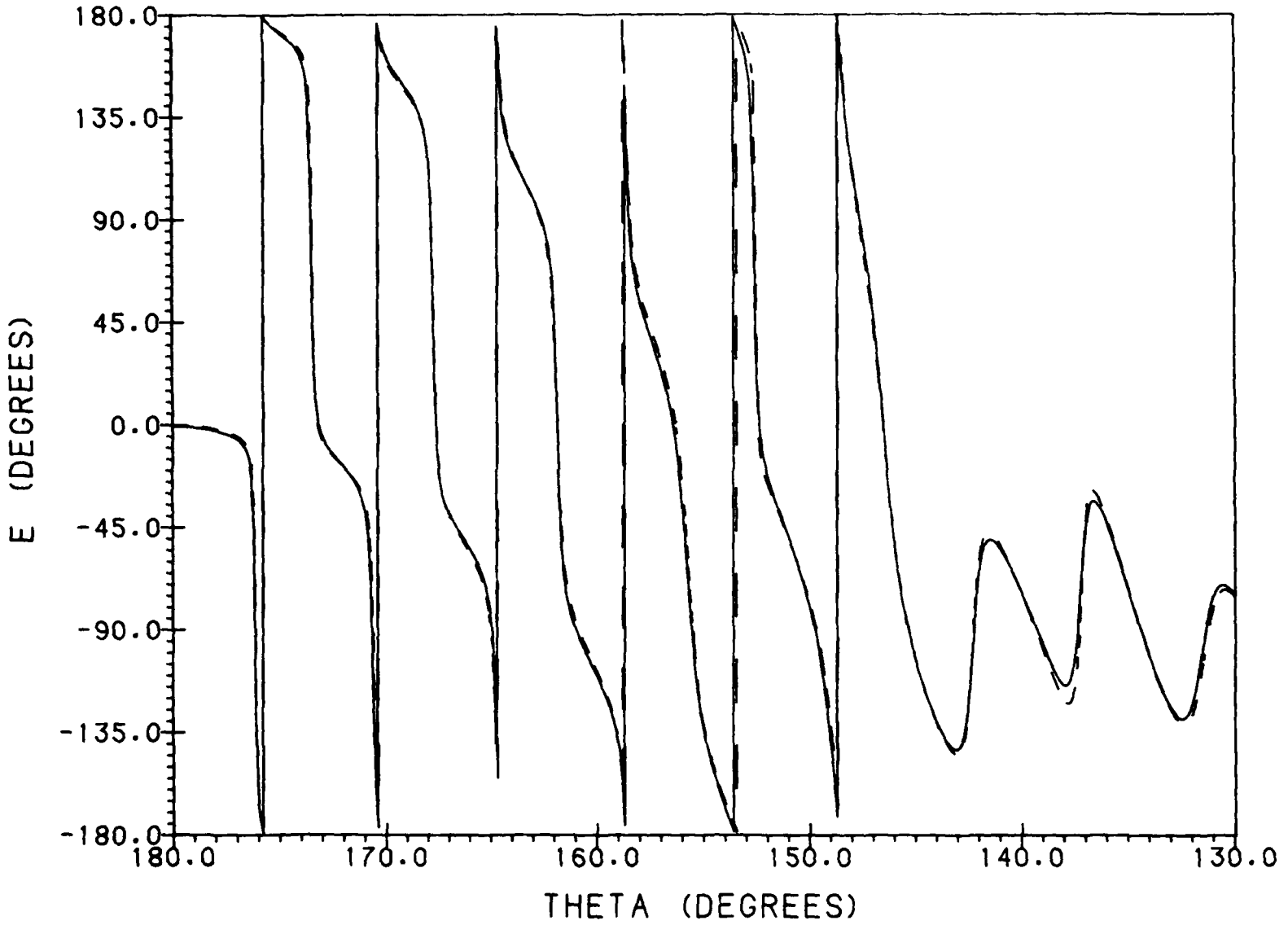

Figure 7b. Co-Polar H-Plane Phase Pattern of Paraboloid With Two Diameter Cracks Defined by $\phi_c' = 45°, -135°$, and by $\phi_c' = 135°, -45°$ (———) and of Paraboloid Without Cracks (------)

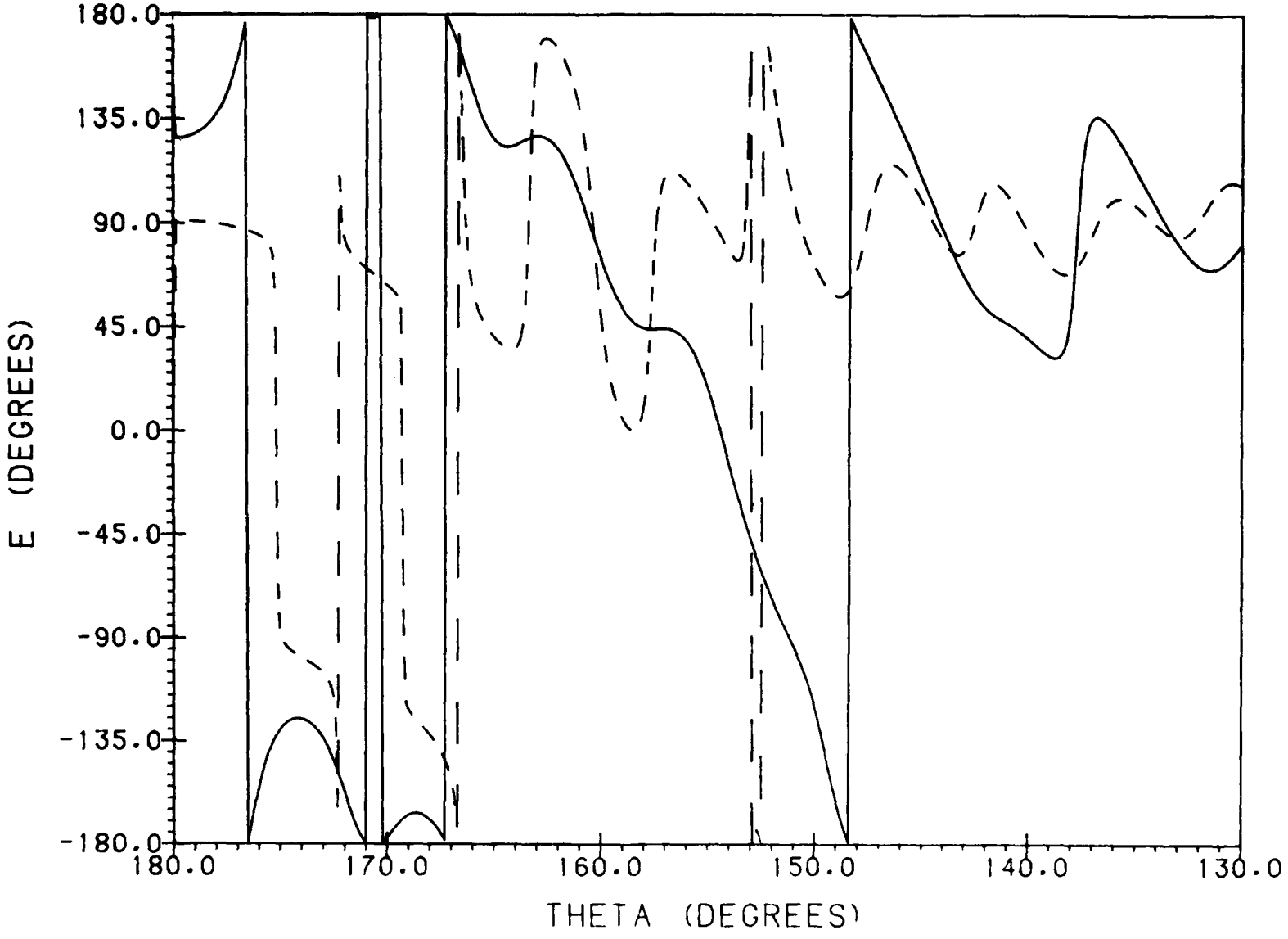

Figure 7c. Cross-Polar Phase Pattern in $\phi = 45^\circ$ Plane of Paraboloid With Two Diameter Cracks Defined by $\phi_c' = 45^\circ$, -135°, and by $\phi_c' = 135^\circ$, -45° (———) and of Paraboloid Without Cracks (------)

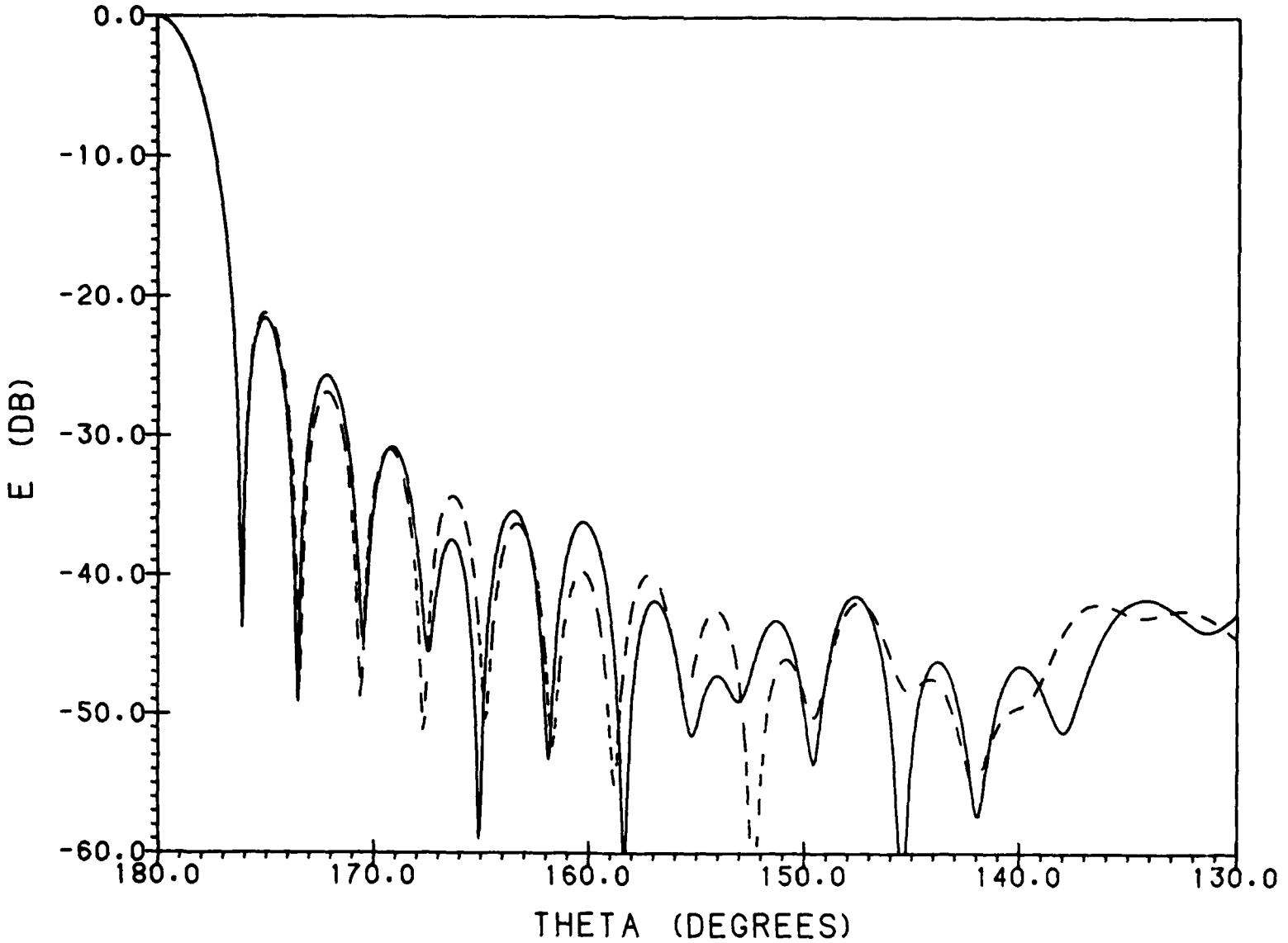

Figure 8a. Co-Polar E-Plane Amplitude Pattern of Paraboloid With Azimuthal Crack Defined by $\theta_c' = 32.01°$ (———) and of Paraboloid Without Cracks (------)

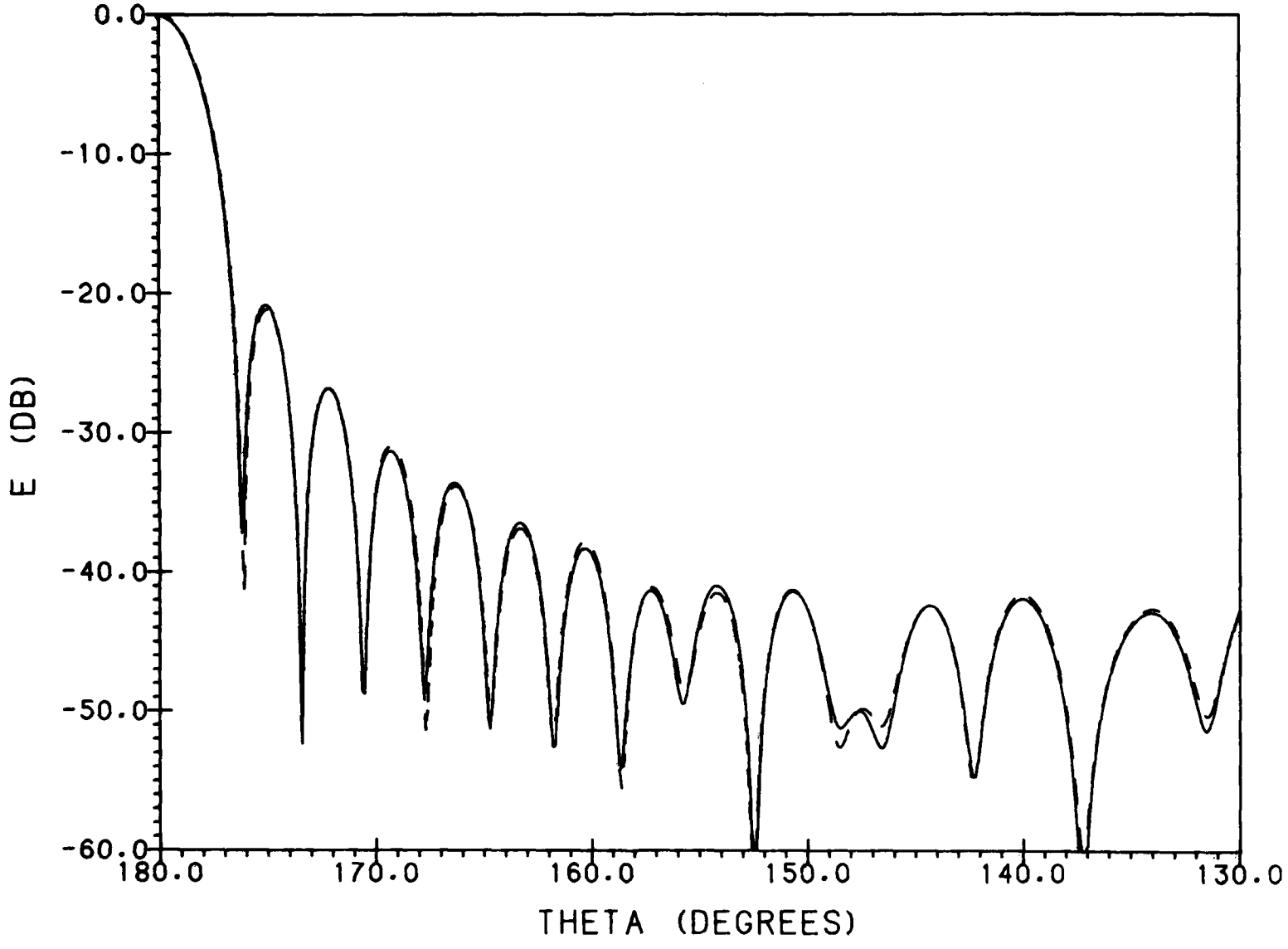

Figure 8b. Co-Polar H-Plane Amplitude Pattern of Paraboloid With Azimuthal Crack Defined by $\theta_c' = 32.01°$ (———) and of Paraboloid Without Cracks (------)

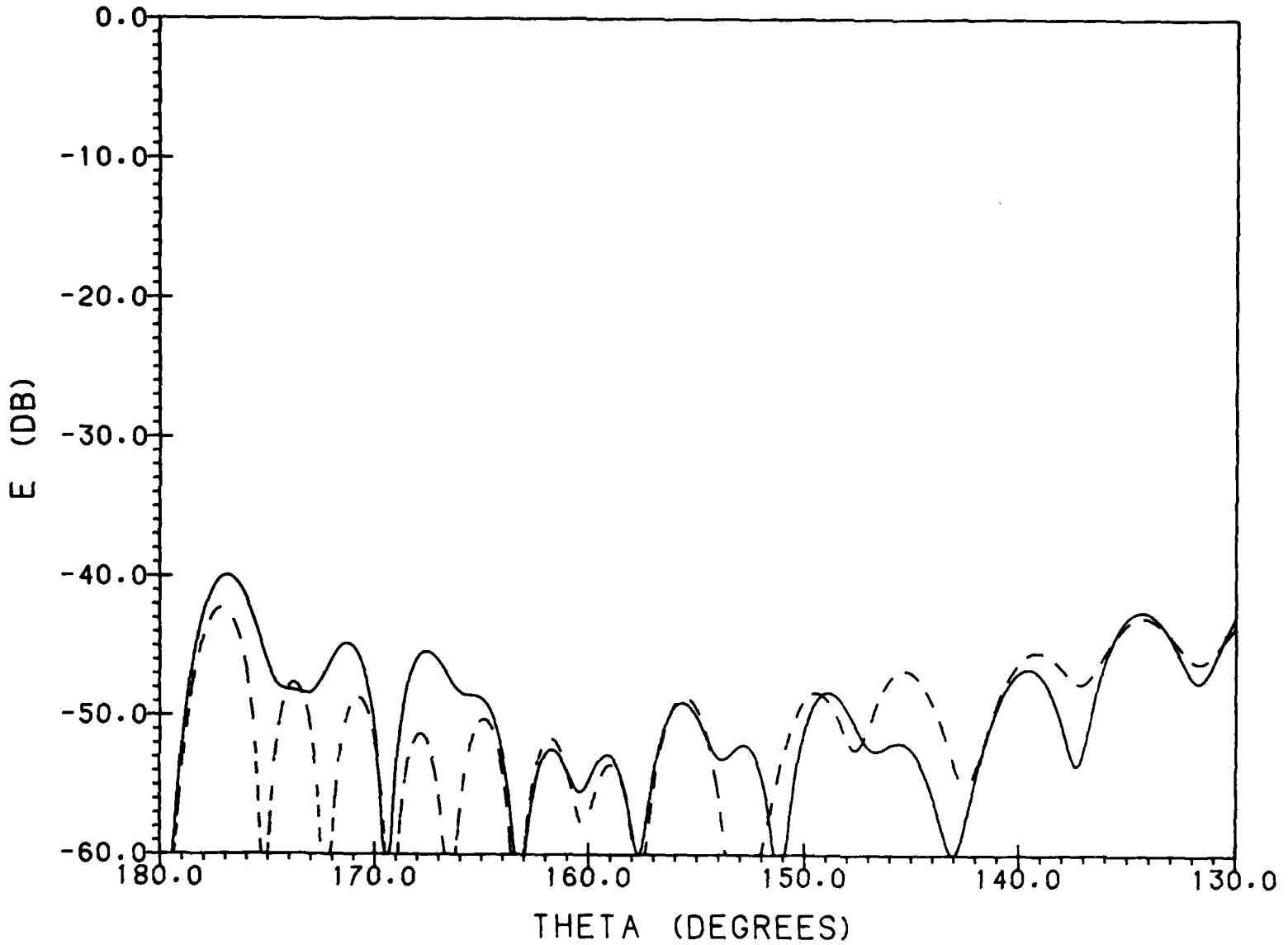

Figure 8c. Cross-Polar Amplitude Pattern in ϕ = 45° Plane of Paraboloid With Azimuthal Crack Defined by θ_c' = 32.01° (———) and of Paraboloid Without Cracks (------)

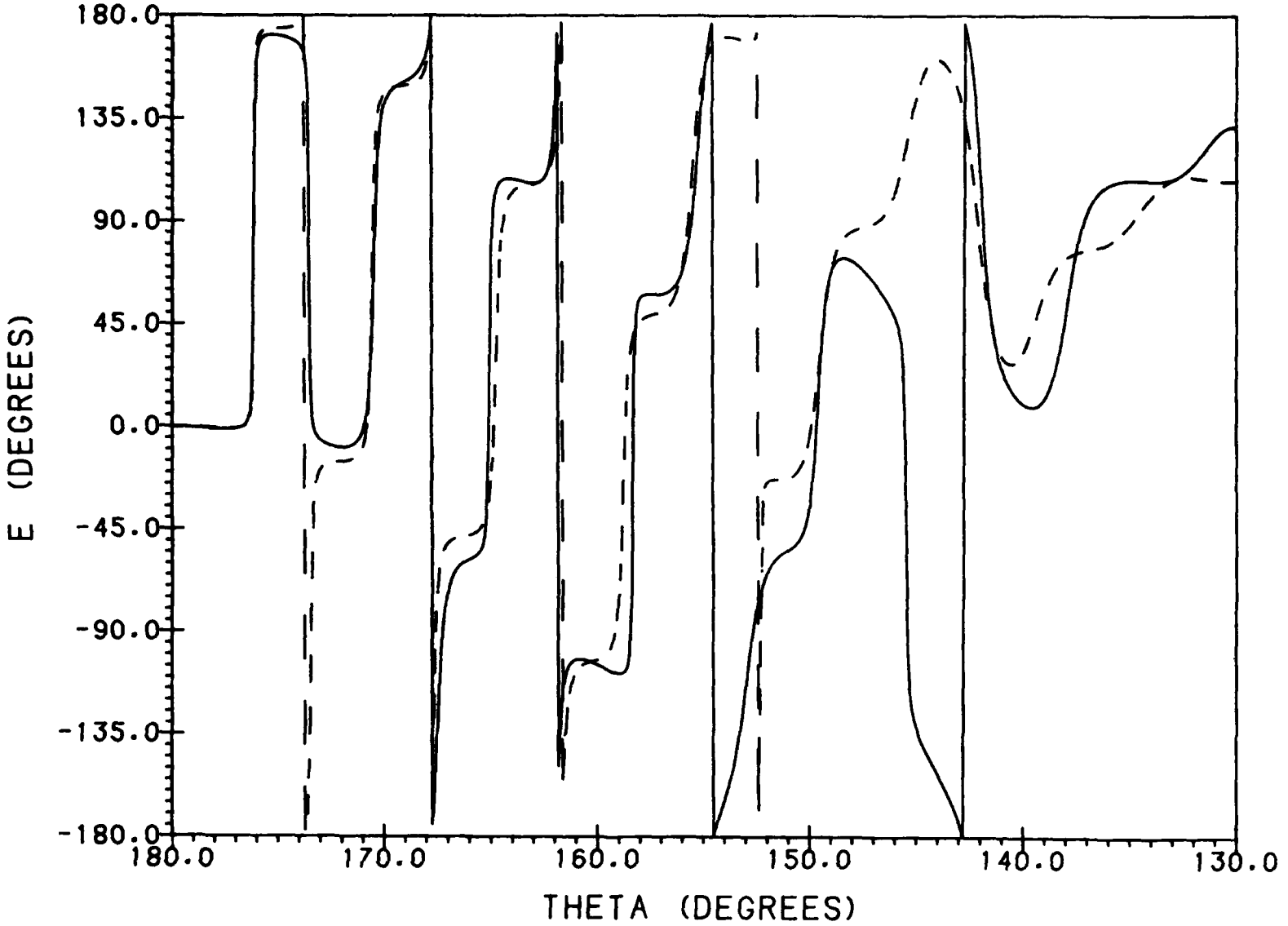

Figure 9a. Co-Polar E-Plane Phase Pattern of Paraboloid With Azimuthal Crack Defined by $\theta_c' = 32.01°$ (———) and of Paraboloid Without Cracks (------)

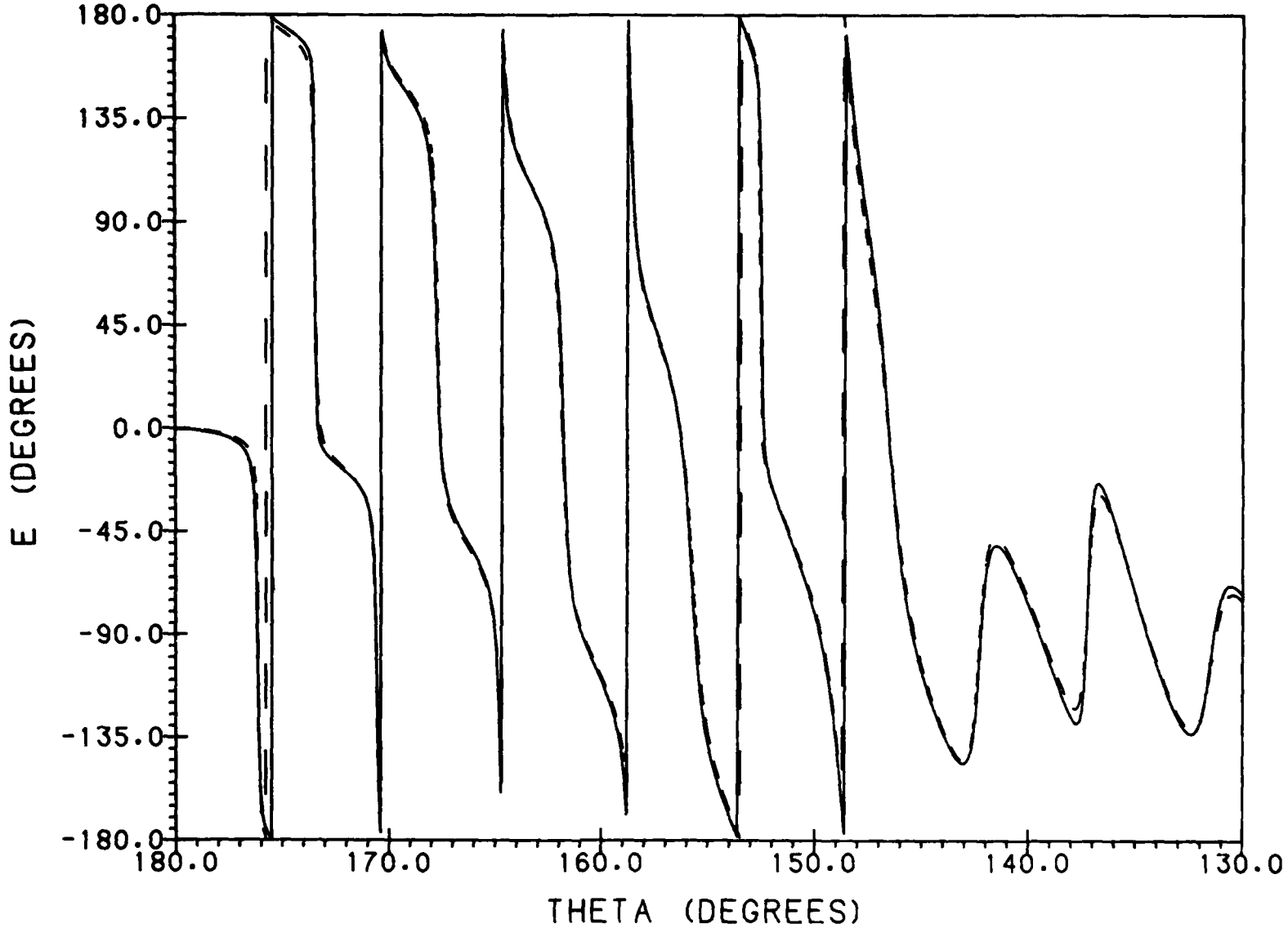

Figure 9b. Co-Polar H-Plane Phase Pattern of Paraboloid With Azimuthal Crack Defined by $\theta_c' = 32.01°$ (———) and of Paraboloid Without Cracks (------)

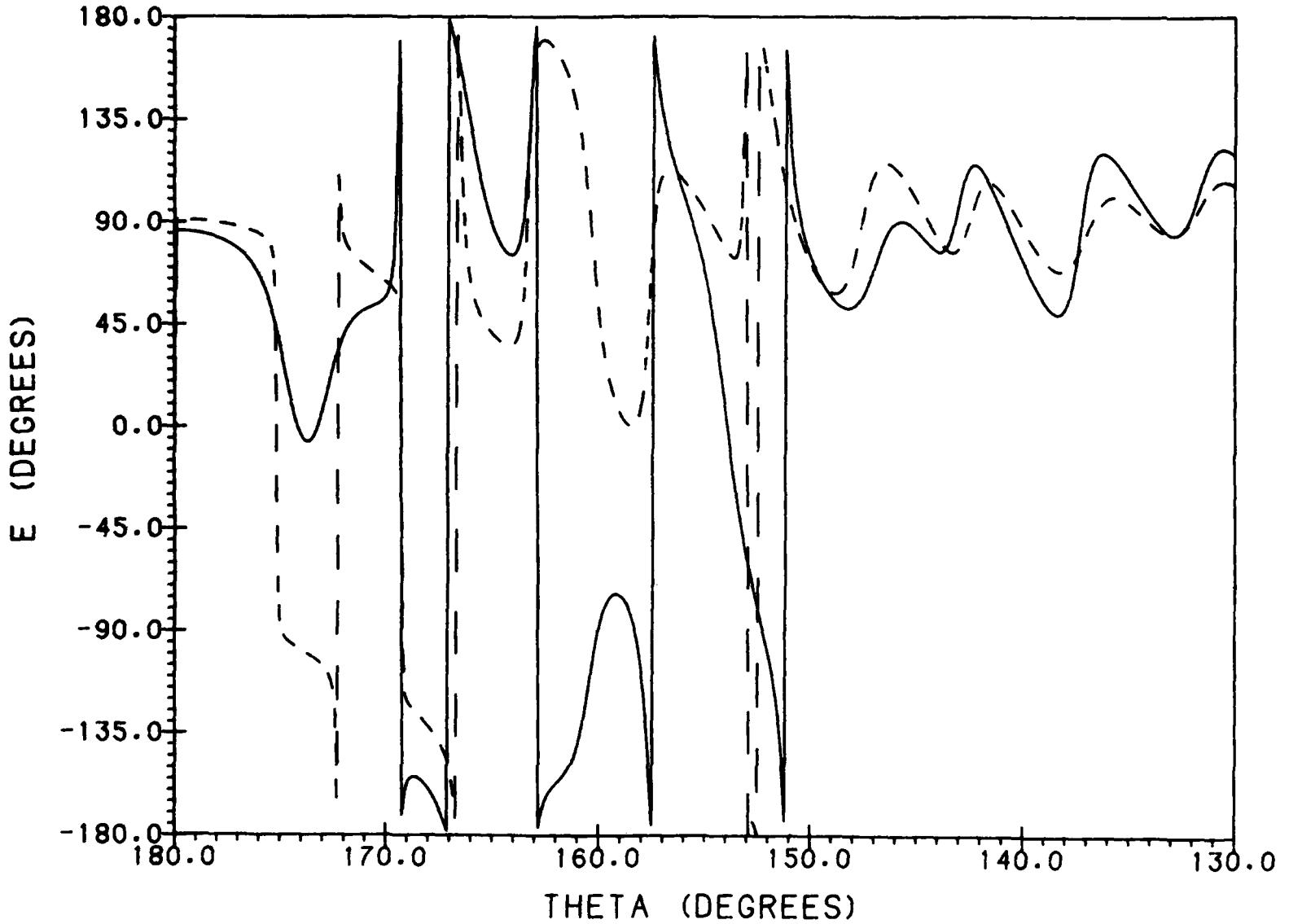

Figure 9c. Cross-Polar Phase Pattern in $\phi = 45°$ Plane of Paraboloid With Azimuthal Crack Defined by $\theta_c' = 32.01°$ (———) and of Paraboloid Without Cracks (------)

crack is present, that the effect of the basic crack configuration on the E- and H-plane patterns is due almost exclusively to the azimuthal crack. For the E-plane pattern, the contribution of the azimuthal crack to the diffracted field comes primarily from the two stationary phase points at 0° and 180°, whereas, for the H-plane pattern, the diffracted field is due in large part to the stationary phase points at ±90°. For a Huygens feed with an electric dipole oriented in the x-direction ($\phi' = 0°$), there is no component of the incident electric field in the direction of the azimuthal crack at $\phi' = 0°$ and 180°, and no component of the incident magnetic field in the crack direction at $\phi' = \pm 90°$, so that in (4) $E_{iz_\ell} = 0$ for differential crack elements at 0° and 180° and $H_{iz_\ell} = 0$ for crack elements at ±90°. (In other words, viewed in terms of the local coordinate system, the azimuthal crack at $\phi' = 0°$ and 180° is illuminated by a TE wave and at $\phi' = \pm 90°$ by a TM wave.) Also the local elevation angle $\theta_{o\ell}$ of the incident illumination is 90° for all points on the azimuthal crack [see (6)]; and θ_ℓ equals 90° for observation directions in the E-plane and differential crack elements at $\phi' = 0°$ and 180°, and for observation directions in the H-plane and differential crack elements at ±90°. Hence from (4) the incremental diffraction coefficient for the crack elements at $\phi' = 0°$ and 180° and observation directions in the E-plane is

$$\overline{\overline{dE}}_d \overset{r_\ell \to \infty}{\sim} dz'_\ell \frac{e^{ikr_\ell}}{4\pi r_\ell} Z_o H_{iz_\ell} 4P_1(\phi_\ell, \phi_{o\ell}, kd)\hat{\phi}_\ell$$

while for crack elements at $\phi' = \pm 90°$ and observation directions in the H-plane

$$\overline{\overline{dE}}_d \overset{r_\ell \to \infty}{\sim} -dz'_\ell \frac{e^{ikr_\ell}}{4\pi r_\ell} E_{iz_\ell} 4P_2(\phi_\ell, \phi_{o\ell}, kd)\hat{\theta}_\ell \quad .$$

Since, for a given θ, the values of r_ℓ, ϕ_ℓ, and $Z_o H_{iz_\ell}$ for $\phi = 0°$ and $\phi' = 0°$ and 180° equal, respectively, the values or r_ℓ, ϕ_ℓ, and E_{iz_ℓ} for $\phi = 90°$ and $\phi' = \pm 90°$; and, since $\phi_{o\ell}$ is a constant [see (7)], it follows that the ratios of the incremental fields in the E-plane diffracted by the crack elements at $\phi' = 0°$ and 180° to the incremental fields in the H-plane diffracted respectively from the crack elements at $\phi_\ell = 90°$ and -90° are

$$\frac{P_1(\phi_\ell, \phi_{o\ell}, kd)}{P_2(\phi_\ell, \phi_{o\ell}, kd)} \quad .$$

Referring to (3a) and (3b) and taking the leading terms in the series representations, however,

$$P_1 \approx \frac{1}{2} \frac{\pi}{\ell n \frac{kd}{8} + \gamma - i\frac{\pi}{2}}$$

and

$$P_2 \approx \frac{\pi}{16} \sin \phi_{o\ell} \sin \phi_{\ell} (kd)^2$$

so that, for the crack width $d = 0.1\lambda$, $|P_1/P_2| \geq 8.1 = 18$ dB. Thus, for the width of cracks we are considering, the effect on the E-plane pattern of azimuthal crack elements at 0° and 180° can be expected to be at least 18 dB larger than the effect on the H-plane of crack elements at ±90°. In brief, when the incident electric field is normal to the crack at the stationary phase point, the crack scatters much more than when it is parallel to the incident electric field.

A much more pronounced effect of the cracks on the antenna pattern than that on the co-polar E-plane pattern we have just discussed is the effect on the cross-polar pattern in the $\phi = 45°$ plane shown in Figures 4(c) and 5(c). Comparison with Figures 6(c) and 7(c), and Figures 8(c) and 9(c) shows that, here, the effect is due largely to the diameter cracks. A further comparison with Figures 10(c) and 11(c) for the amplitude and phase of the cross-polar pattern in the $\phi = 45°$ plane when only the diameter crack defined by $\phi_c' = 135°$ and -45° is present, and with Figures 12(c) and 13(c) for the patterns when only the diameter crack defined by $\phi_c' = 45°$ and -135° is present, shows that the effect is almost exclusively the result of diffraction from the diameter crack at $\phi_c' = 135°$, -45°, located in the plane perpendicular to the $\phi = 45°$ plane. A simple explanation of why the diameter crack defined by $\phi_c' = 135°$ and -45° dominates the diffraction effect shown in Figures 4(c) and 5(c) may be found by regarding the diameter cracks as line sources (neglecting the curvature of the paraboloid) which, because of the symmetry of the crack configuration with respect to the feed, are excited equally by the feed illumination. The diameter crack perpendicular to the $\phi = 45°$ plane has a broad pattern in this plane and hence a large effect on the pattern, whereas the diameter crack parallel to the $\phi = 45°$ plane has a narrow mainbeam and sidelobes that decay rapidly in this plane and hence a noticeable effect only in the forward direction.

Figures 14(a), 14(b) and 14(c) show the co-polar amplitude patterns in the E- and H-planes and the cross-polar amplitude pattern in the $\phi = 45°$ plane for the paraboloid antenna with a single diameter crack defined by $\phi_c' = 0°$ and 180°. The corresponding phase patterns are shown in Figures 15(a), 15(b) and 15(c). Figures 16(a), 16(b) and 16(c), and Figures 17(a), 17(b) and 17(c) show the patterns when the paraboloid has a single diameter crack defined by $\phi_c' = 90°$ and -90°.

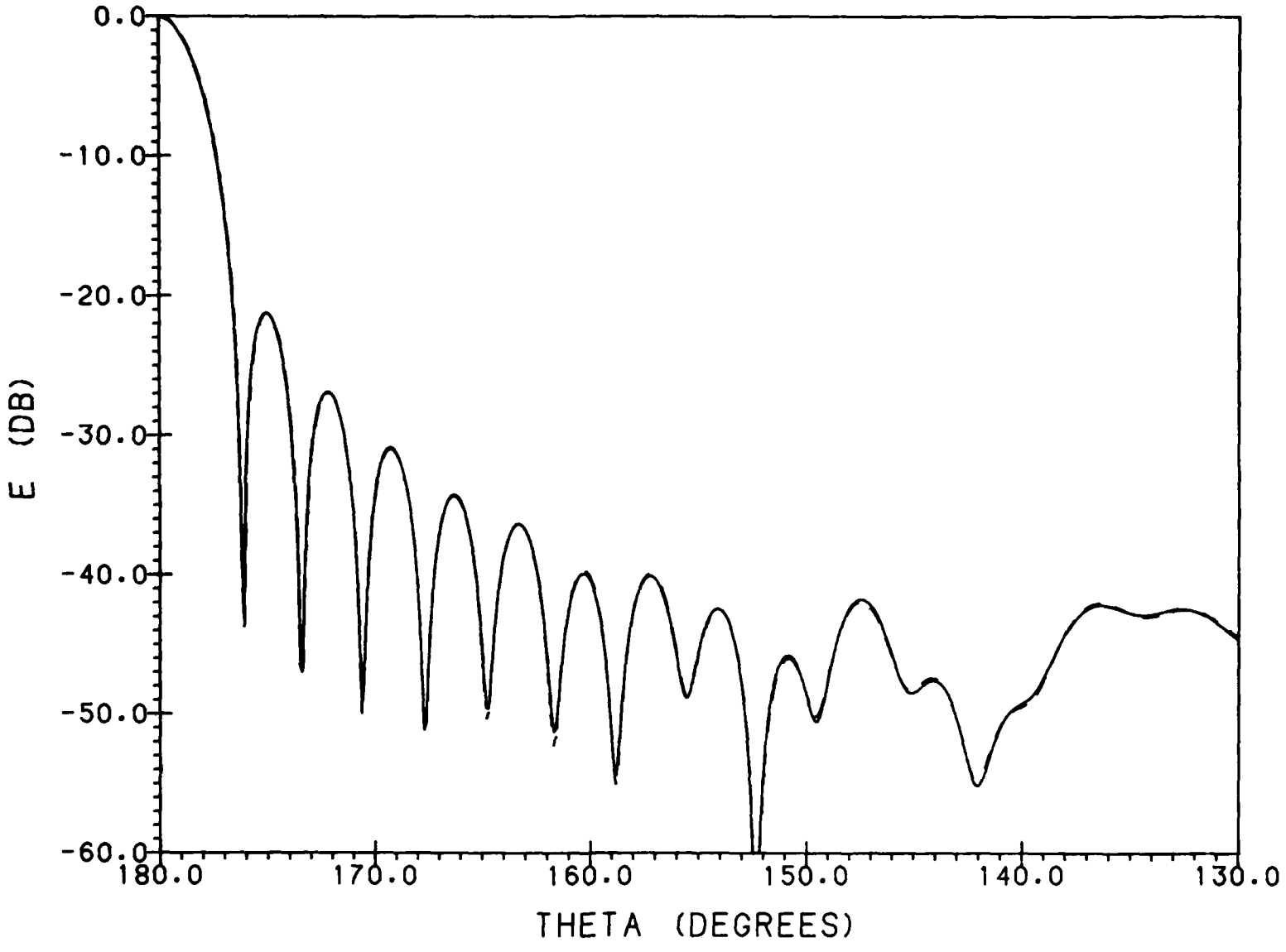

Figure 10a. Co-Polar E-Plane Amplitude Pattern of Paraboloid With a Single Diameter Crack Defined by $\phi_c' = 135°, -45°$ (———) and of Paraboloid Without Cracks (------)

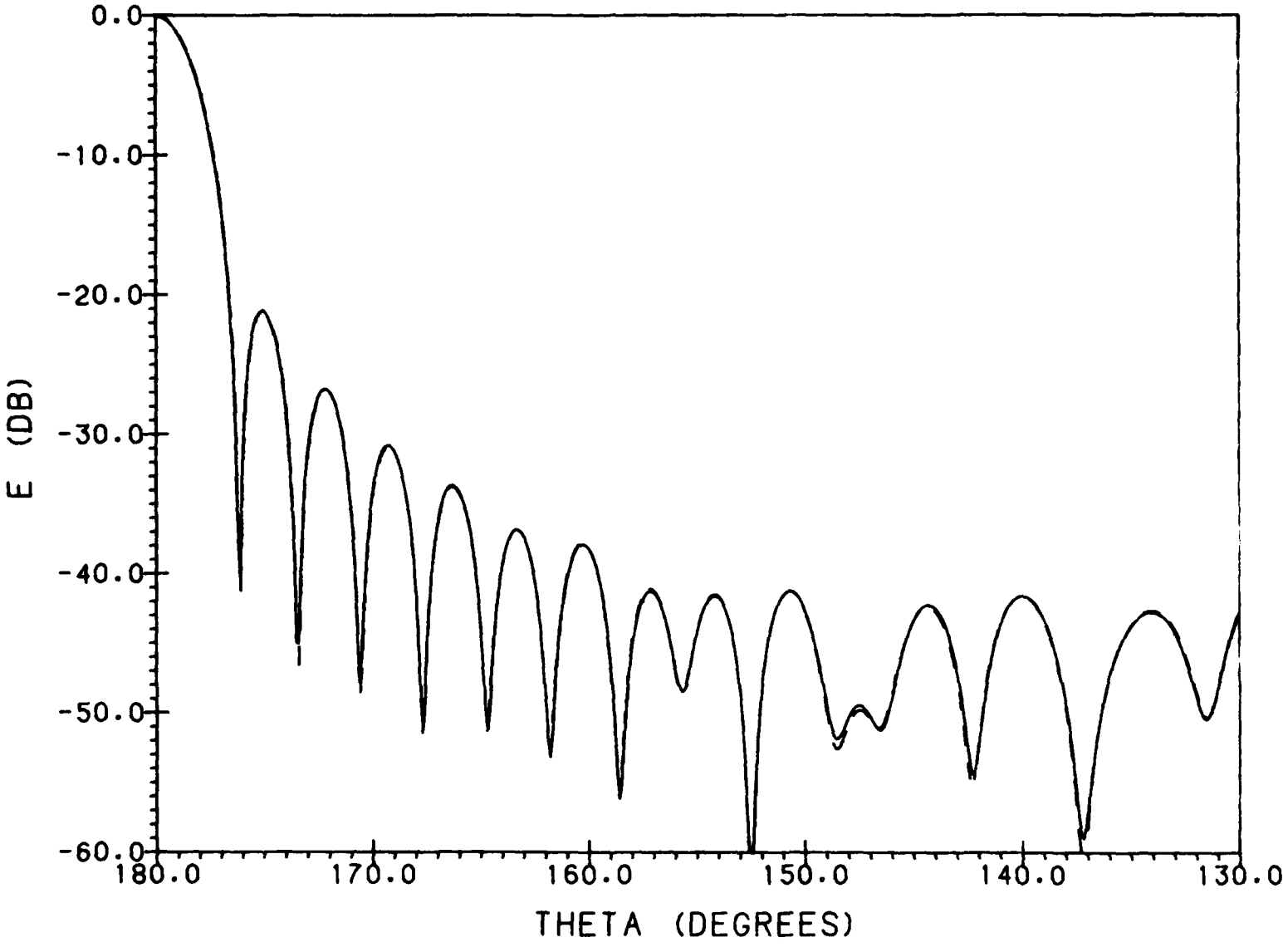

Figure 10b. Co-Polar H-Plane Amplitude Pattern of Paraboloid With a Single Diameter Crack Defined by $\phi_c' = 135°, -45°$ (———) and of Paraboloid Without Cracks (------)

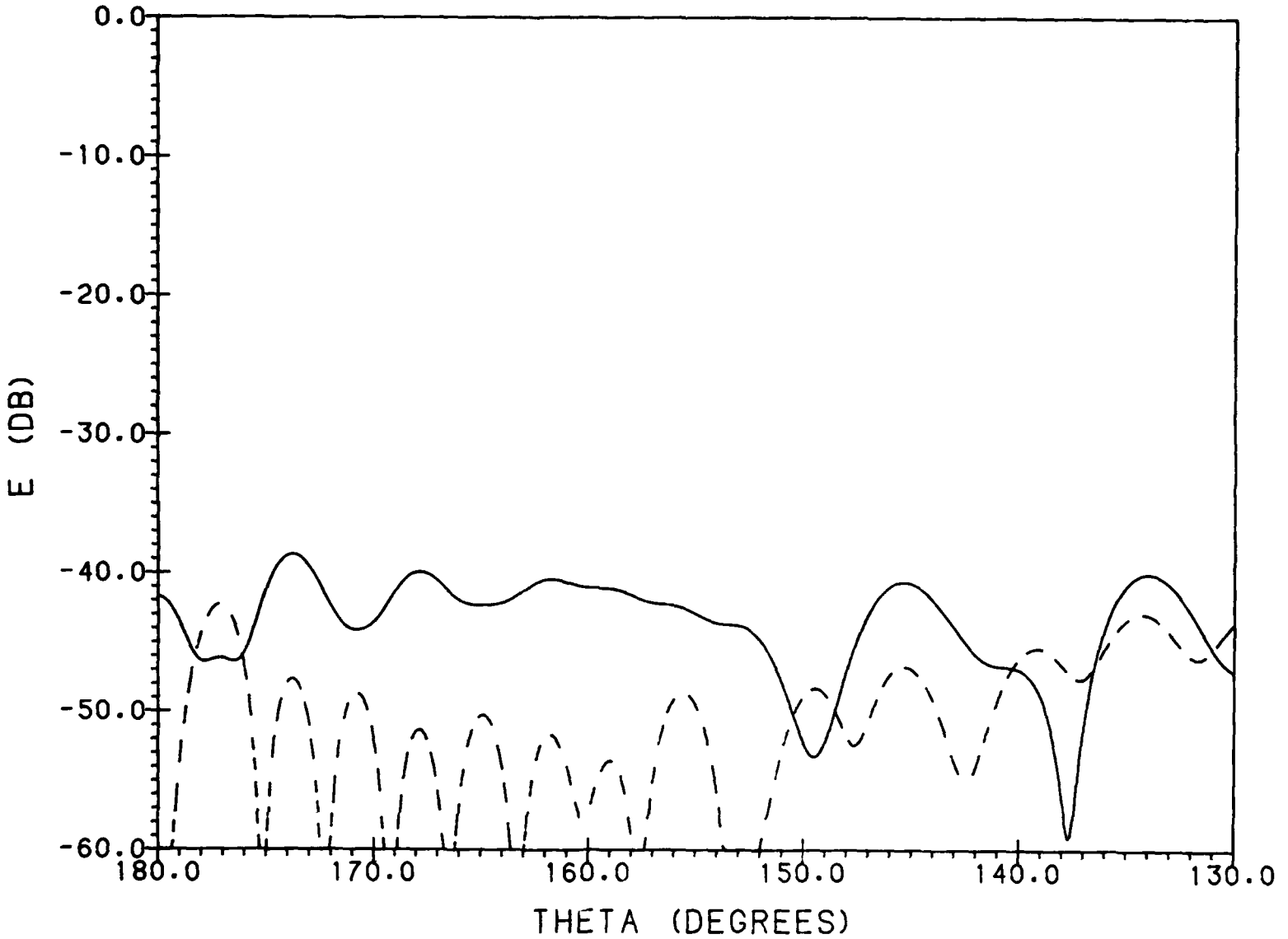

Figure 10c. Cross-Polar Amplitude Pattern in $\phi = 45°$ Plane of Paraboloid With a Single Diameter Crack Defined by $\phi_c' = 135°, -45°$ (———) and of Paraboloid Without Cracks (------)

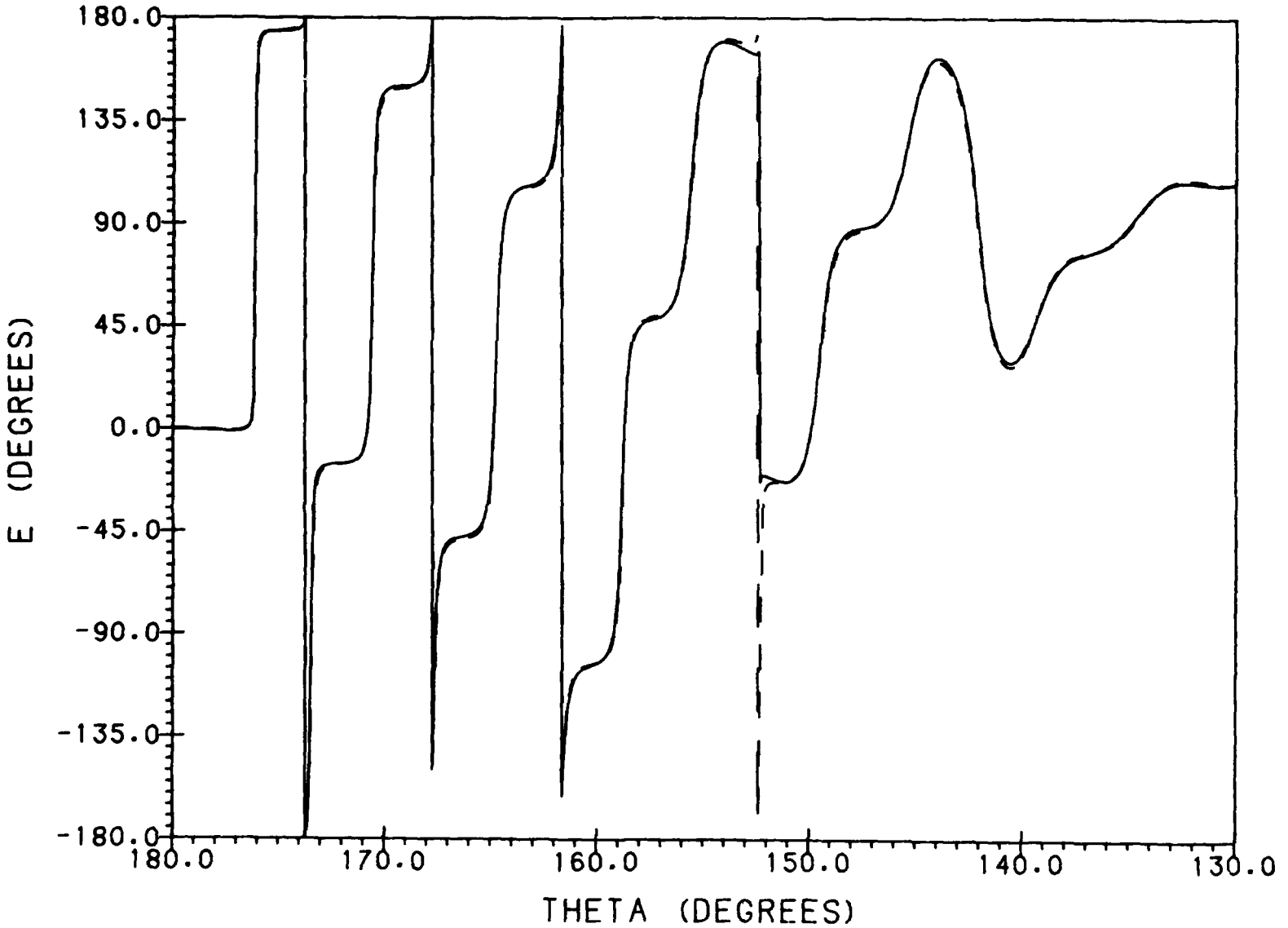

Figure 11a. Co-Polar E-Plane Phase Pattern of Paraboloid With a Single Diameter Crack Defined by $\phi_c' = 135^\circ, -45^\circ$ (———) and of Paraboloid Without Cracks (------)

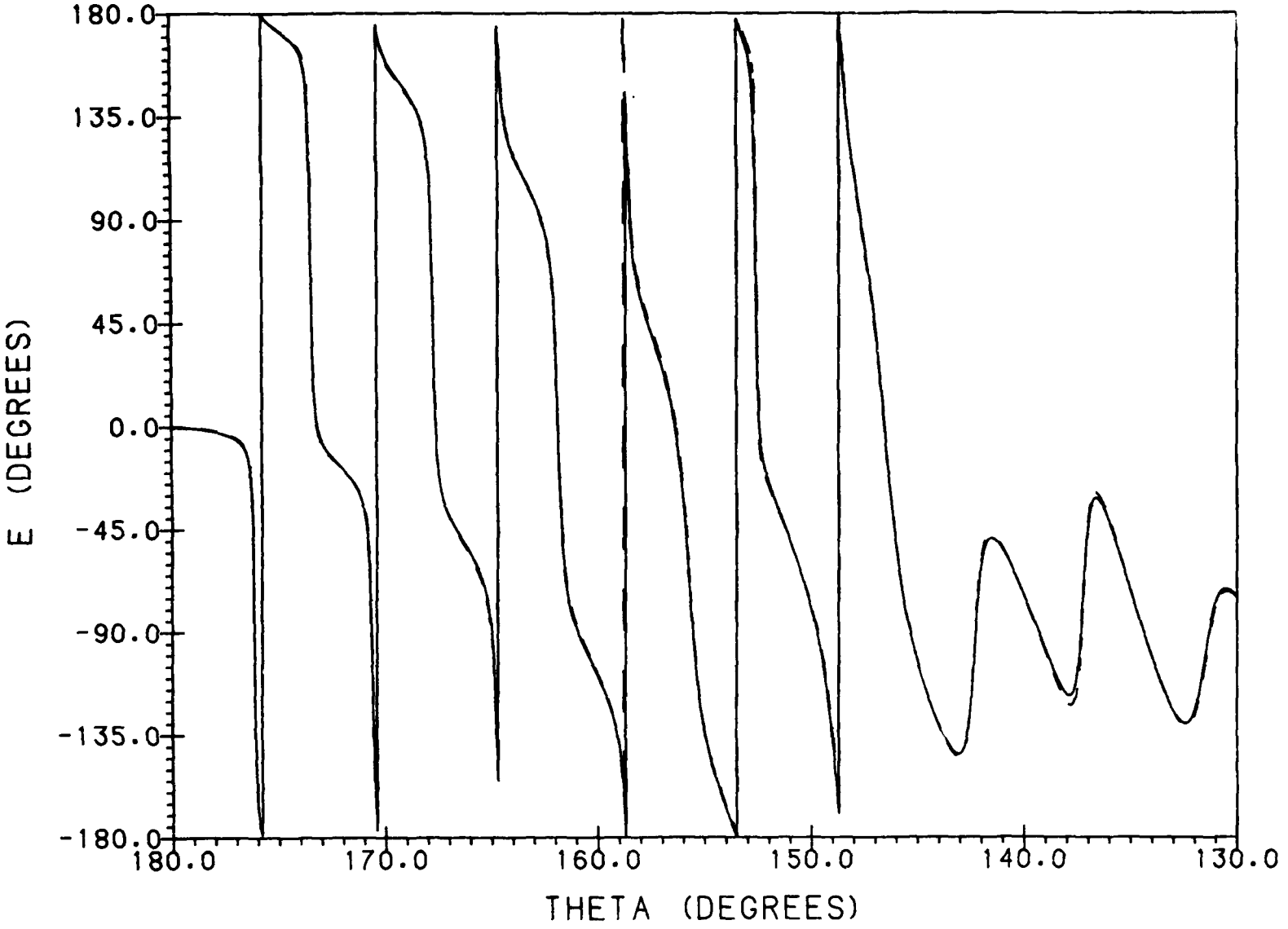

Figure 11b. Co-Polar H-Plane Phase Pattern of Paraboloid With a Single Diameter Crack Defined by $\phi_c' = 135°, -45°$ (———) and of Paraboloid Without Cracks (------)

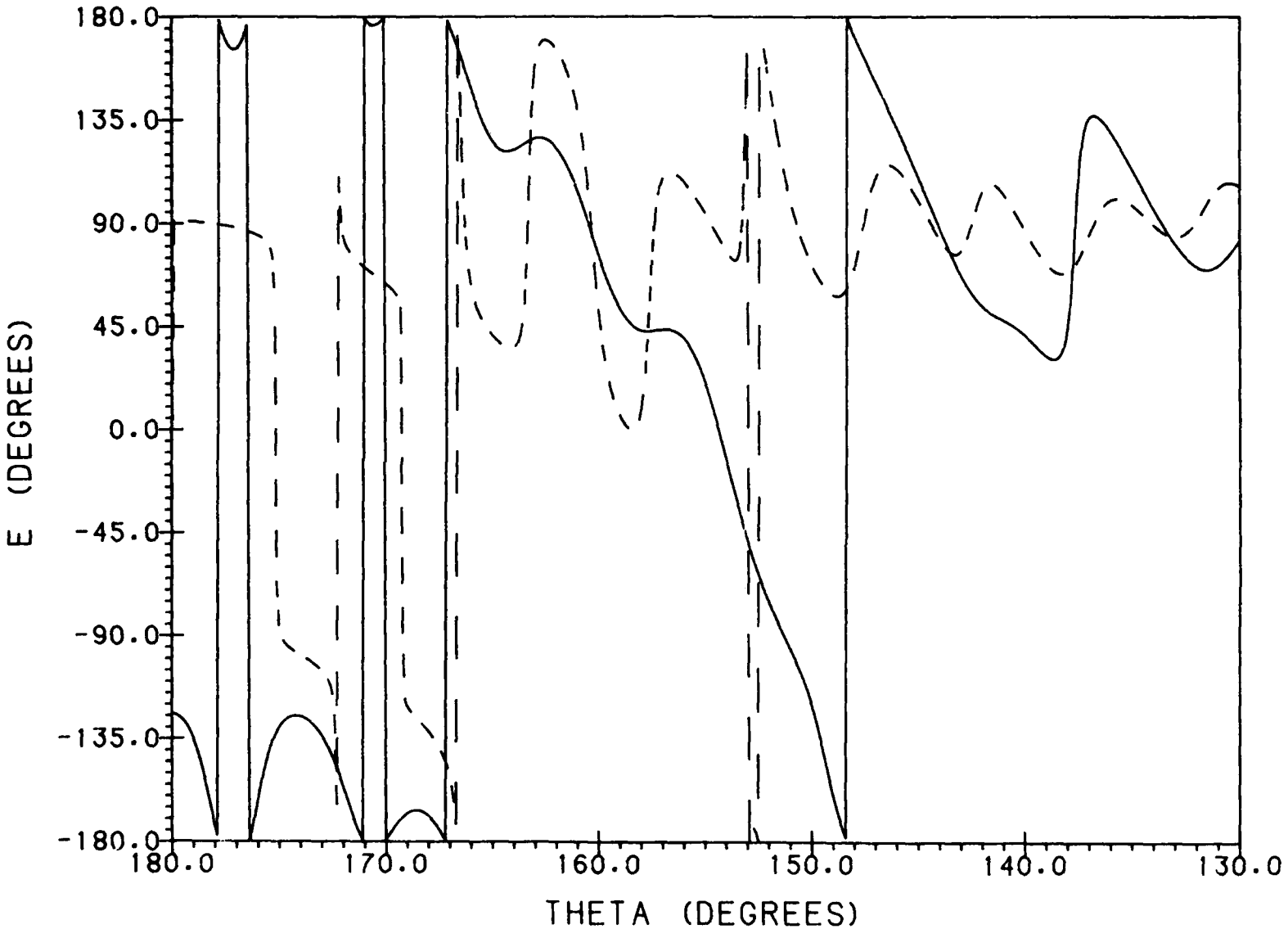

Figure 11c. Cross-Polar Phase Pattern in $\phi = 45°$ Plane of Paraboloid With a Single Diameter Crack Defined by $\phi_c' = 135°, -45°$ (———) and of Paraboloid Without Cracks (------)

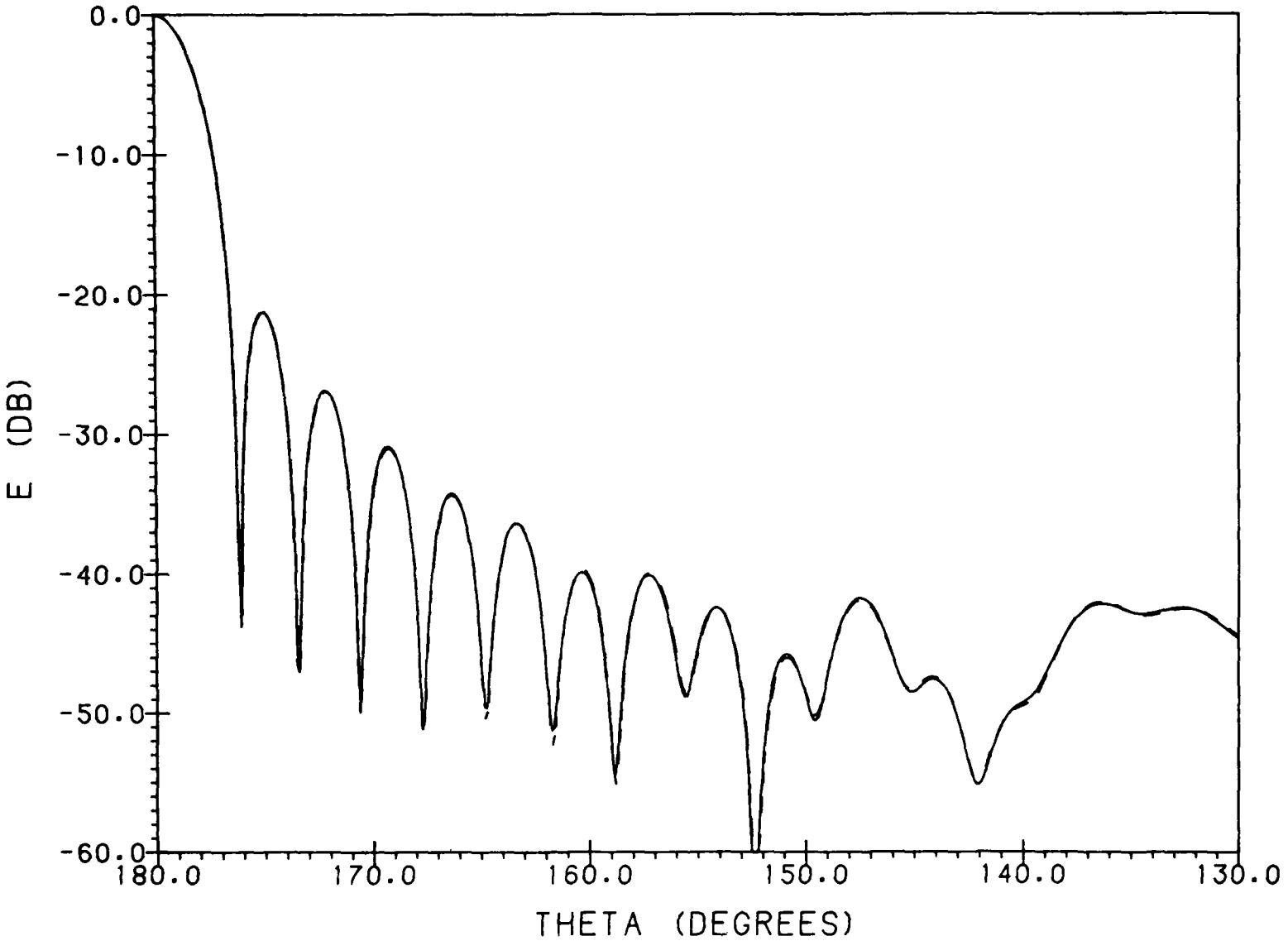

Figure 12a. Co-Polar E-Plane Amplitude Pattern of Paraboloid With a Single Diameter Crack Defined by $\phi_c' = 45°, -135°$ (———) and of Paraboloid Without Cracks (------)

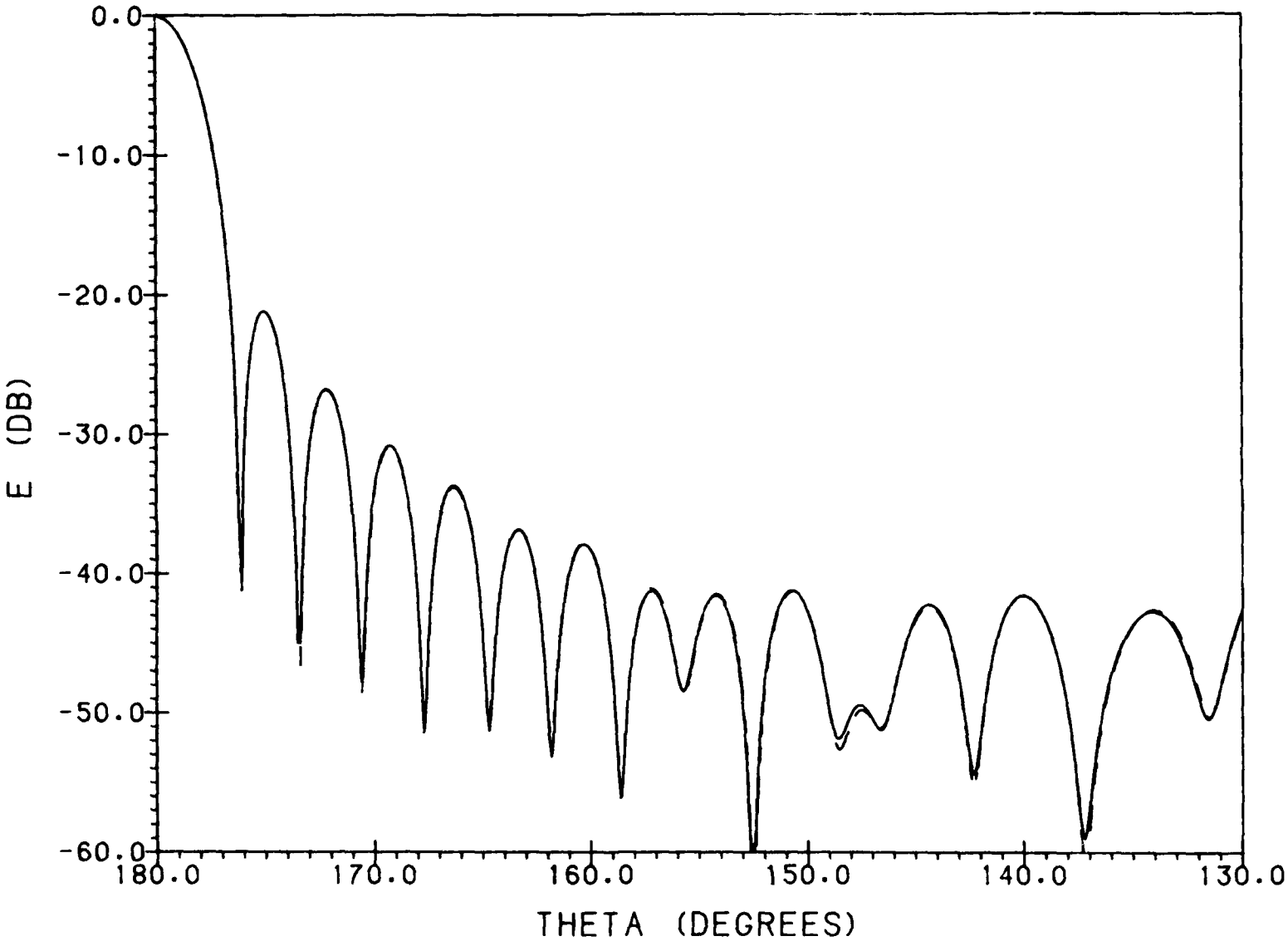

Figure 12b. Co-Polar H-Plane Amplitude Pattern of Paraboloid With a Single Diameter Crack Defined by $\phi_c' = 45^\circ, -135^\circ$ (———) and of Paraboloid Without Cracks (------)

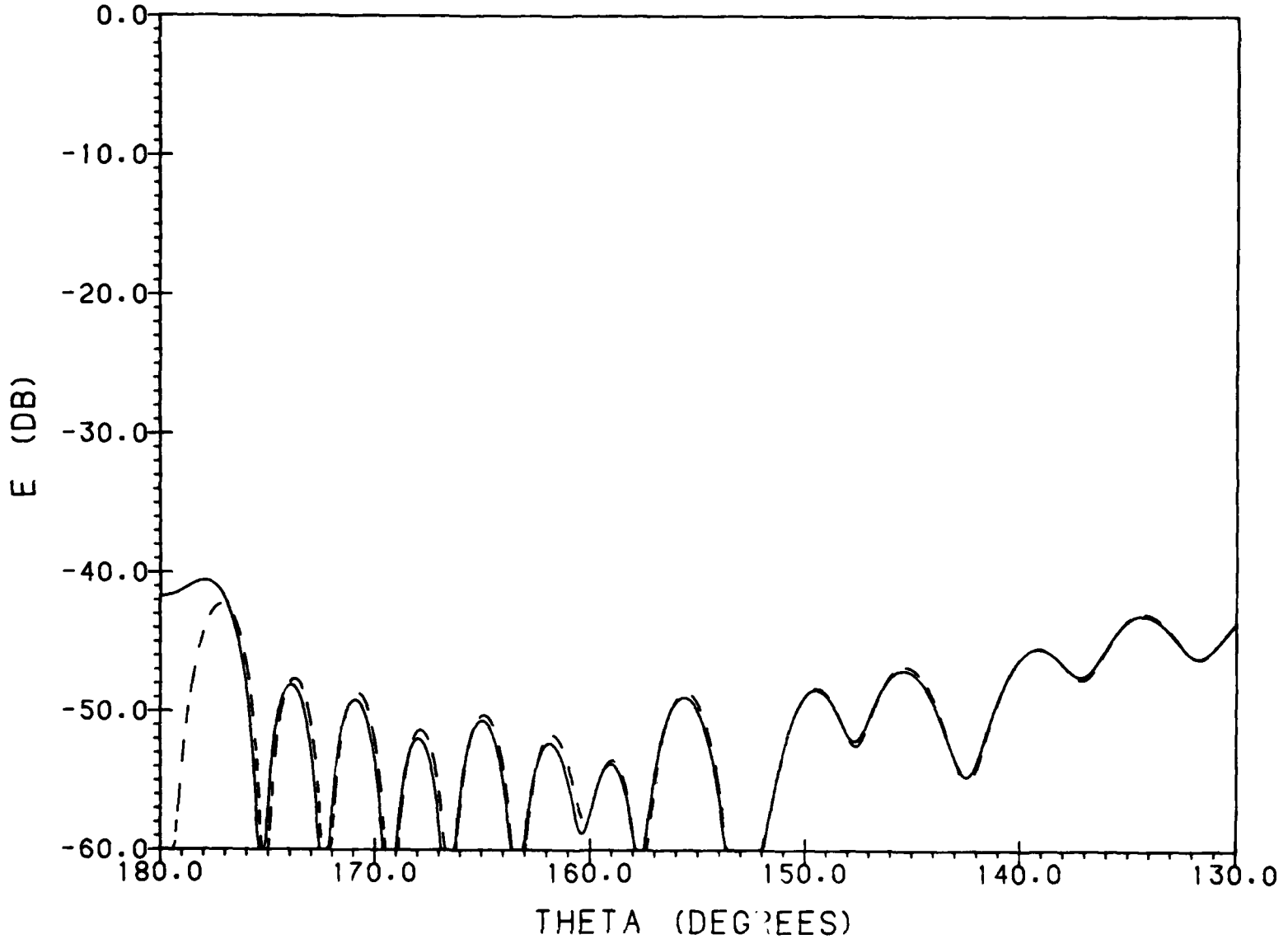

Figure 12c. Cross-Polar Amplitude Pattern in $\phi = 45°$ Plane of Paraboloid With a Single Diameter Crack Defined by $\phi_c' = 45°$, $-135°$ (———) and of Paraboloid Without Cracks (------)

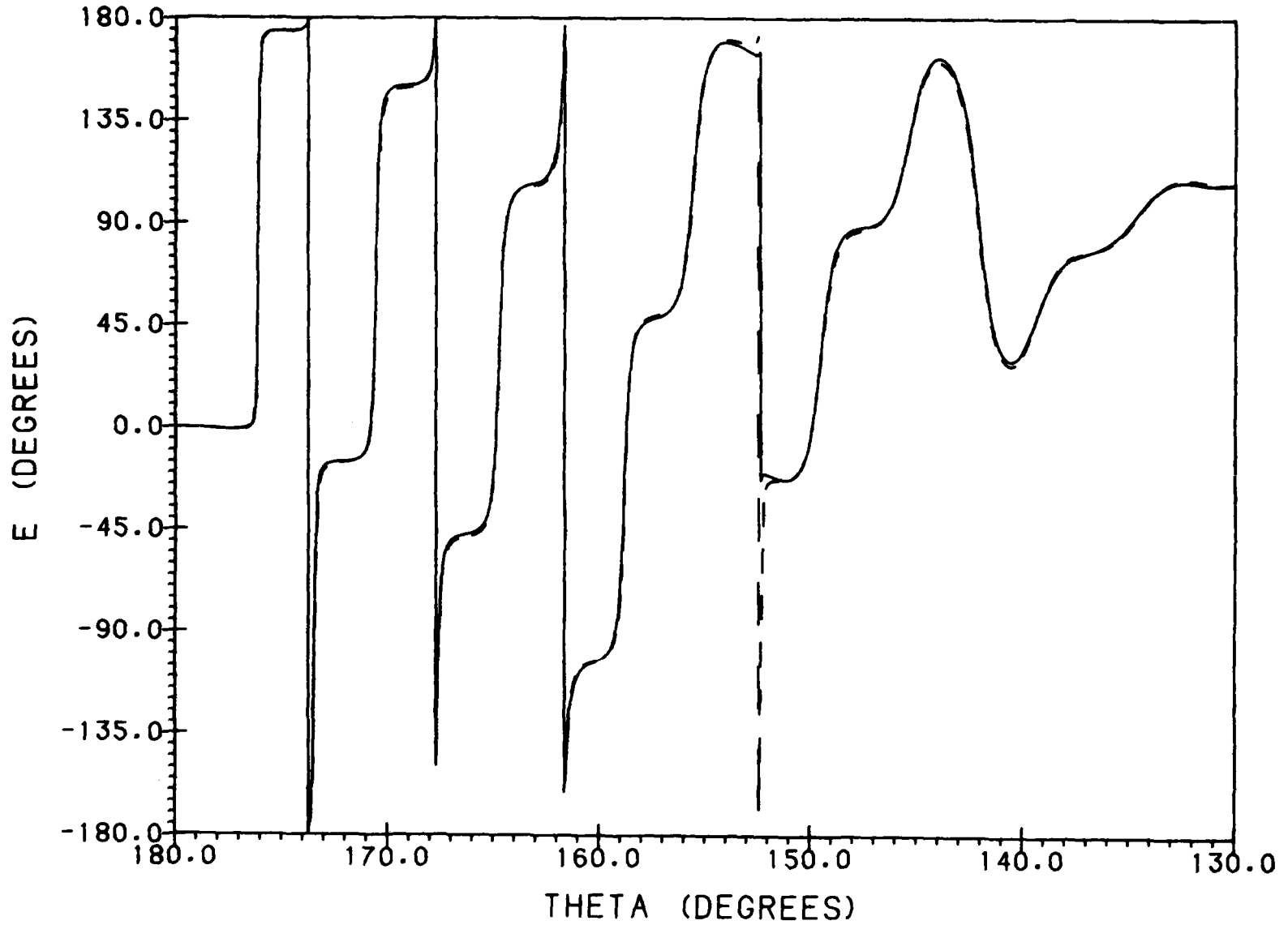

Figure 13a. Co-Polar E-Plane Phase Pattern of Paraboloid With a Single Diameter Crack Defined by $\phi_c' = 45°, -135°$ (———) and of Paraboloid Without Cracks (------)

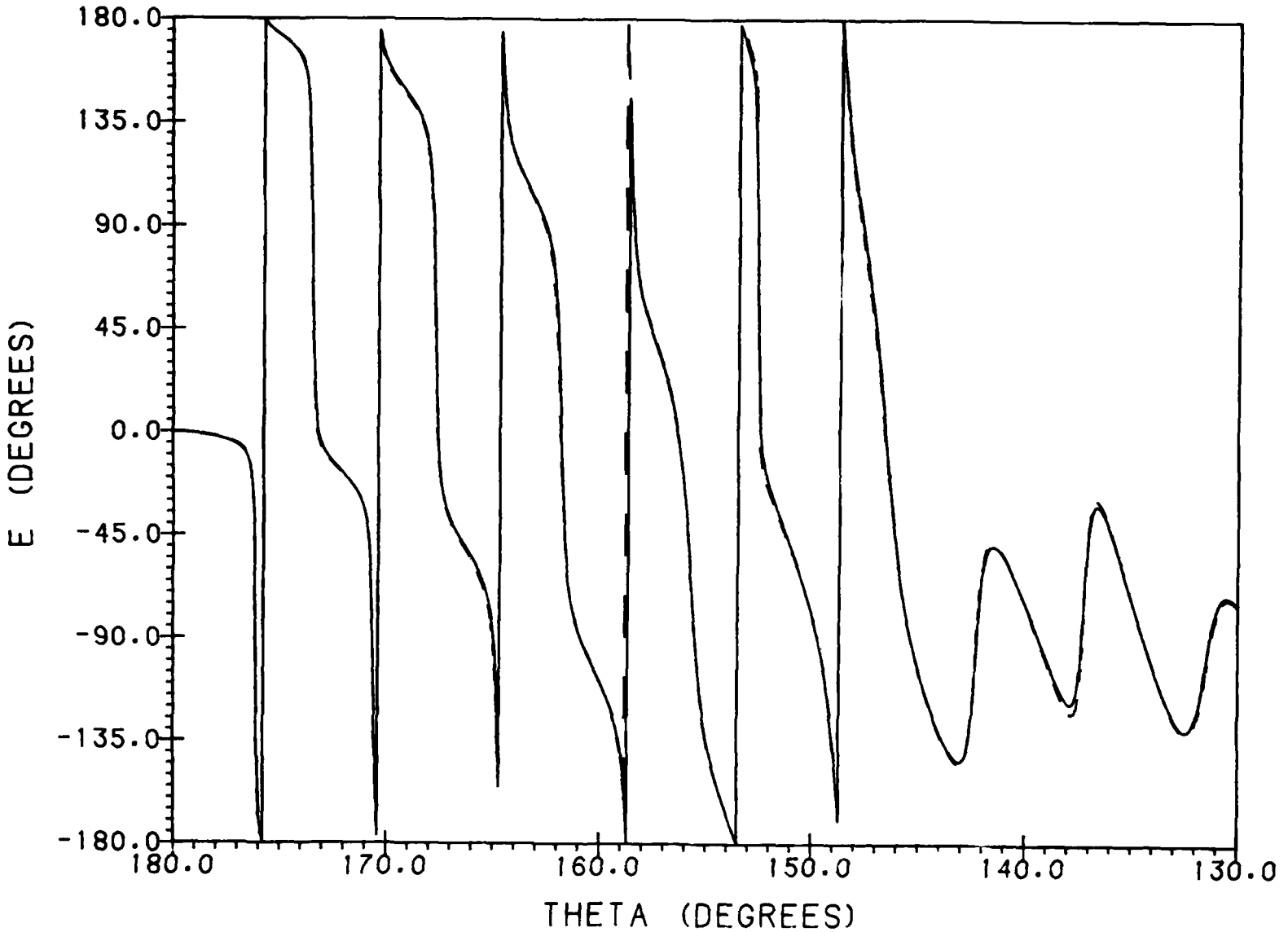

Figure 13b. Co-Polar H-Plane Phase Pattern of Paraboloid With a Single Diameter Crack Defined by $\phi_c' = 45°, -135°$ (———) and of Paraboloid Without Cracks (------)

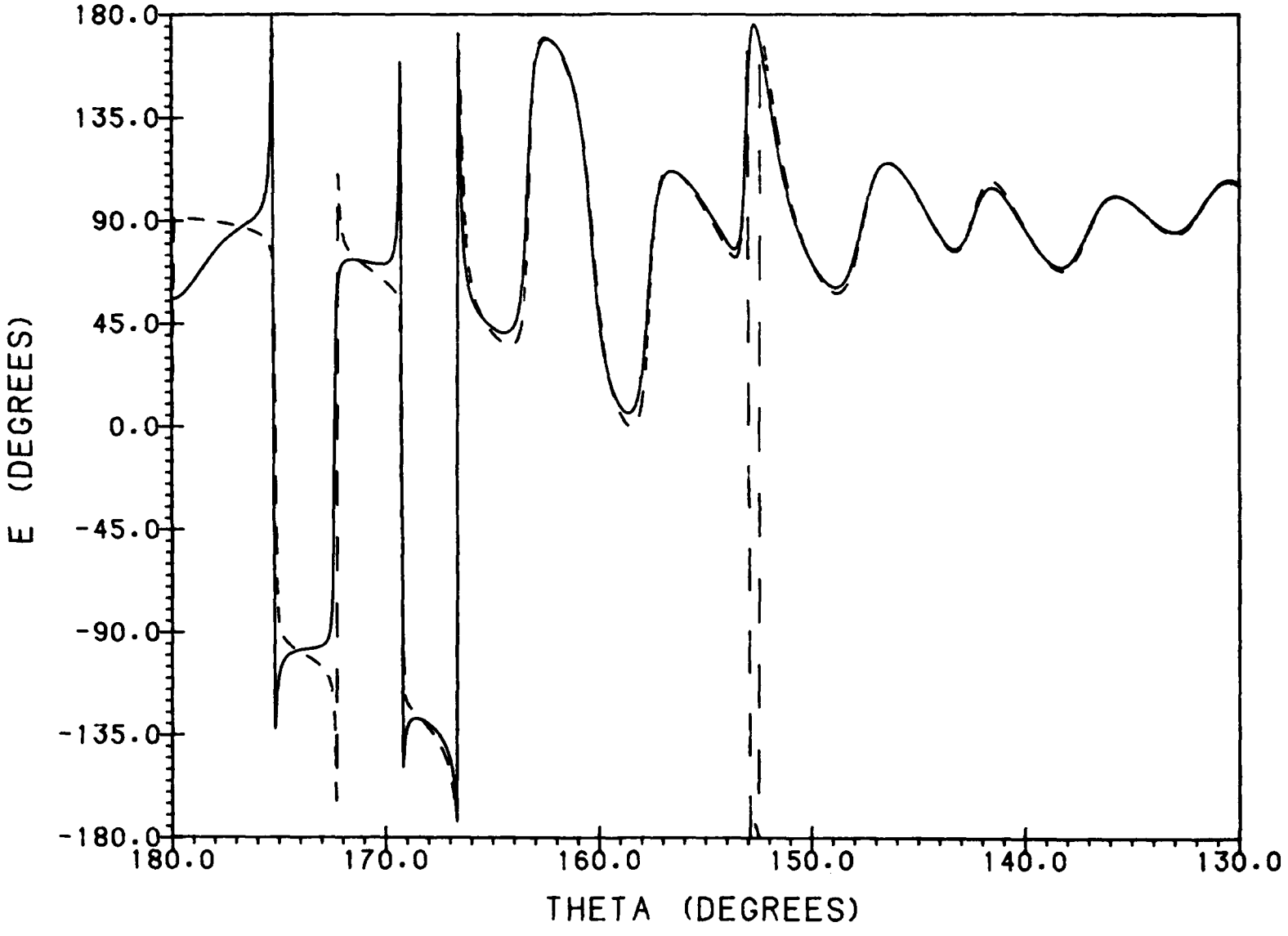

Figure 13c. Cross-Polar Phase Pattern in $\phi = 45°$ Plane of Paraboloid With a Single Diameter Crack Defined by $\phi_c' = 45°$, $-135°$ (———) and of Paraboloid Without Cracks (------)

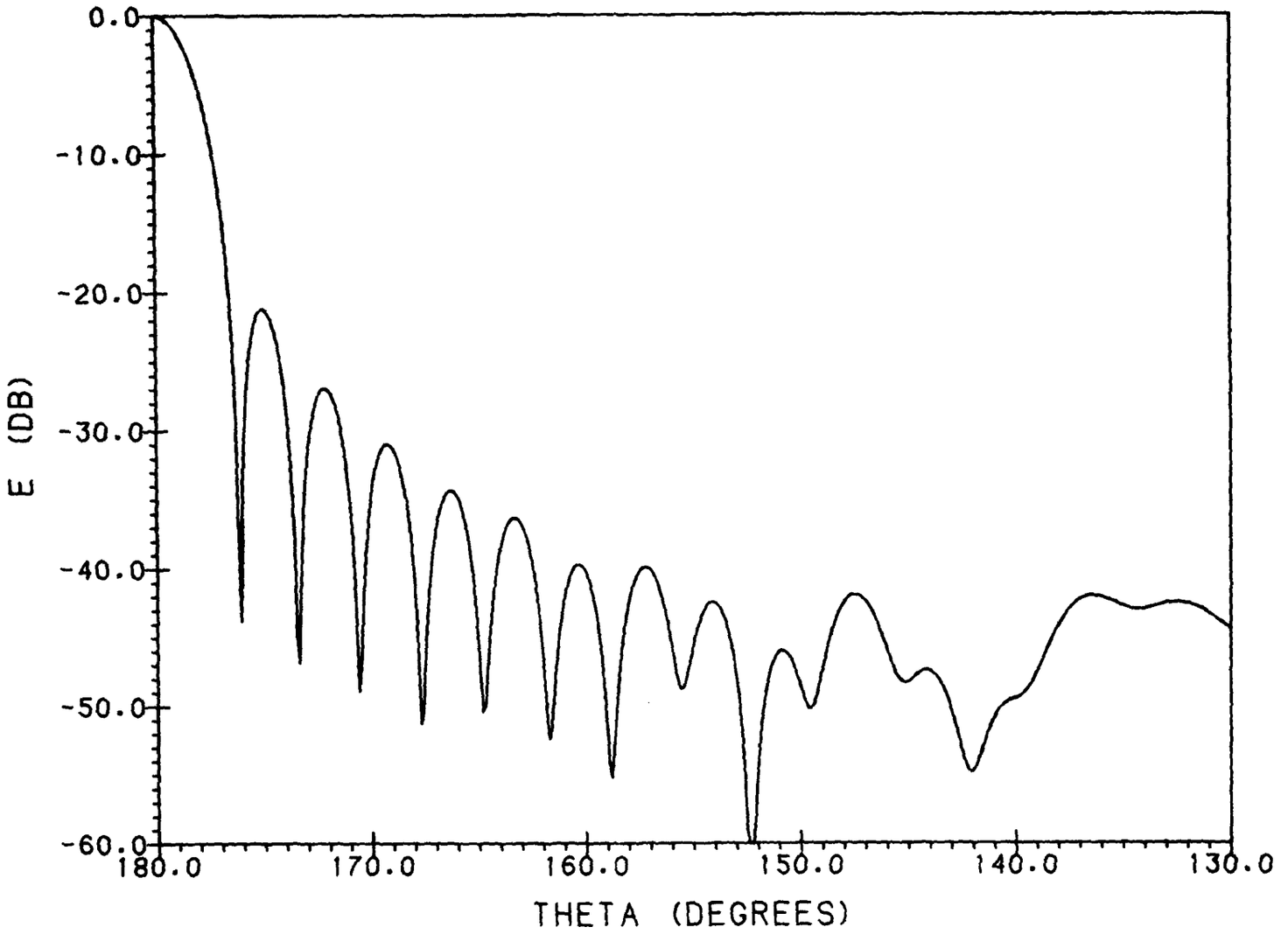

Figure 14a. Co-Polar E-Plane Amplitude Pattern of Paraboloid With a Single Diameter Crack Defined by $\phi_c' = 0^\circ$, 180° (———) and of Paraboloid Without Cracks (------)

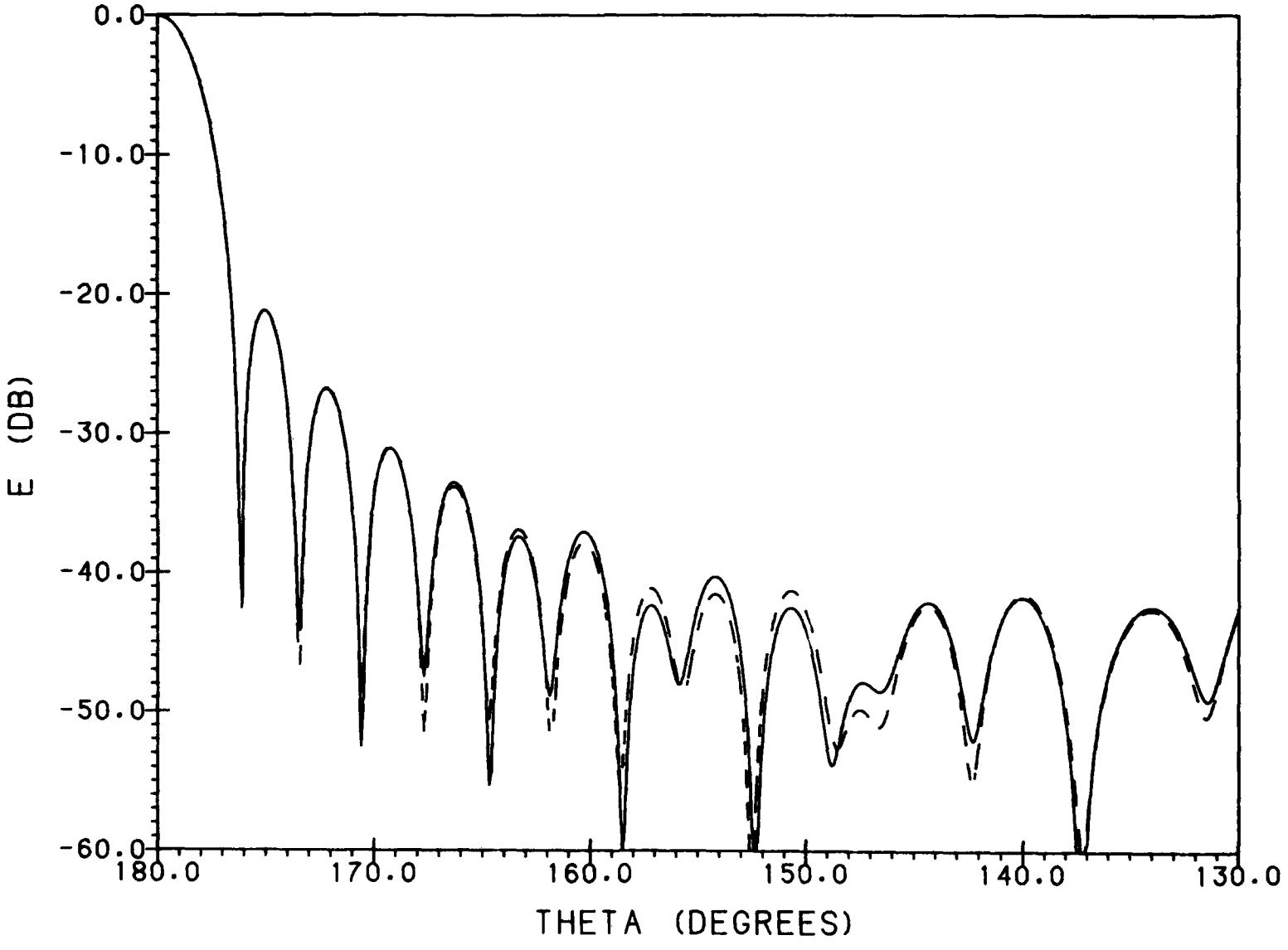

Figure 14b. Co-Polar H-Plane Amplitude Pattern of Paraboloid With a Single Diameter Crack Defined by $\phi_c' = 0°$, 180° (———) and of Paraboloid Without Cracks (------)

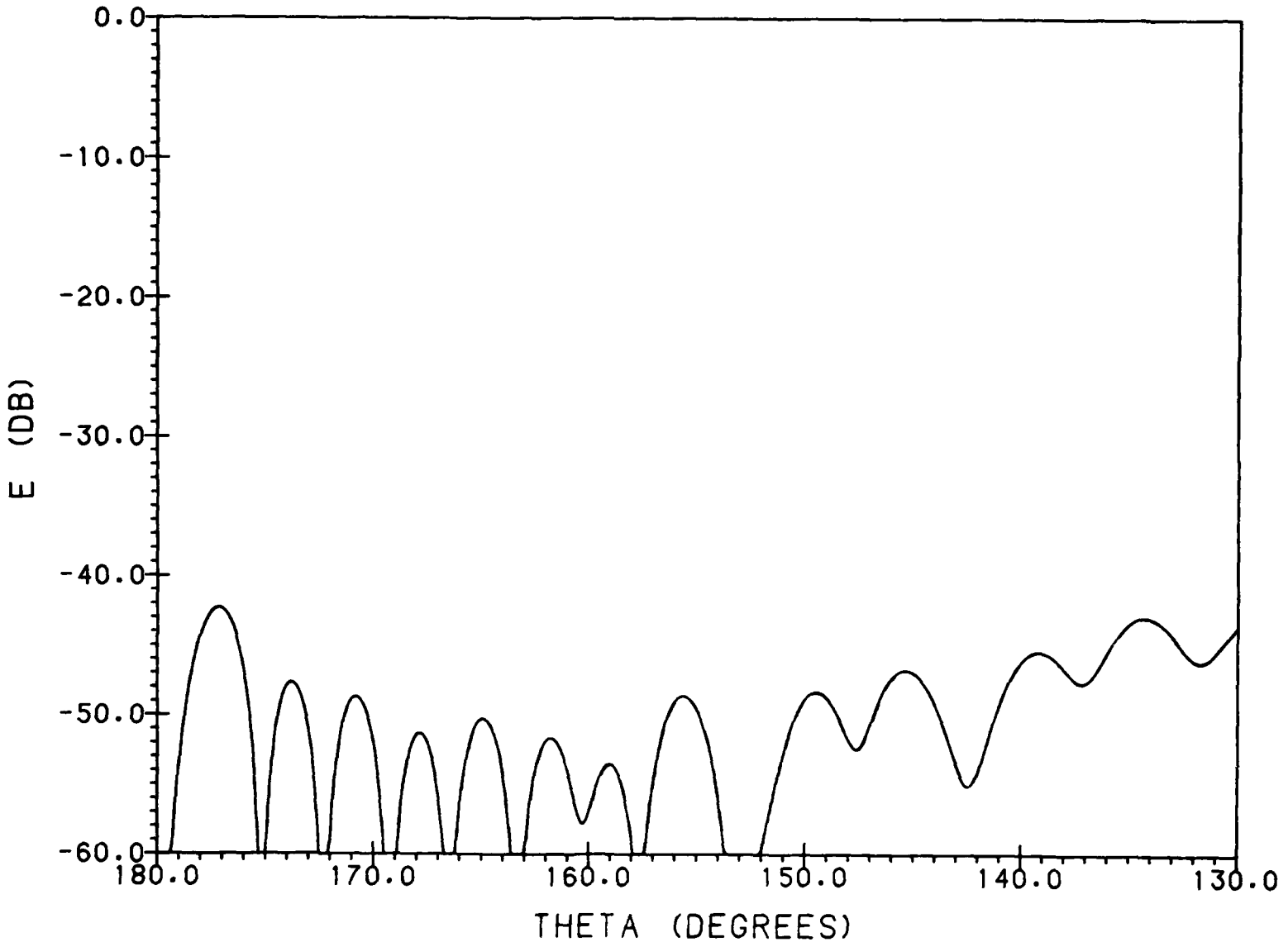

Figure 14c. Cross-Polar Amplitude Pattern in $\phi = 45°$ Plane of Paraboloid With a Single Diameter Crack Defined by $\phi_c' = 0°$, 180° (———) and of Paraboloid Without Cracks (------)

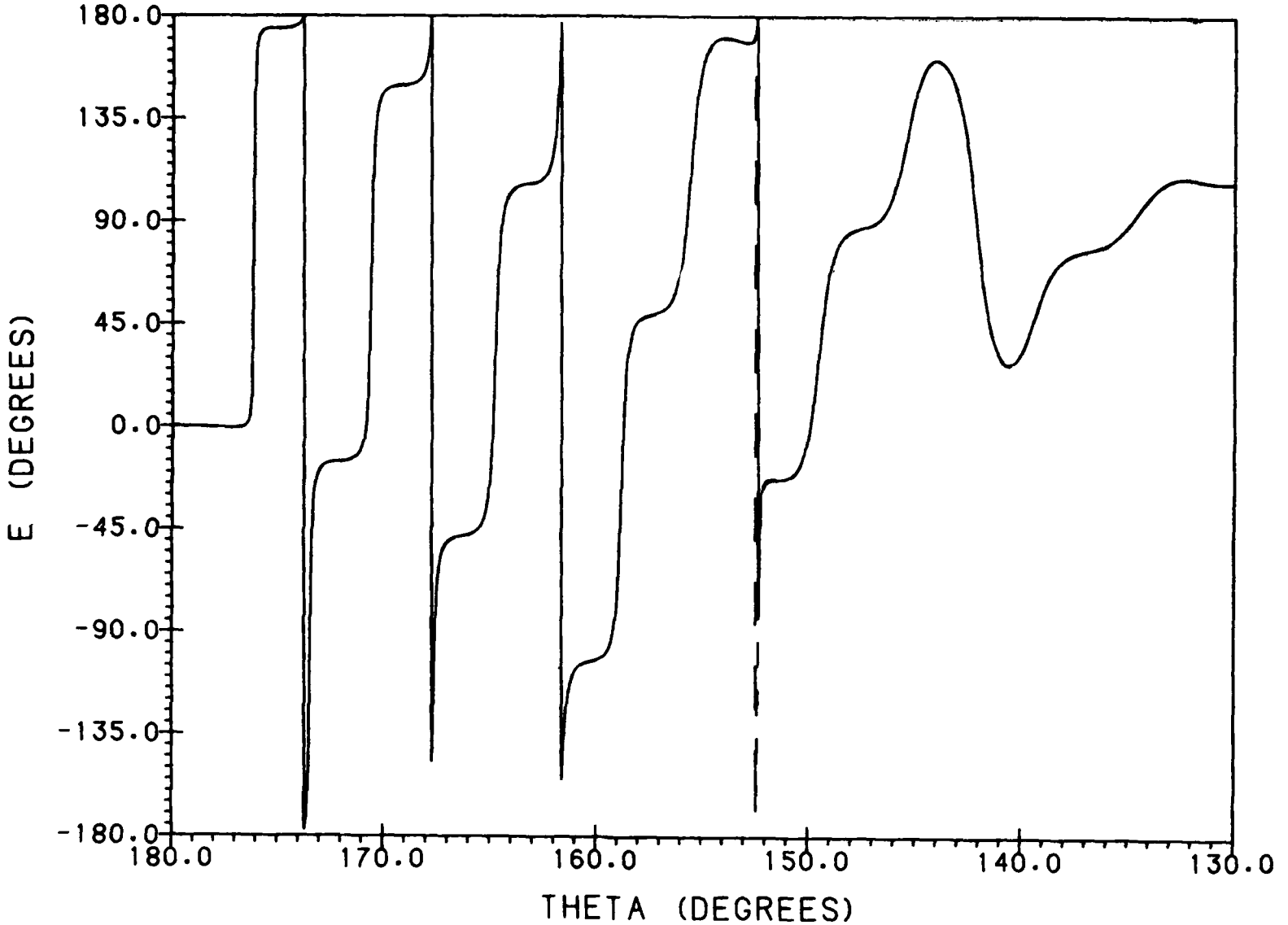

Figure 15a. Co-Polar E-Plane Phase Pattern of Paraboloid With a Single Diameter Crack Defined by $\phi'_c = 0^\circ, 180^\circ$ (———) and of Paraboloid Without Cracks (------)

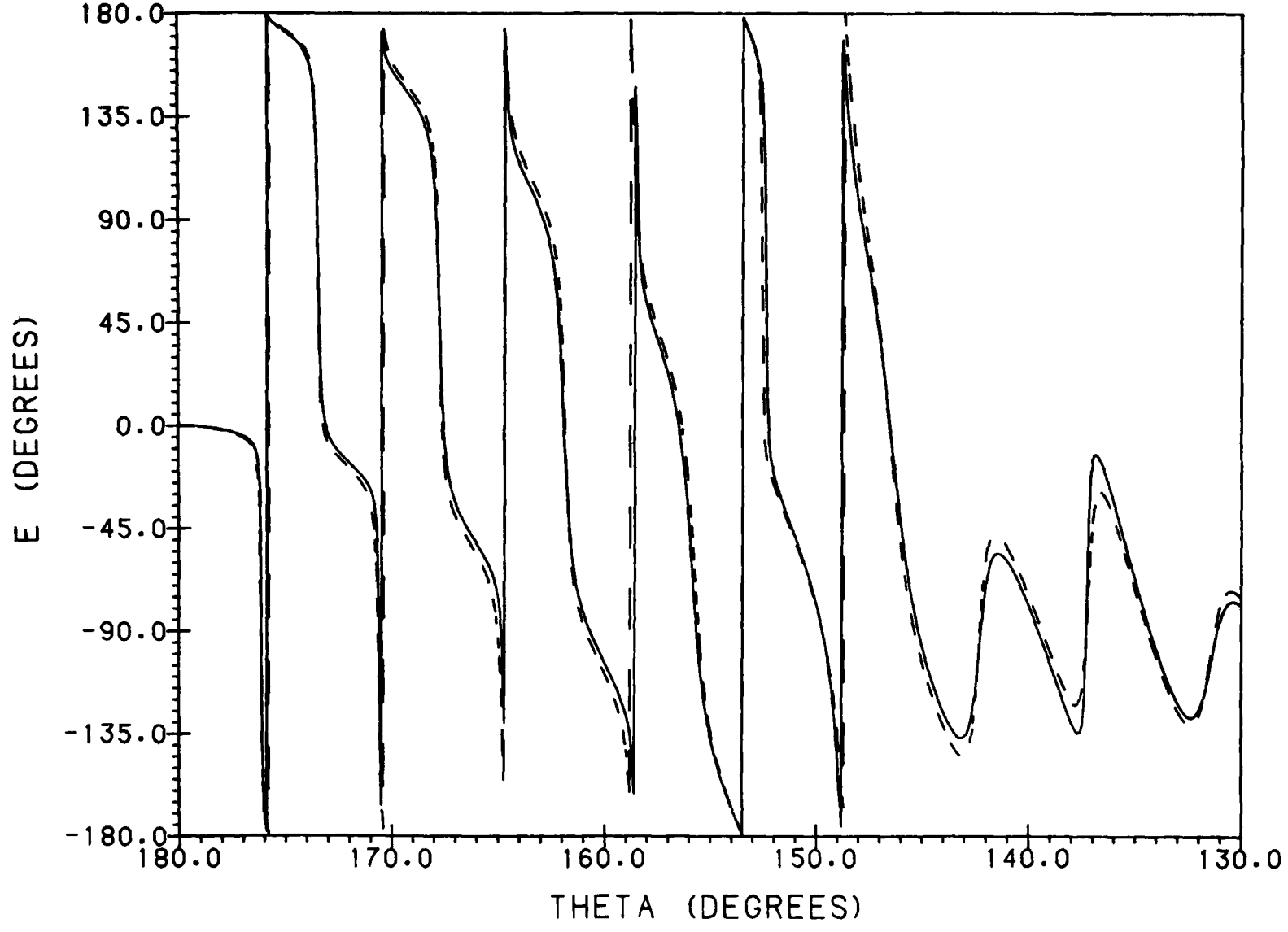

Figure 15b. Co-Polar H-Plane Phase Pattern of Paraboloid With a Single Diameter Crack Defined by $\phi_c' = 0°, 180°$ (———) and of Paraboloid Without Cracks (------)

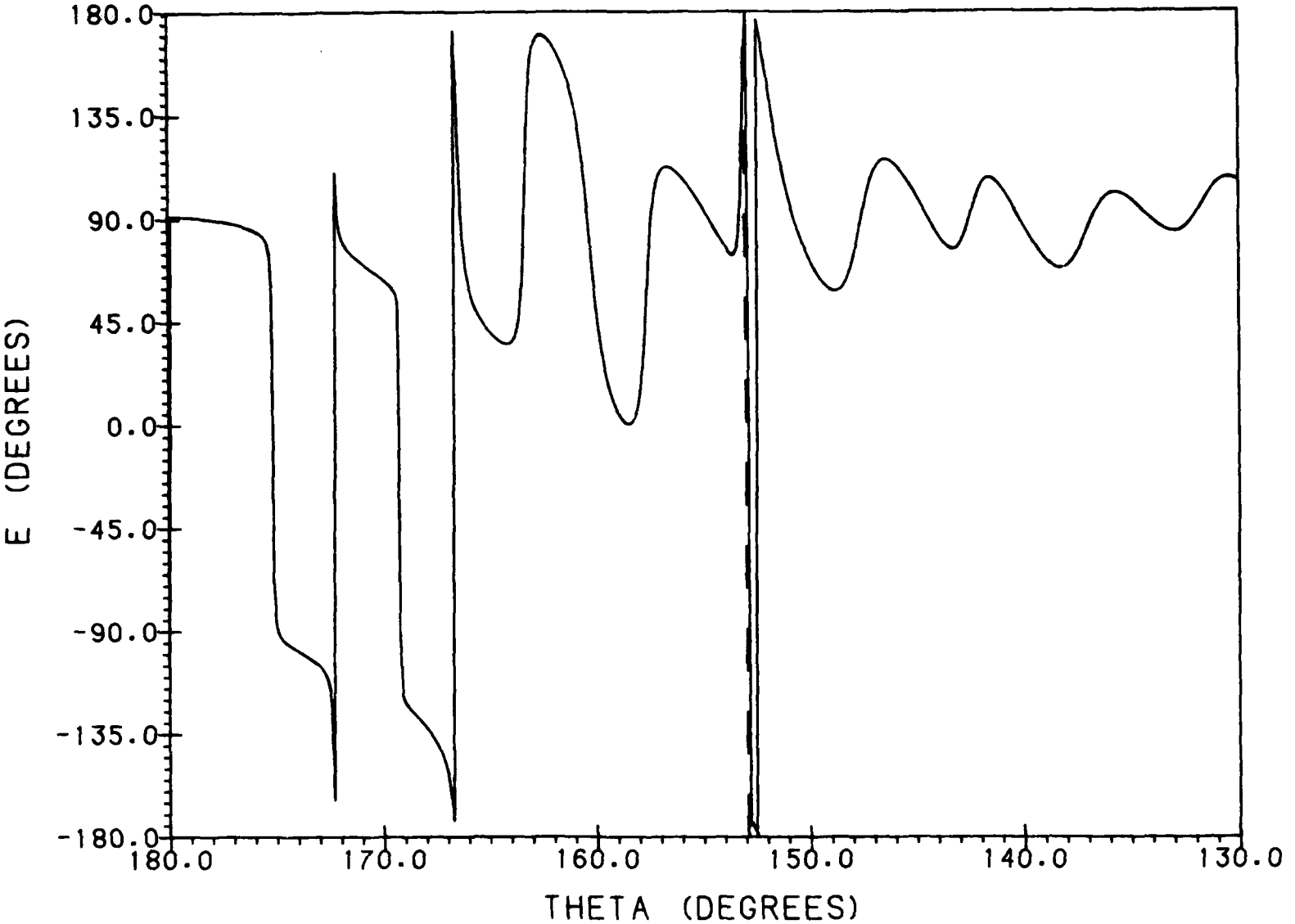

Figure 15c. Cross-Polar Phase Pattern in $\phi = 45°$ Plane of Paraboloid With a Single Diameter Crack Defined by $\phi'_c = 0°$, 180° (———) and of Paraboloid Without Cracks (------)

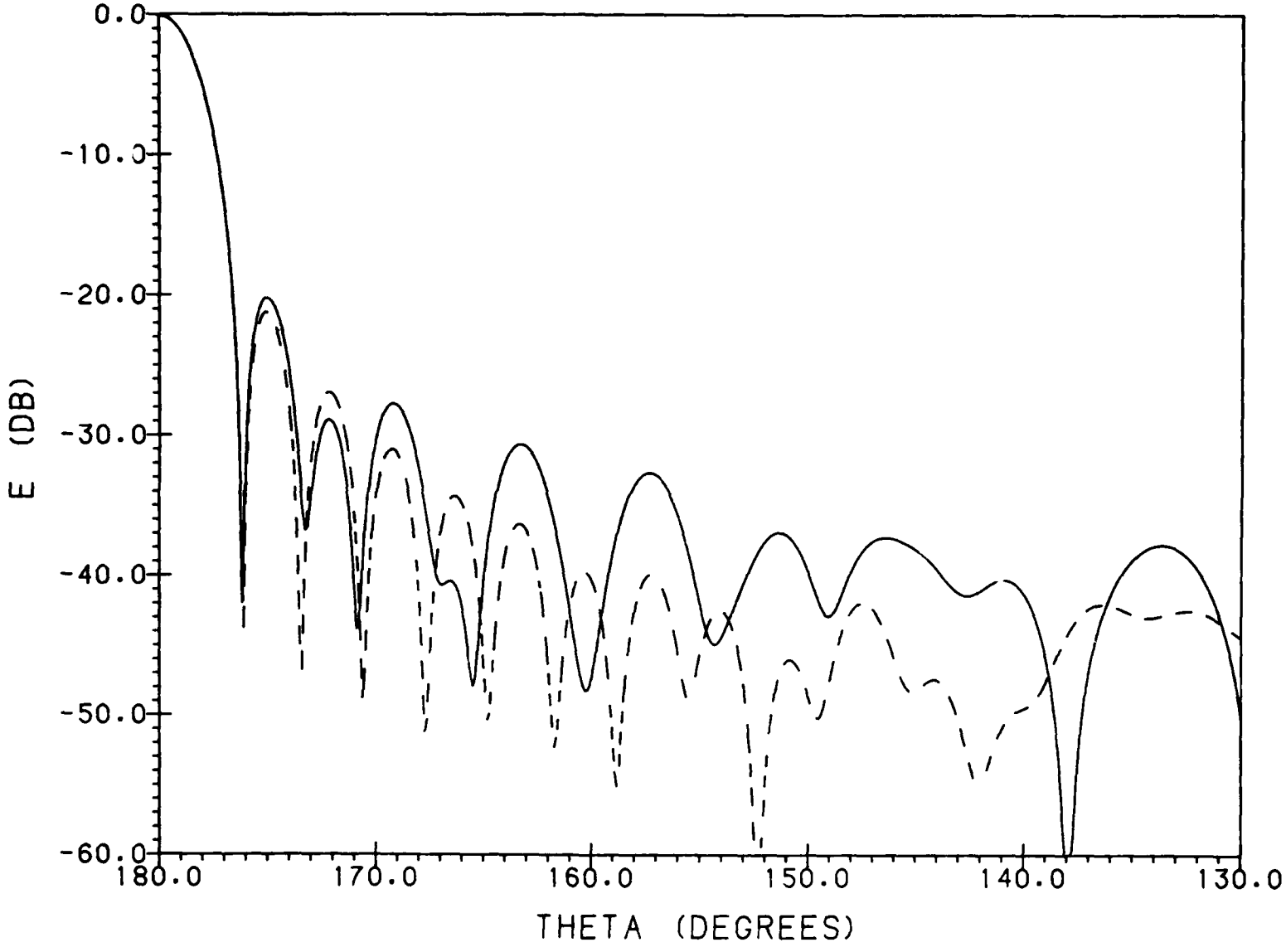

Figure 16a. Co-Polar E-Plane Amplitude Pattern of Paraboloid With a Single Diameter Crack Defined by $\phi'_c = \pm 90°$ (———) and of Paraboloid Without Cracks (------)

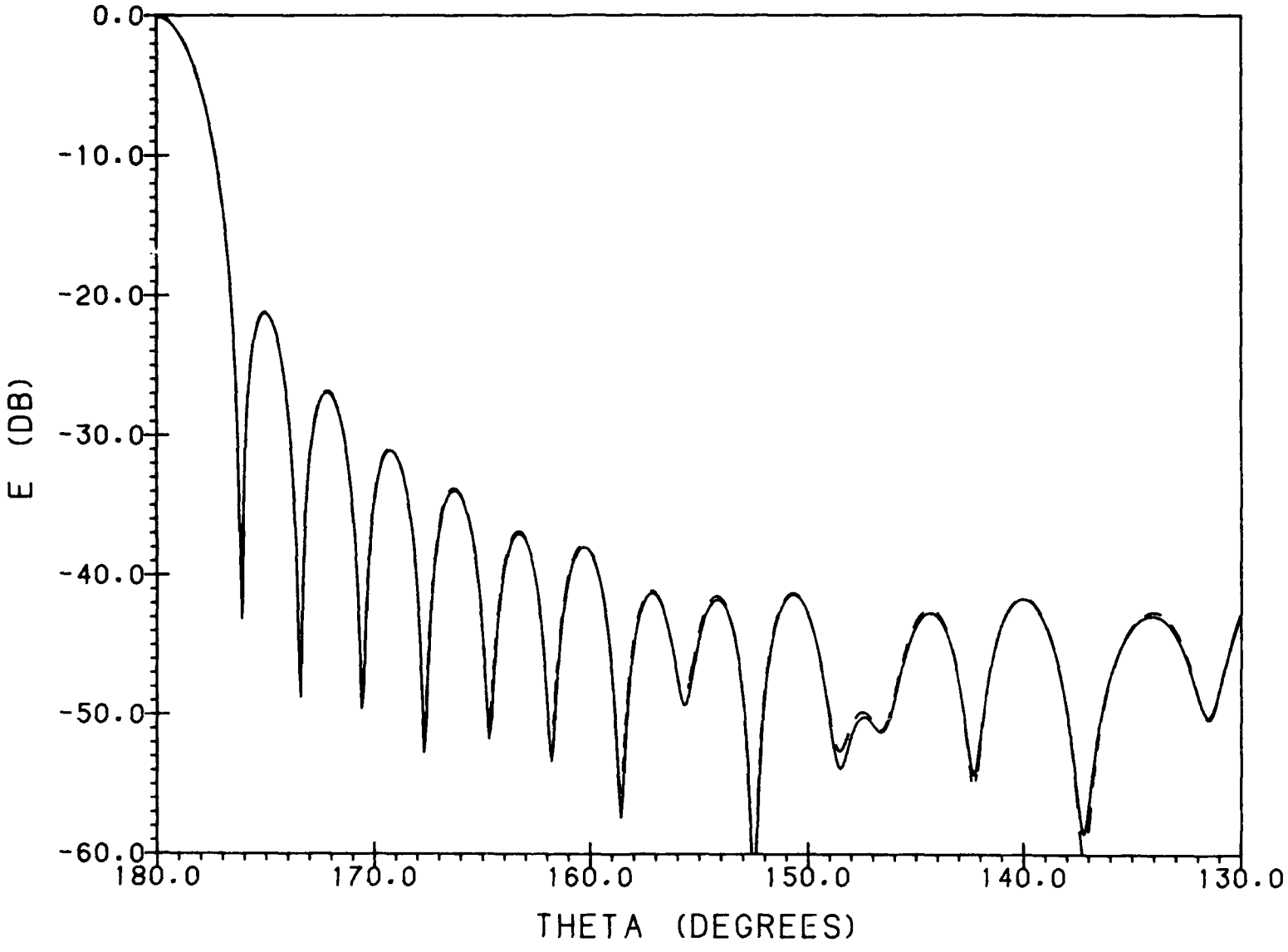

Figure 16b. Co-Polar H-Plane Phase Pattern of Paraboloid With a Single Diameter Crack Defined by $\phi'_c = \pm 90^\circ$ (———) and of Paraboloid Without Cracks (- - - - -)

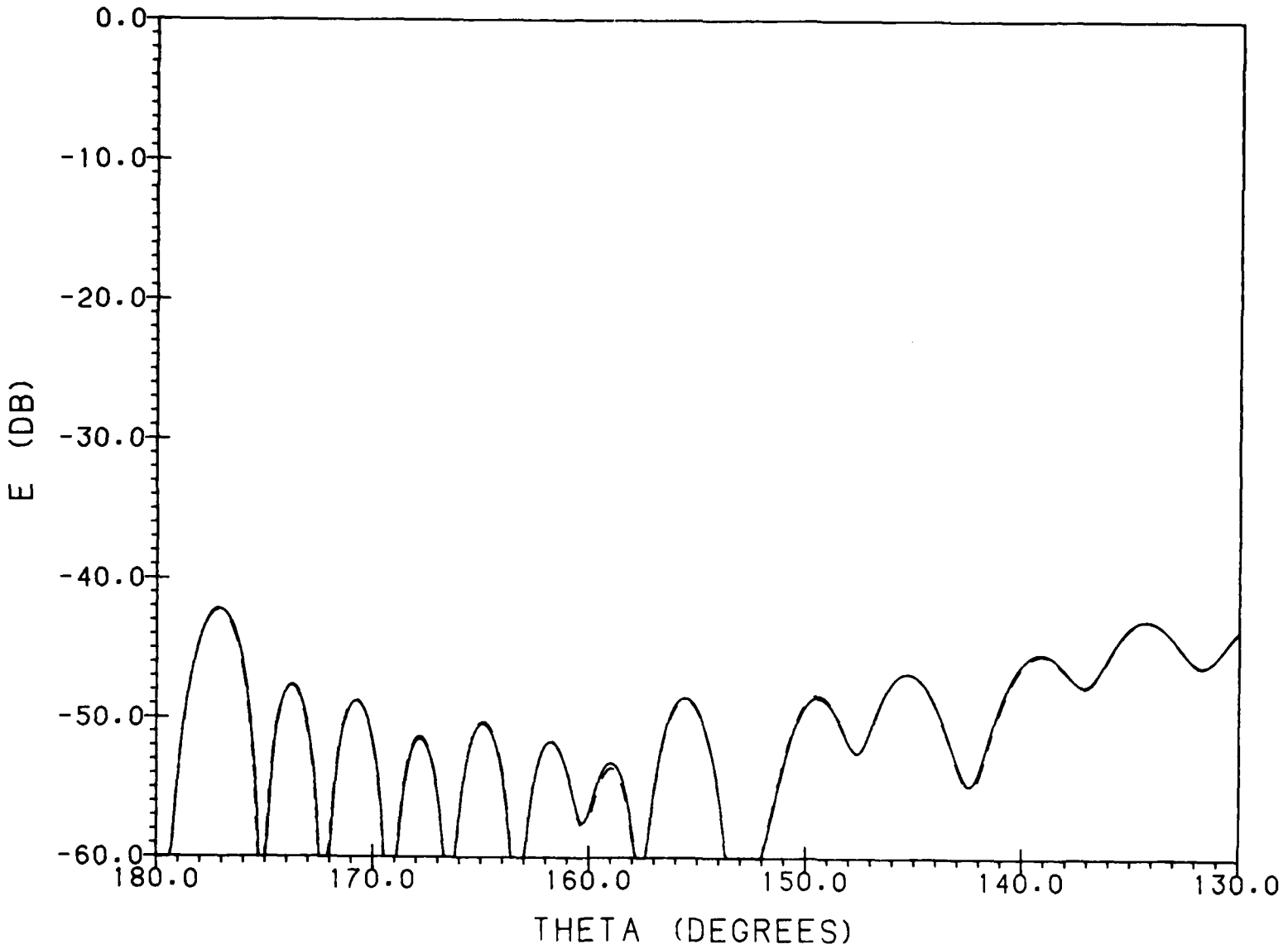

Figure 16c. Cross-Polar Amplitude Pattern in $\phi = 45^\circ$ Plane of Paraboloid With a Single Diameter Crack Defined by $\phi_c' = \pm 90^\circ$ (———) and of Paraboloid Without Cracks (------)

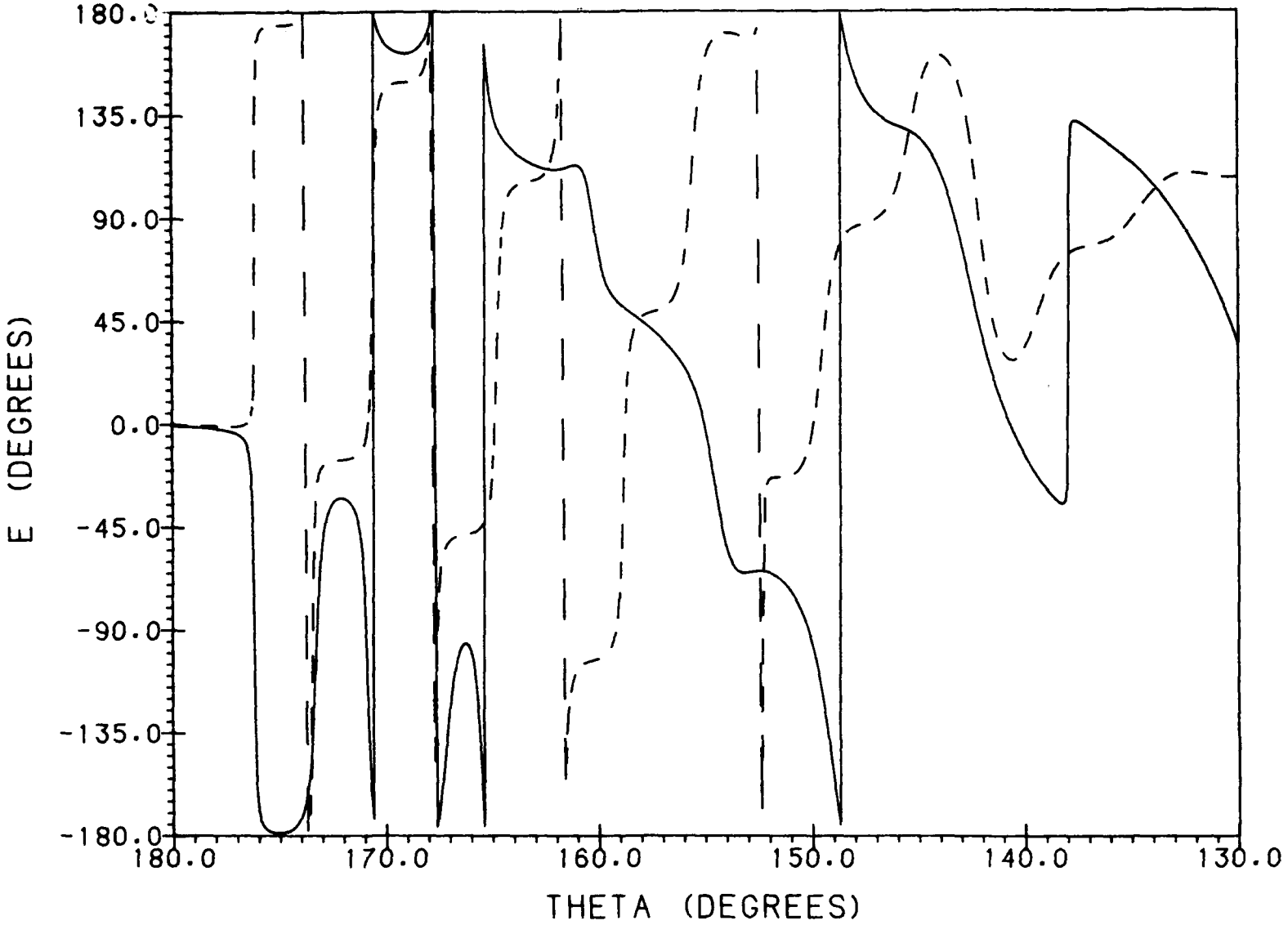

Figure 17a. Co-Polar E-Plane Phase Pattern of Paraboloid With a Single Diameter Crack Defined by $\phi'_c = \pm 90^\circ$ (———) and of Paraboloid Without Cracks (------)

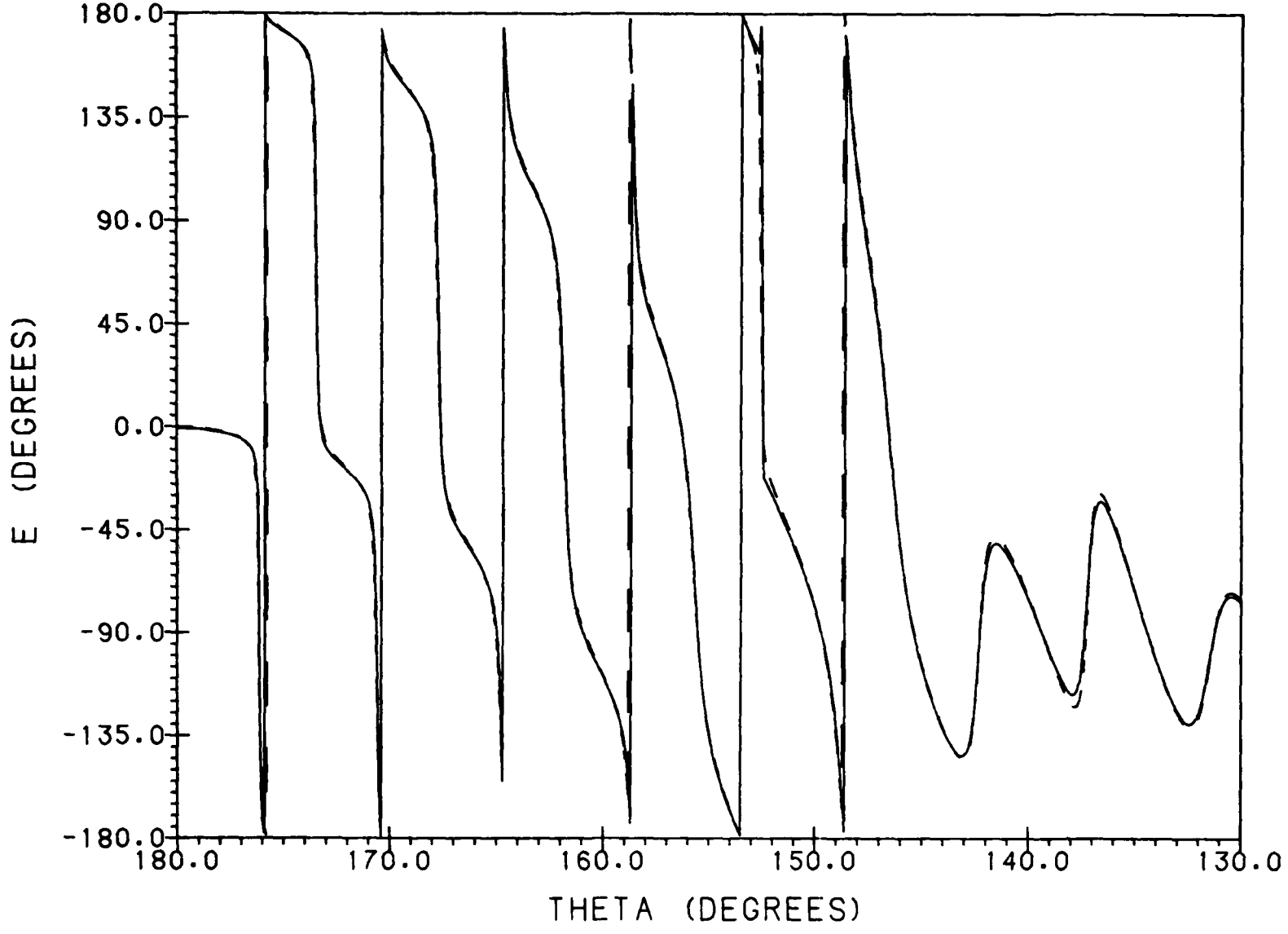

Figure 17b. Co-Polar H-Plane Phase Pattern of Paraboloid With a Single Diameter Crack Defined by $\phi_c' = \pm 90°$ (———) and of Paraboloid Without Cracks (------)

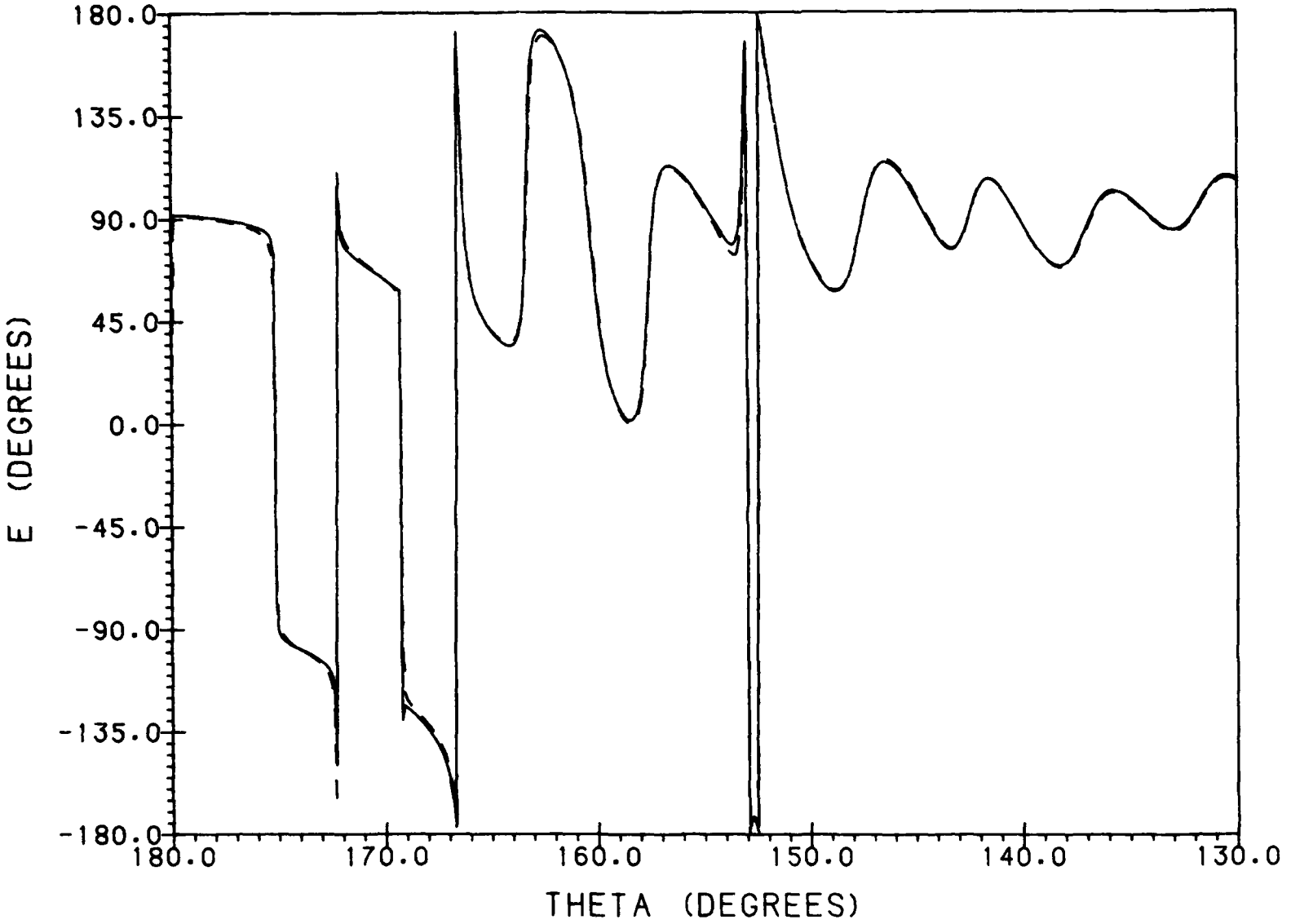

Figure 17c. Cross-Polar Phase Pattern in $\phi = 45°$ Plane of Paraboloid With a Single Diameter Crack Defined by $\phi'_c = \pm 90°$ (———) and of Paraboloid Without Cracks (------)

Comparing Figures 14(a) and 15(a) for the E-plane with Figures 14(b) and 15(b) for the H-plane, it is seen that the dominant effect of the cracks is on the E-plane pattern, with the H-plane pattern being almost unaffected. This difference can again be explained with the same line source model used above in explaining the dominant effect of the diameter crack defined by $\phi_c' = 135°$ and $-45°$ on the $\phi = 45°$ cross-polar pattern. Here the crack in the yz-plane has a broad pattern in the E-plane normal to the plane of the crack, and a narrow pattern in the H-plane parallel to the plane of the crack.

Comparing Figures 16(a) and 17(a) for the E-plane with Figures 16(b) and 17(b) for the H-plane for a single diameter crack in the yz-plane, we see that the dominant effect here is on the pattern in the H-plane, because the H-plane rather than the E-plane is now the plane normal to the plane of the crack. Additionally if we compare Figures 14(a) and 15(a) with Figures 16(b) and 17(b), it is clear that the effect on the E-plane in Figures 14(a) and 15(a) is considerably greater than the effect on the H-plane shown in Figures 16(b) and 17(b). This difference can be explained in much the same way as the difference in the effect of the azimuthal crack on the E- and H-plane patterns was explained above. The diameter crack in the yz-plane is illuminated locally by a TE wave while the diameter crack in the xz-plane is illuminated locally by a TM wave, and the TE incremental diffracted field is considerably stronger than the TM diffracted field.

As an indication of how the effect of the cracks on the paraboloid pattern varies with the width of the cracks, Figure 18 shows the cross-polar amplitude pattern in the $\phi = 45°$ plane of the paraboloid with the basic crack configuration for a crack width of 0.01λ. Also shown in the same figure for reference is the pattern for a crack width of 0.1λ and the pattern of the paraboloid without cracks. It is seen that the effect of the cracks on the paraboloid pattern decreases quite slowly with the crack width, the effect still being quite significant even for the 0.01λ crack width. The reason for this slow decrease is the logarithmic dependence of the slit width of the leading term of the series expansion for P_1 of the slit TE incremental diffraction coefficient [see (1a)]

$$P_1 \approx \frac{1}{2} \frac{\pi}{\ln \frac{kd}{8} + \gamma - i\frac{\pi}{2}} \quad .$$

For $d = 0.1\lambda$, $|P_1| \approx 0.624$, while for $d = 0.01\lambda$, $|P_1| \approx 0.345$, a decrease of only 5 dB.

It should be pointed out, however, that the slit model we have adopted in this report for investigating the pattern effects of cracks in the surface of reflectors may exaggerate the magnitude of the actual effects in real antennas. One would

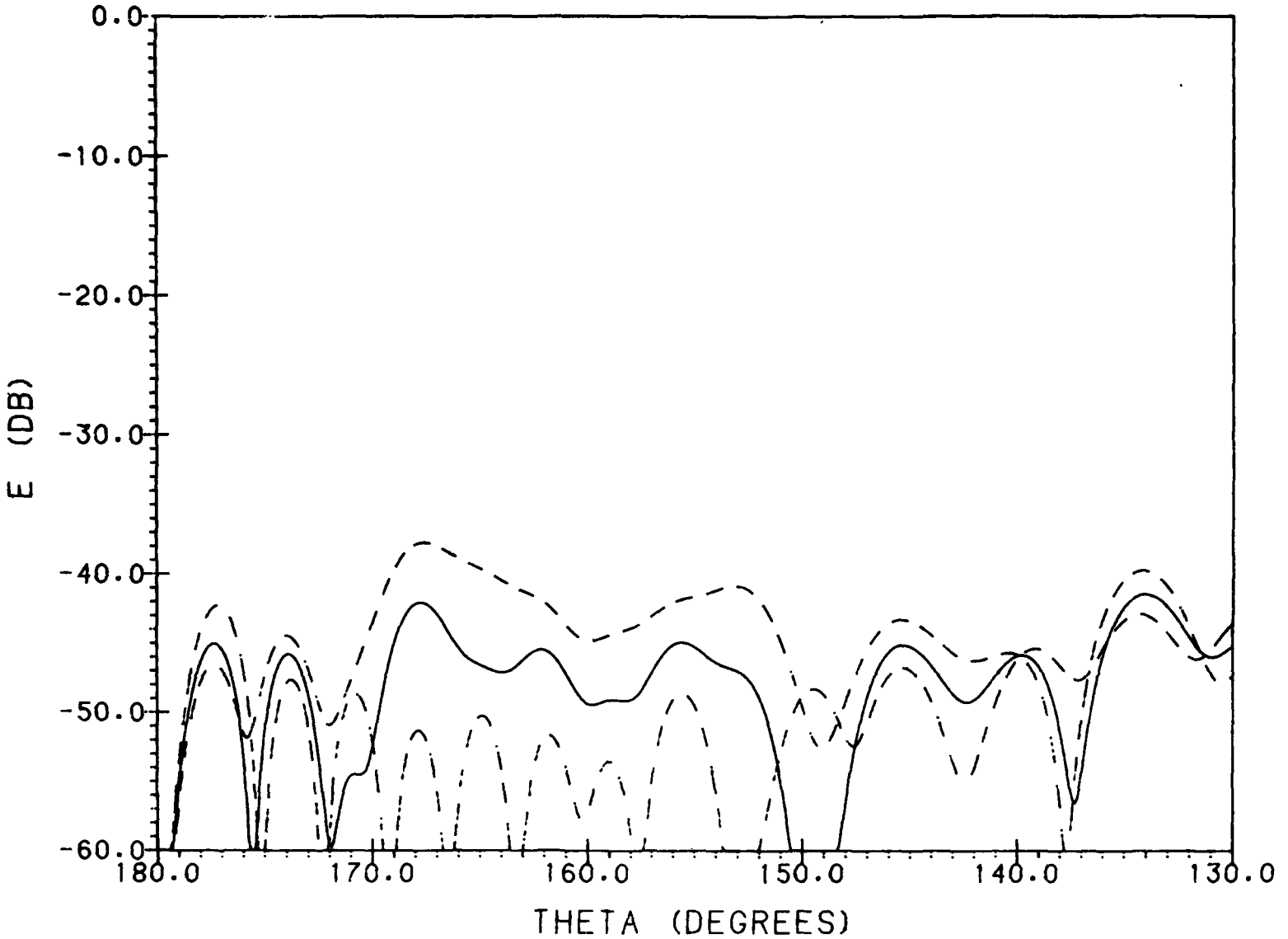

Figure 18. Cross-Polar Amplitude Pattern in $\phi = 45°$ Plane of Paraboloid With Basic Crack Configuration and Crack Width of 0.01 (———), Crack Width of 0.1λ (------) and of Paraboloid Without Cracks (-.-.-.-.)

not expect the cracks resulting from joining panels together in actual large reflectors to go clear through to the other side; some kind of metallic backing would probably be used. In this event, the currents excited in a direction transverse to the crack axis would be able to continue down one side of a crack and up the other, so that the crack would not cause a total break in the current sheet, as happens for the slit model used here. A more realistic model of the cracks, consisting of narrow troughs rather than slits, might very well indicate a significantly smaller effect on the patterns. To employ the same method we have used in this report, however, it would be necessary to have an expression for the incremental diffraction coefficients of a narrow trough in a perfectly conducting surface. It is hoped that this can be accomplished in future work.

3.2 Comparison With Scattered Fields Obtained by Asymptotic Evaluation of the Diffraction Integrals

In the previous section, we calculated the scattered far fields of the azimuthal and radial cracks by numerically integrating the incremental diffraction coefficients for the slit (multiplied by the incident field) along the cracks. Alternatively, we can evaluate these integrals asymptotically by the method of stationary phase to obtain closed-form approximate expressions for far fields scattered by the cracks.

Proceeding as we did in Section 3.2 of Part II,[2] we find the following asymptotic expressions for the scattered far fields of the azimuthal crack:

(E-plane)

$$E_\theta^{az}(\theta) = H_{i\phi'}(\phi' = 0)\, Z_o \left(\frac{D_c \lambda}{2 \sin\theta}\right)^{1/2} \frac{e^{i(kR+\pi/4}}{\pi R}$$

$$\cdot \left[e^{-i\pi D_c \cos(\theta-\theta_c')/\lambda \sin\theta \sin\theta_c'} P_1(\theta_1, \theta_1', kd) \right.$$

$$\left. - ie^{-i\pi D_c \cos(\theta+\theta_c')/(\lambda \sin\theta \sin\theta_c')} P_1(\theta_2, \theta_1', kd) \right] , \qquad (36)$$

(H-plane)

$$E_{\phi}^{az}(\theta) = E_{i\phi'}(\phi' = \pi/2) \left(\frac{D_c \lambda}{2 \sin \theta}\right)^{1/2} \frac{e^{i(kR+\pi/4)}}{\pi R}$$

$$\cdot \left[e^{-i\pi D_c \cos(\theta-\theta'_c)/(\lambda \sin\theta \sin\theta'_c)} P_1(\theta_1, \theta'_1, kd) \right.$$

$$\left. - i e^{-i\pi D_c \cos(\theta+\theta'_c)/(\lambda \sin\theta \sin\theta'_c)} P_1(\theta_2, \theta'_1, kd) \right] , \qquad (37)$$

where all the parameters in (36) and (37) have been defined previously except for (see Figure 19)

$$\theta_1 = 2\pi - (\theta + \beta'_c) ,$$

$$\theta_2 = \theta - \beta'_c ,$$

$$\theta'_1 = \pi - \beta'_c - \theta'_c ,$$

$$\beta'_c = \frac{\pi}{2} - \frac{\theta'_c}{2} ,$$

and

D_c = diameter of azimuthal crack

$$= 4F \frac{\sin \theta'_c}{4 \cos \theta'_c} = 4F \tan \frac{\theta'_c}{2} .$$

Similarly, the E-plane far fields scattered by a single diameter crack (that is, two radial cracks) in the H-plane of the reflector can be approximated by the method of stationary phase as

$$E_{\theta}^{di}(\theta) = H_{oy} Z_o \left(\frac{2F\lambda}{1 + \cos \theta}\right) \frac{e^{i(kR+\pi/4)}}{\pi R} e^{-ikF\cos\theta} P_1\left(\theta - \frac{\pi}{2}, \frac{\pi}{2}, kd\right) , \qquad (38)$$

and the H-plane far fields scattered by a diameter crack in the E-plane of the reflector can be approximated as

$$E_{\phi}^{di}(\theta) = - E_{ox} \left(\frac{2F\lambda}{1 + \cos \theta}\right) \frac{e^{i(kR+\pi/4)}}{\pi R} e^{-ikF\cos\theta} P_1\left(\theta - \frac{\pi}{2}, \frac{\pi}{2}, kd\right) . \qquad (39)$$

The constants H_{oy} and E_{ox} are the incident magnetic and electric fields illuminating the center of the cracks. From (27a) and (27b),

$$H_{oy} = -\frac{e^{ikF}}{Z_o F} d(0) \quad ,$$

$$E_{ox} = \frac{e^{ikF}}{Z_o F} a(0) \quad ,$$

where $a(\theta')$ and $d(\theta')$ are given respectively by (28) and (29) for an x-directed electric dipole source and a Huygens source with an x-directed electric dipole and y-directed magnetic dipole.

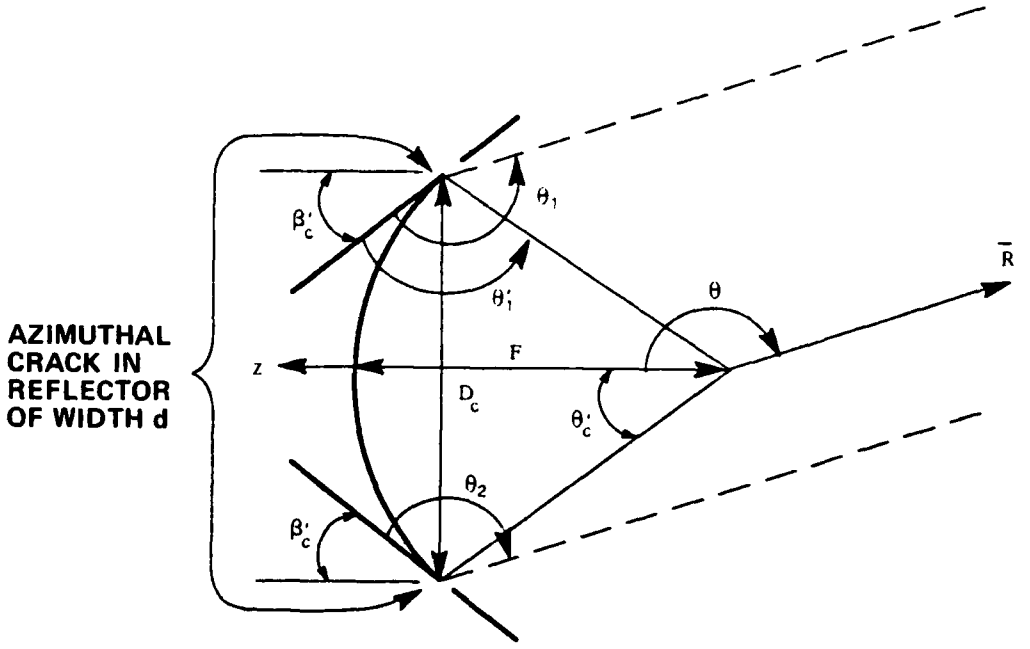

Figure 19. Geometry of Reflector Antenna With Azimuthal Crack

The amplitude of the diffracted far fields E^{az}, E^{az}, E^{di}, and E^{di} for the Huygens source given by the asymptotic expressions (36) through (39) are plotted in Figures 20(a) through 20(d). Also shown in these figures are the same diffracted fields computed by numerical integration of the incremental diffraction coefficients. The agreement between the asymptotically and numerically evaluated E-plane far fields of the azimuthal crack is quite good except in the forward

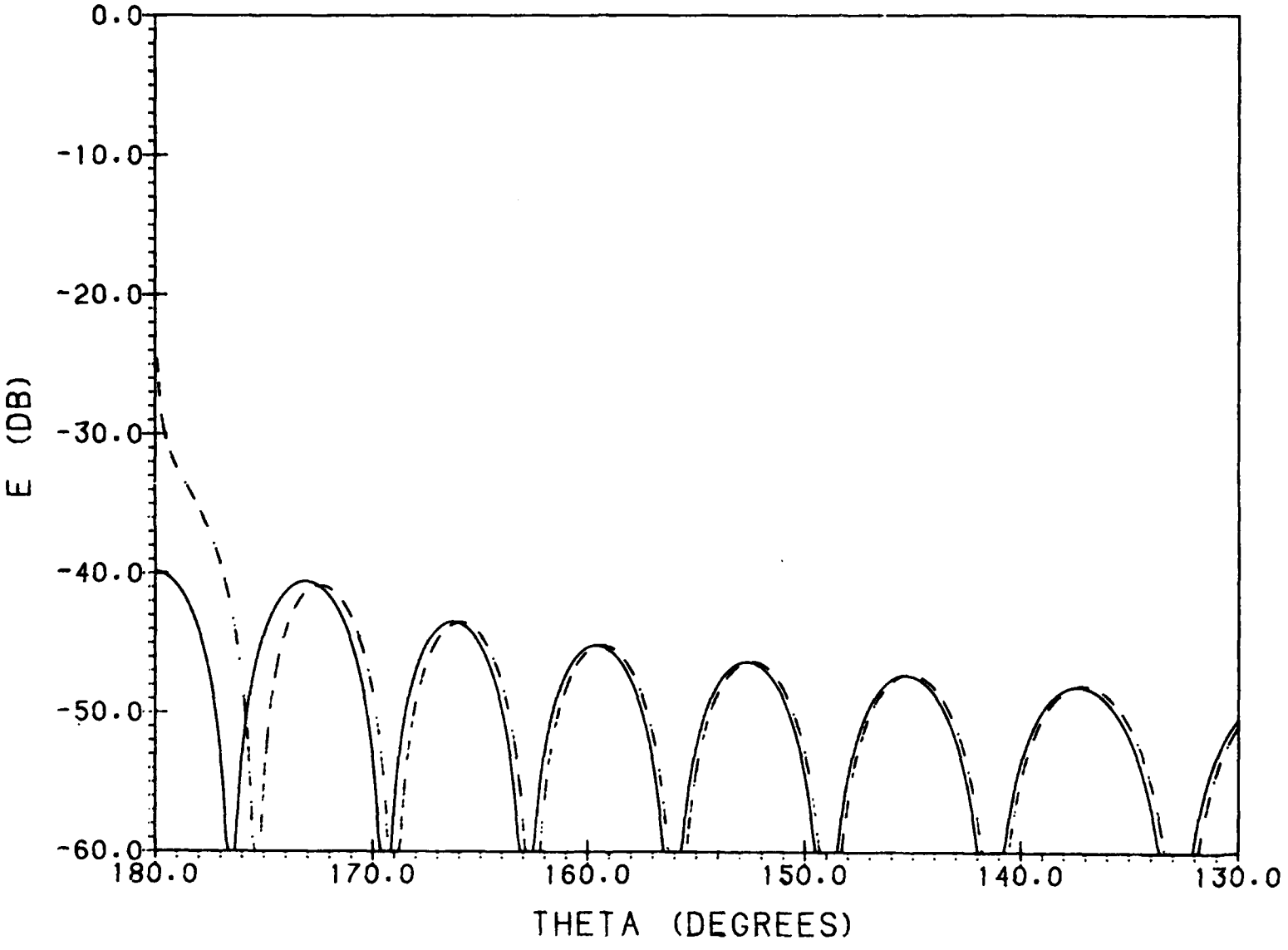

Figure 20a. E-Plane Amplitude Pattern of Azimuthal Crack Diffracted Fields of a 20λ Huygens Source-Fed Paraboloid Antenna; ------ Asymptotic, Eq. (36), ——— Numerical Integration, Eq. (34a); F/D = 0.4, θ =[180°, 130°]

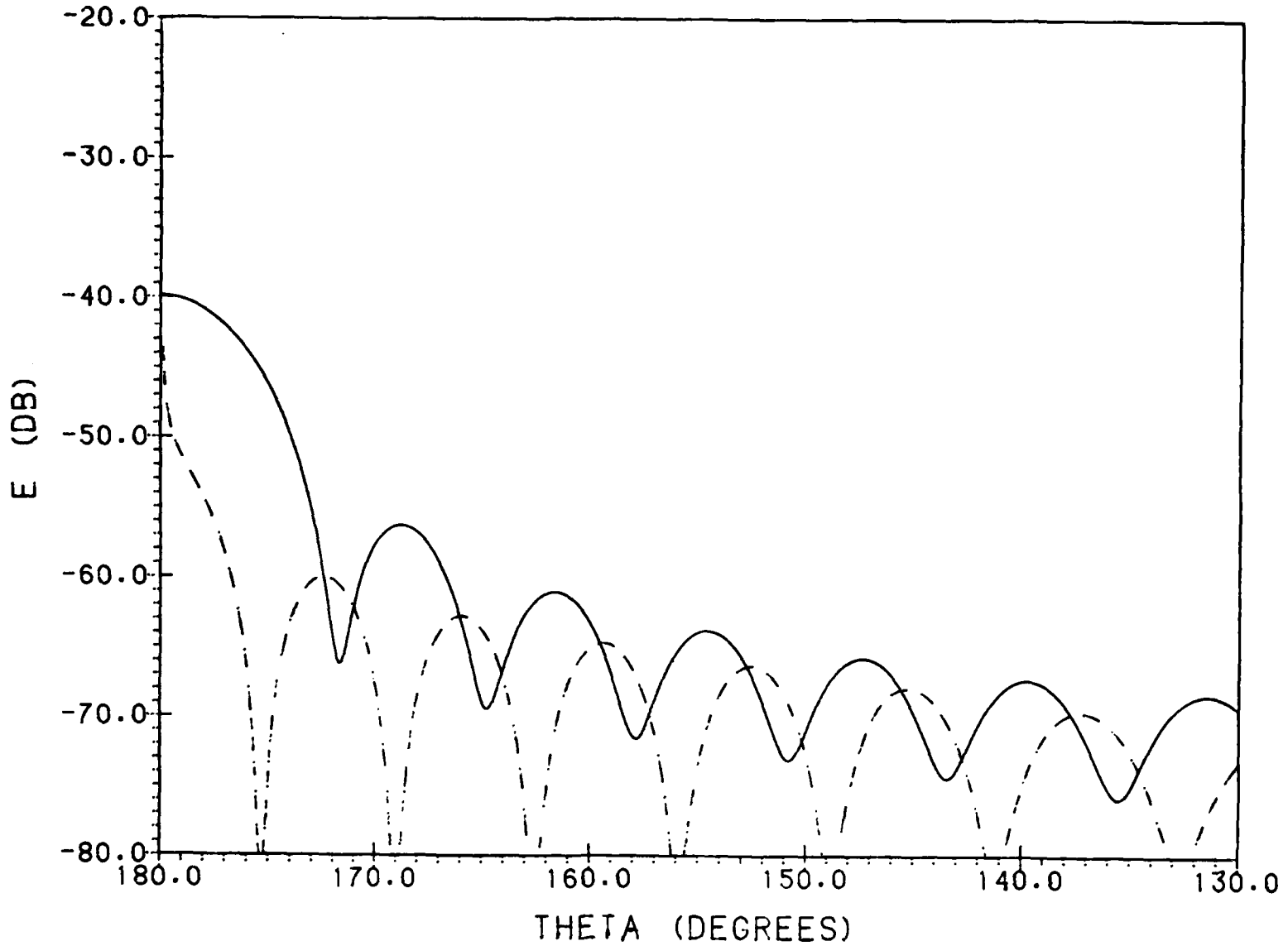

Figure 20b. H-Plane Amplitude Pattern of Azimuthal Crack Diffracted Fields of a 20λ Huygens Source-Fed Paraboloid Antenna; ------ Asymptotic, Eq. (37), ——— Numerical Integration, Eq. (34b); F/D = 0.4, $\theta = [180^{\circ}, 130^{\circ}]$

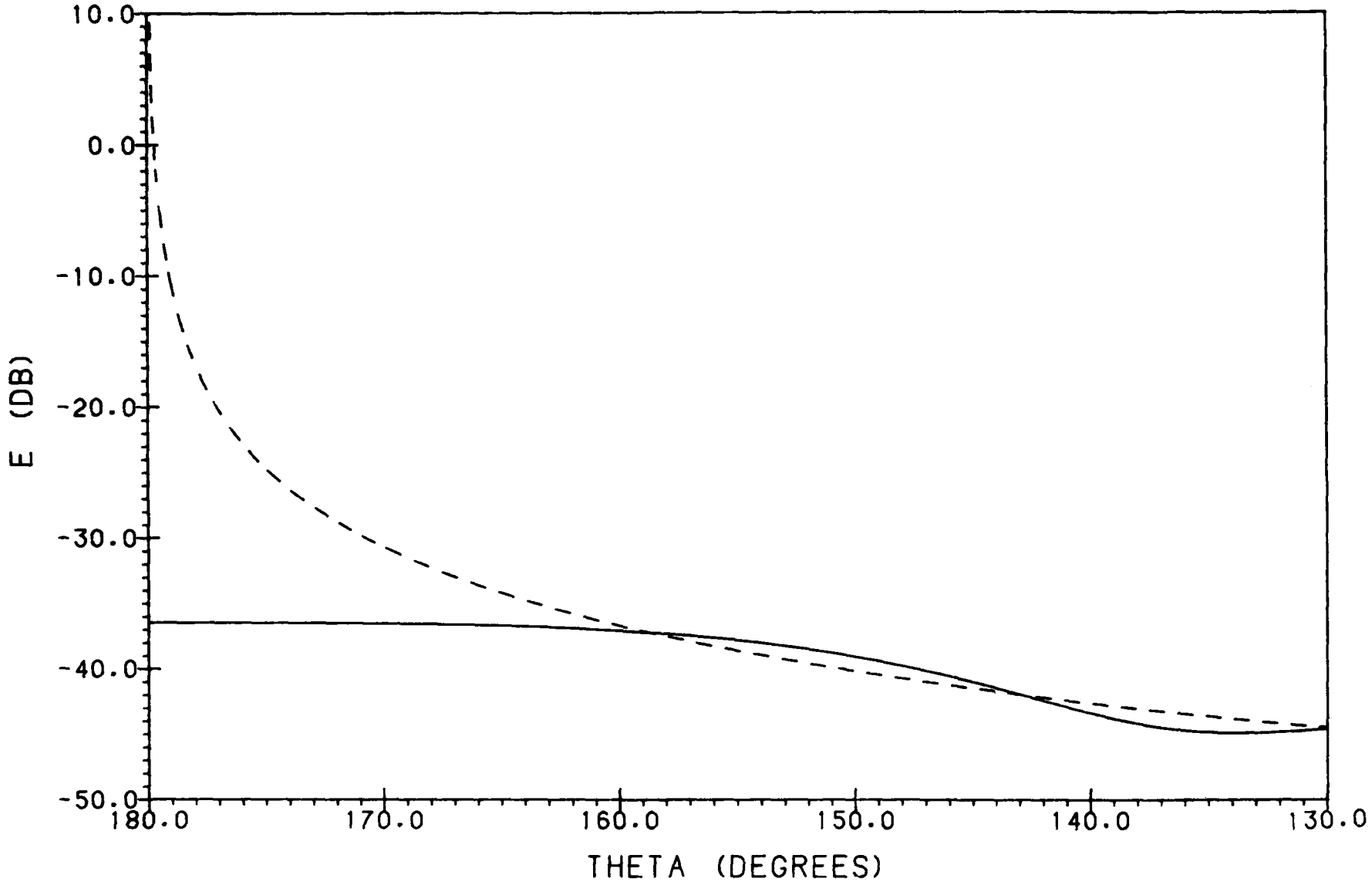

Figure 20c. E-Plane Amplitude Pattern of Fields Diffracted by a Diameter Crack in the H-Plane of a 20λ Huygens Source-Fed Paraboloid Antenna; ------ Asymptotic, Eq. (38), ——— Numerical Integration, Eq. (33a); F/D = 0.4, $\theta = [180°, 130°]$

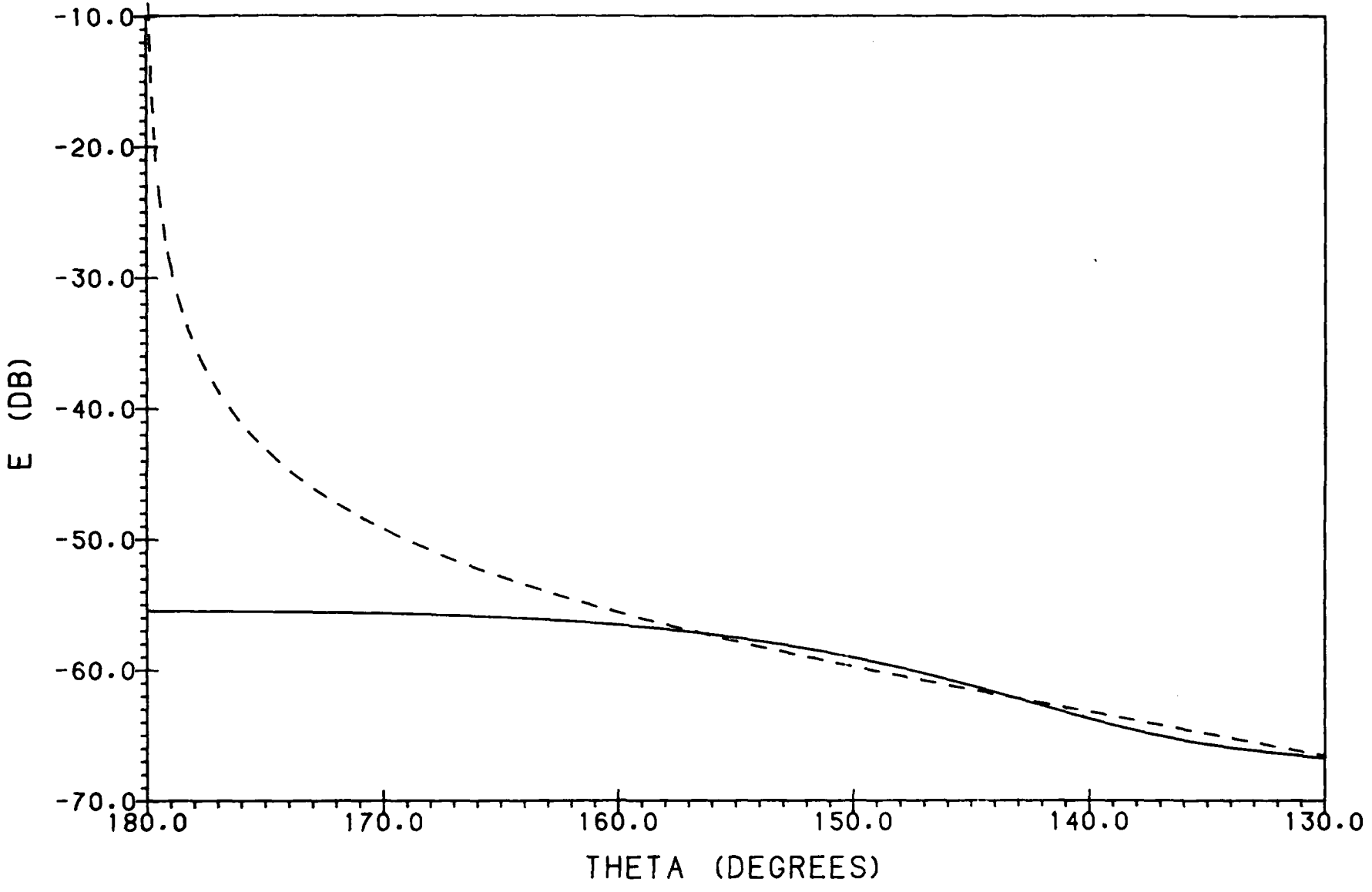

Figure 20d. H-Plane Amplitude Pattern of Fields Diffracted by a Diameter Crack in the E-Plane of a 20λ Huygens Source-Fed Paraboloid Antenna; ------ Asymptotic, Eq. (39), ——— Numerical Integration, Eq. (33b); F/D = 0.4, θ = [180°, 130°]

direction ($\theta = 180°$), because the method of stationary phase produces divergent results in this focal direction of the paraboloidal reflector.

The poor agreement in the H-plane for the azimuthal crack [Figure 20(b)] was traced to the small values of the diffracted far fields from the two stationary phase points where the incident E-field is parallel to the azimuthal crack. Although the normal component of the incident E-field is zero at these two points, the normal component away from the stationary phase points produces large diffracted far-fields that contribute significantly to the numerical integration but do not contribute to the first order asymptotic evaluation (37) of the integral by the method of stationary phase.

The discrepancy between the numerical and asymptotic calculations of the diffracted fields of the radial cracks in a fairly large forward sector of the patterns was traced to the lack of a sufficient number of Fresnel zones in the neighborhood of the stationary phase point at the center of the reflector to insure that the first order asymptotic approximations, (38) and (39), are accurate for a reflector with $F/\lambda = 8$. Indeed, as we increased F/λ, we found that the agreement between the numerically and asymptotically calculated far fields became increasingly better except, of course, very close to the forward direction.

In conclusion, we emphasize that conventional asymptotic high frequency diffraction formulas applied to cracks can predict highly inaccurate crack scattered fields over the entire far field sphere of reflectors many wavelengths in both diameter and focal length.

References

1. Shore, R.A., and Yaghjian, A.D. (1987) Incremental Diffraction Coefficients for Planar Surfaces, Part I: Theory, RADC-TR-87-35.

2. Shore, R.A., and Yaghjian, A.D. (1987) Incremental Diffraction Coefficients for Planar Surfaces, Part II: Calculation of the Nonuniform Current Correction to PO Reflector Antenna Patterns, RADC-TR-87-213.

3. Millar, R.F. (1960) A note on diffraction by an infinite slit, Can. J. Phys., 38:38-47.

4. Asvestas, J.S., and Kleinman, R.E. (1969) The strip, Ch. 4 of Electromagnetic and Acoustic Scattering by Simple Shapes, Bowman, J.J., Senior, T.B.A., and Uslenghi, P.L.E., Eds., Amsterdam: North-Holland.

5. Ludwig, A.C. (1973) The definition of cross polarization, IEEE Trans. Antennas and Propagat., AP-21:116-119.

MISSION
of
Rome Air Development Center

RADC plans and executes research, development, test and selected acquisition programs in support of Command, Control, Communications and Intelligence (C^3I) activities. Technical and engineering support within areas of competence is provided to ESD Program Offices (POs) and other ESD elements to perform effective acquisition of C^3I systems. The areas of technical competence include communications, command and control, battle management, information processing, surveillance sensors, intelligence data collection and handling, solid state sciences, electromagnetics, and propagation, and electronic, maintainability, and compatibility.